Walter A. Rosenblith New Investigator Award
RESEARCH REPORT

HEALTH EFFECTS INSTITUTE

Number 179
June 2014

Development and Application of an Aerosol Screening Model for Size-Resolved Urban Aerosols

Charles O. Stanier and Sang-Rin Lee

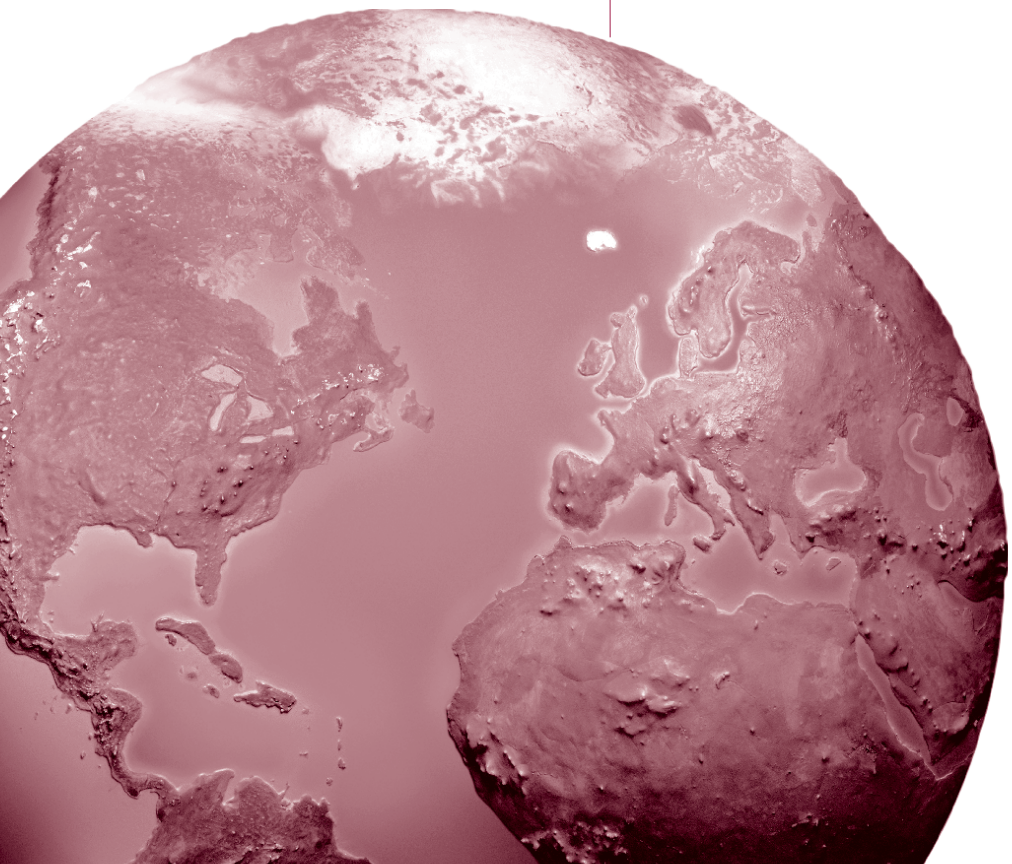

Development and Application of an Aerosol Screening Model for Size-Resolved Urban Aerosols

Charles O. Stanier and Sang-Rin Lee

with a Critique by the HEI Health Review Committee

Research Report 179
Health Effects Institute
Boston, Massachusetts

Trusted Science • Cleaner Air • Better Health

Publishing history: This document was posted at *www.healtheffects.org* in June 2014.

Citation for document:

Stanier CO, Lee S-R. 2014. Development and Application of an Aerosol Screening Model for Size-Resolved Urban Aerosols. Research Report 179. Boston, MA: Health Effects Institute.

CONTENTS

Research Report 179

ABOUT HEI

The Health Effects Institute is a nonprofit corporation chartered in 1980 as an independent research organization to provide high-quality, impartial, and relevant science on the effects of air pollution on health. To accomplish its mission, the institute

- Identifies the highest-priority areas for health effects research;
- Competitively funds and oversees research projects;
- Provides intensive independent review of HEI-supported studies and related research;
- Integrates HEI's research results with those of other institutions into broader evaluations; and
- Communicates the results of HEI's research and analyses to public and private decision makers.

HEI typically receives half of its core funds from the U.S. Environmental Protection Agency and half from the worldwide motor vehicle industry. Frequently, other public and private organizations in the United States and around the world also support major projects or research programs. HEI has funded more than 330 research projects in North America, Europe, Asia, and Latin America, the results of which have informed decisions regarding carbon monoxide, air toxics, nitrogen oxides, diesel exhaust, ozone, particulate matter, and other pollutants. These results have appeared in more than 260 comprehensive reports published by HEI, as well as in more than 1000 articles in the peer-reviewed literature.

HEI's independent Board of Directors consists of leaders in science and policy who are committed to fostering the public–private partnership that is central to the organization. The Health Research Committee solicits input from HEI sponsors and other stakeholders and works with scientific staff to develop a Five-Year Strategic Plan, select research projects for funding, and oversee their conduct. The Health Review Committee, which has no role in selecting or overseeing studies, works with staff to evaluate and interpret the results of funded studies and related research.

All project results and accompanying comments by the Health Review Committee are widely disseminated through HEI's Web site *(www.healtheffects.org)*, printed reports, newsletters and other publications, annual conferences, and presentations to legislative bodies and public agencies.

ABOUT THIS REPORT

Research Report 179, *Development and Application of an Aerosol Screening Model for Size-Resolved Urban Aerosols*, presents a research project funded by the Health Effects Institute and conducted by Dr. Charles O. Stanier of the Department of Chemical and Biochemical Engineering at the University of Iowa, Iowa City, and his colleague Dr. Sang-Rin Lee. This research was funded under HEI's Walter A. Rosenblith New Investigator Award Program, which provides support to promising scientists in the early stages of their careers. The report contains three main sections.

The HEI Statement, prepared by staff at HEI, is a brief, nontechnical summary of the study and its findings; it also briefly describes the Health Review Committee's comments on the study.

The Investigators' Report, prepared by Stanier and Lee, describes the scientific background, aims, methods, results, and conclusions of the study.

The Critique is prepared by members of the Health Review Committee with the assistance of HEI staff; it places the study in a broader scientific context, points out its strengths and limitations, and discusses remaining uncertainties and implications of the study's findings for public health and future research.

This report has gone through HEI's rigorous review process. When an HEI-funded study is completed, the investigators submit a draft final report presenting the background and results of the study. This draft report is first examined by outside technical reviewers and a biostatistician. The report and the reviewers' comments are then evaluated by members of the Health Review Committee, an independent panel of distinguished scientists who have no involvement in selecting or overseeing HEI studies. During the review process, the investigators have an opportunity to exchange comments with the Review Committee and, as necessary, to revise their report. The Critique reflects the information provided in the final version of the report.

HEI STATEMENT

Synopsis of Research Report 179

Development and Application of an Aerosol Screening Model for Size-Resolved Urban Aerosols

BACKGROUND

Dr. Charles O. Stanier, a recipient of HEI's Walter A. Rosenblith New Investigator Award, and Dr. Sang-Rin Lee developed, tested, and evaluated an aerosol screening model for estimating the number concentrations and size distribution of ultrafine particles, defined as particles less than 100 nm in aerodynamic diameter, in near-road environments with high spatial resolution (~10 m). In the urban atmosphere, ultrafine particles are derived primarily from motor vehicles, and their concentrations vary greatly because of steep concentration gradients near traffic sources. Thus assessing exposure to ultrafine particles is challenging, and there is a need for improved models.

APPROACH

The main goal of the study was to develop, test, and evaluate an aerosol screening model of hourly size-resolved number concentrations and distributions for particles in the size range of 3 nm to 2.5 μm. The aerosol screening model is an integrated model based on the Lagrangian modeling framework, which assumes columns of air parcels that move downwind with larger steps when far from receptors and smaller steps when close to receptors. The assumptions used by the aerosol screening model include rapid mixing of tailpipe emissions, emissions evenly mixed horizontally across the road width and carried beyond the edge of the road by diffusion and advection with the wind (i.e., downwind transport), and rapid mixing into a predefined vertical distribution.

Model design and construction were guided by the desire for the model, first, to have the ability to model concentrations over short (1-hour) and longer (24-hour) periods at sites with various traffic volumes and patterns and at various distances from roads and, second, to use a large database of road segments and emission factors derived from different data sources. It was also important that the model estimates could be compared with field measurements made with a condensation particle counter (CPC) and a scanning mobility particle sizer (SMPS), which have different lower size cutoffs.

What This Study Adds

- Stanier and Lee developed and tested an aerosol screening model to simulate the dispersion of ultrafine particles near roadways using a Lagrangian dispersion framework. The model estimated particle numbers and size distributions at 11 sites in Los Angeles and Riverside counties in California.
- The performance of the model was mixed. The model predictions for the 24-hour average number concentrations were close to the preset performance targets; the predictions for the 1-hour average number concentrations were poor and did not capture the diurnal variations observed at several sites. Particle size distributions also were not well represented by the model.
- The study demonstrates the challenges involved in modeling ultrafine particles in urban areas. Although it remains unclear what the most useful applications of this model will be, it offers promise for further improvements.

This Statement, prepared by the Health Effects Institute, summarizes a research project funded by HEI and conducted by Dr. Charles O. Stanier and Dr. Sang-Rin Lee at the University of Iowa, Iowa City. Research Report 179 contains both the detailed Investigators' Report and a Critique of the study prepared by the Institute's Health Review Committee.

The model was run to predict hourly and 24-hour concentrations and size distributions of particle number and mass at 11 sites in California where real-time measurements were made in previous studies. These included seven sites around the port of Long Beach (one of the busiest commercial ports in the United States) that were part of the Harbor Community Monitoring Study (HCMS) and four sites near retirement communities in Los Angeles and Riverside counties that were part of the Cardiovascular Health and Air Pollution Study (CHAPS).

RESULTS AND INTERPRETATION

The investigators assessed the performance of the aerosol screening model by comparing the 1-hour and 24-hour-average simulations with the corresponding measured concentrations. Correlations between the modeled and measured 1-hour and 24-hour average number concentrations differed.

For the 24-hour measurement, the model's performance was not far from the preset targets. For the 1-hour average number concentrations, the model's performance was poor and did not capture the diurnal variations observed at several sites. In general, the performance was better at the CHAPS sites, which were further from freeways and had a lower volume of heavy-duty vehicles compared with the majority of the HCMS sites. The investigators found that when the modeled values failed to fall in the specified ranges, the model typically underestimated the particle concentrations. Sensitivity analysis showed that the model was sensitive to traffic volume and type, as well as to road class.

The investigators compared modeled and measured size distributions at two of the Long Beach sites, LB4 and LB5. The modeled size distributions differed from the measured distributions for many of the simulations. The investigators concluded that the model underpredicts particle number concentrations for all particles sizes $\geq$ 15 nm and overpredicts concentrations for particle sizes < 15 nm.

CONCLUSIONS

Modeling the number and size distributions of ultrafine particles in epidemiologic studies is challenging, and only a few approaches have so far been tested. Thus the Committee thought that the study addressed an important research need. This ambitious study was carefully planned and performed, and the work was of high quality. The Committee felt that Stanier and Lee had chosen a high level of complexity for a screening model, that the model would require additional simplifications for actual screening applications, and that additional information would be needed for more detailed applications.

The strengths of the model are its flexibility to incorporate additional processes, the automated procedure to process road network and traffic data, and the synthesis of emission data for particle number by size from various research groups (a complex task). Model limitations are implicit in the Lagrangian approach, which assumes that all the air parcels move downwind at the same rate and communicate by diffusion, but which does not allow any movement through their boundaries associated with changes in wind speed and direction.

Evaluation of the model indicated that the predictions of the 24-hour average number concentrations were close to the preset performance targets; the predictions of the 1-hour average number concentrations were poor and did not capture the diurnal variations observed at several sites. Particle size distributions were not well represented by the model, at least in part because of uncertainties in the emission factors.

The Committee agreed with the investigators' overall assessment that the performance of the model in predicting particle number and size distribution was mixed. The results suggest that the model might be more suitable for studies that require long-term (i.e., 24-hour or longer) averages.

The study reflected the challenges involved in modeling dynamic concentrations of UFPs in urban areas, including the complex behavior of UFPs in the atmosphere as well as our limited knowledge not only of size-resolved emission factors as a function of vehicle types and operating modes, but also of emissions from non-mobile sources. Given the complexity of the model and the limitations of the Lagrangian framework in modeling the behavior of ultrafine particles, it remains unclear what the most useful application of this model will be. However, the model offers promise for further improvements and has the flexibility of incorporating additional inputs such as fleet information and emissions from off-road sources.

Development and Application of an Aerosol Screening Model for Size-Resolved Urban Aerosols

Charles O. Stanier and Sang-Rin Lee

Department of Chemical and Biochemical Engineering (C.O.S.), IIHR–Hydroscience & Engineering Institute (C.O.S. and S-R.L.), and Center for Global and Regional Environmental Research (C.O.S.), University of Iowa, Iowa City

ABSTRACT

Predictive models of vehicular ultrafine particles less than 0.1 μm in diameter (UFPs*) and other urban pollutants with high spatial and temporal variation are useful and important in applications such as (1) decision support for infrastructure projects, emissions controls, and transportation-mode shifts; (2) the interpretation and enhancement of observations (e.g., source apportionment, extrapolation, interpolation, and gap-filling in space and time); and (3) the generation of spatially and temporally resolved exposure estimates where monitoring is unfeasible.

The objective of the current study was to develop, test, and apply the Aerosol Screening Model (ASM), a new physically based vehicular UFP model for use in near-road environments. The ASM simulates hourly average outdoor concentrations of roadway-derived aerosols and gases. Its distinguishing features include user-specified spatial resolution; use of the Weather Research and Forecasting (WRF) meteorologic model for winds estimates; use of a database of more than 100,000 road segments in the Los Angeles, California, region, including freeway ramps and local streets; and extensive testing against more than 9000 hours of observed particle concentrations at 11 sites.

This Investigators' Report is one part of Health Effects Institute Research Report 179, which also includes a Critique by the Health Review Committee and an HEI Statement about the research project. Correspondence concerning the Investigators' Report may be addressed to Dr. Charles O. Stanier, University of Iowa, 4122 Seamans Center for the Engineering Arts and Sciences, Iowa City, IA 52242-1527; email: *charles-stanier@uiowa.edu*.

Although this document was produced with partial funding by the United States Environmental Protection Agency under Assistance Award CR-83467701 to the Health Effects Institute, it has not been subjected to the Agency's peer and administrative review and therefore may not necessarily reflect the views of the Agency, and no official endorsement by it should be inferred. The contents of this document also have not been reviewed by private party institutions, including those that support the Health Effects Institute; therefore, it may not reflect the views or policies of these parties, and no endorsement by them should be inferred.

* A list of abbreviations and other terms appears at the end of the Investigators' Report.

After initialization of air parcels at an upwind boundary, the model solves for vehicle emissions, dispersion, coagulation, and deposition using a Lagrangian modeling framework. The Lagrangian parcel of air is subdivided vertically (into 11 levels) and in the crosswind direction (into 3 parcels). It has overall dimensions of 10 m (downwind), 300 m (vertically), and 2.1 km (crosswind). The simulation is typically started 4 km upwind from the receptor, that is, the location at which the exposure is to be estimated. As parcels approach the receptor, depending on the user-specified resolution, step size is decreased, and crosswind resolution is enhanced through subdivision of parcels in the crosswind direction.

Hourly concentrations and size distributions of aerosols were simulated for 11 sites in the Los Angeles area with large variations in proximal traffic and particle number concentrations (ranging from 6000 to 41,000/cm^3). Observed data were from the 2005–2007 Harbor Community Monitoring Study (HCMS; Moore et al. 2009), in Long Beach, California, and the Coronary Health and Air Pollution Study (CHAPS; Delfino et al. 2008), in the Los Angeles area. Meteorologic fields were extracted from 1-km-resolution meteorologic simulations, and observed wind direction and speed were incorporated. Using on-road and tunnel measurements, size-resolved emission factors ranging from 1.4×10^{15} to 16×10^{15} particles/kg fuel were developed specifically for the ASM. Four separate size-resolved emissions were used. Traffic and emission factors were separately estimated for heavy-duty diesel and light-duty vehicles (LDV), and both cruise and acceleration emission factors were used. The light-duty cruise size-resolved number emission factor had a single prominent mode at 12 nm. The diesel cruise size-resolved number emission factor was bimodal, with a large mode at 16 nm and a secondary mode at around 100 nm. Emitted particles were assumed to be nonvolatile. Data on traffic activity came from a 2008 travel-demand model, supplemented by data on diurnal patterns. Simulated ambient number size distributions and number

concentrations were compared to observations taking into account estimated losses from particle transmission efficiency in instrument inlet tubing.

The skill of the model in predicting number concentrations and size distributions was mixed, with some promising prediction features and some other areas in need of substantial improvement. For long-term (~15-day) average concentrations, the variability from site to site could be modeled with a coefficient of determination (r^2) of 0.76. Model underprediction was more common than overprediction. The average of the absolute normalized bias was 0.30; in other words, long-term mean particle concentrations at each site were on average predicted to within 30% of the measured values. Observed 24-hour number concentrations were simulated to within a factor of 1.6 on 48% of days at HCMS sites and 81% at CHAPS sites, lower than the original design goal of 90%.

Extensive evaluation of hourly concentrations, diurnal patterns, size distributions, and directional patterns was performed. At two sites with heavy freeway and heavy-duty-vehicle (HDV) influences and extensive size-resolved measurements, the ASM made significant errors in the diurnal pattern, concentration, and mode position of the aerosol size distribution. Observations indicated a shift in concentrations and size distributions corresponding to the afternoon development of offshore wind at the HCMS sites. The model did not reproduce the changes in particles associated with this wind shift and suffered from overprediction for particles of less than 15 nm and underprediction for particles of between 15 and 500 nm, raising doubt about the applicability of the HDV emission factors and the model's assumptions that particles were nonvolatile.

The model's temporal prediction skill at individual monitoring sites was variable; the index of agreement (IOA) for hourly values at single sites ranged from 0.30 to 0.56. The model's ability to reproduce diurnal patterns in aerosol concentrations was site dependent; midday underprediction as well as underprediction for particle sizes greater than 15 nm were typical errors. Despite some problems in model skill, the number of time periods and locations evaluated as well as the extent of our qualitative and quantitative evaluations versus physical measurements well exceeded other published size-resolved modeling efforts.

As a trial of a typical application, the sensitivity of the concentrations at each receptor site to LDV traffic, HDV traffic, and various road classes was evaluated. The sensitivity of overall particle numbers to all types of traffic ranged from 0.87 at the site with the heaviest traffic to 0.28 at the site with the lightest traffic, meaning that a 1% reduction in traffic could yield a reduction in particle number of 0.87% to 0.28%.

Key conclusions and implications of the study are the following:

1. That variable-resolution (down to 10 m) modeling in a relatively simple framework is feasible and can support most of the applications mentioned above;
2. That model improvements will be required for some applications, especially in the areas of the HDV emission factor and the parameterization of meteorologic dispersion;
3. That particle loss from instrument transmission efficiency can be significant for particles smaller than 50 nm, and especially significant for particles smaller than 20 nm. In cases where loss corrections are not accounted for, or are inaccurate, this loss can cause disagreements in observation–model and observation–observation comparisons.
4. That LDV traffic exposures likely exceed HDV traffic exposures in some locations;
5. That variable step size and adaptive parcel width are critical to balancing computational efficiency and resolution; and
6. That the effects of roadways on air quality depend on both traffic volume and distance — in other words, low traffic volumes at close proximity need to be considered in health and planning studies just as much as do high traffic volumes at distances up to several kilometers.

Future improvements to the model have been identified. They include improved emission factors; integration with the U.S. Environmental Protection Agency (EPA) Motor Vehicle Emission Simulator (MOVES) model; nesting with three-dimensional (3D) Eulerian models such as the Community Multi-scale Air Quality (CMAQ) model; increased emission dependence on acceleration, load, grade, and speed as well as evaporation and condensation of semivolatile aerosol species; and modeling of carbon dioxide (CO_2) as an on-road and near-road dilution tracer. In addition, comparison with other statistically and physically based models would be highly beneficial.

INTRODUCTION

Models that predict human exposure to combustion-derived and other ultrafine particles are desirable for use in a number of applications related to human health. These applications include (1) decision support for infrastructure projects, emissions controls, and transportation-mode shifts; (2) the interpretation and enhancement of measured data (e.g., source apportionment, extrapolation, interpolation,

and gap-filling in space and time); and (3) the generation of spatially and temporally resolved exposure estimates where monitoring is not feasible. The quantification of both short-term and long-term exposures is needed to continue to assess the human health effects of gases and particulate matter (PM) from combustion sources, including UFPs. Compared with particles in other size ranges, UFPs have large surface areas and high deposition efficiencies in the respiratory system, resulting in the delivery of adsorbed and condensed toxins, which are associated with oxidative stress and inflammatory responses (Oberdörster 2001; Delfino et al. 2005). Roadway exposures might be the single largest factor in personal exposures (Fruin et al. 2008). In a critical review of the literature, considering traffic pollution in general (and not UFPs in particular), the HEI Panel on the Health Effects of Traffic-Related Air Pollution (2010) found the evidence sufficient to support a causal relationship between exposure and the exacerbation of asthma. The Panel also found the evidence sufficient to suggest causal relationships between exposure and the onset of childhood asthma, non-asthma respiratory symptoms, impaired lung function, total and cardiovascular mortality, and cardiovascular morbidity.

Unlike PM $\leq$ 2.5 μm in aerodynamic diameter ($PM_{2.5}$), for which measures obtained from central monitors are often accurately representative of personal exposures, UFPs and other vehicle exhaust components can vary in concentration substantially over short distances. Two meta-analyses characterized roadway pollutant concentrations as decreasing by 50% from their peak on the road at distances of 100 to 300 m (Zhou and Levy 2007; Karner et al. 2010); the concentration gradient can extend to larger distances during periods of reduced atmospheric mixing, such as nighttime (Zhu et al. 2006; Hu et al. 2009).

EXPOSURE MODELS: POTENTIAL APPLICATIONS AND DESIGN CHOICES

The HEI Panel on the Health Effects of Traffic-Related Air Pollution (2010) identified at least six types of models for the prediction of vehicular pollutants: proximity-based, geostatistical interpolation, land-use regression (LUR), dispersion, hybrid, and regional three-dimensional (3D) air quality models. The model presented in the current study is a dispersion model. Key questions for dispersion models are the following:

1. How much detail about fluid flow and aerosol processes is needed for various applications?
2. To what extent do the physics- and chemistry-based features of dispersion models or the model skill justify the extra computational and input-data requirements compared with those of LUR and proximity-based models?
3. What levels of accuracy are possible with physically based models as a function of modeling choices (e.g., neglecting topography, vehicle wake particle dynamics, or condensation and evaporation)?
4. What are appropriate emission factors and what is an appropriate level of detail in describing variability in emissions? For example, UFP emission factors for both total particle number and size-resolved particle numbers are needed.

The distinction between a screening model and a detailed model is useful in this connection. For the purposes of the current study, a screening model is considered to be one that is run to determine if a more detailed model or additional measurements are warranted. Ideally, a screening model needs only a minimal set of inputs to make this determination. A detailed model is a model that has demonstrated sufficient skill to make predictions useful for a given application without having to resort to a more detailed model or to additional measurements. The working assumption underlying the current study is that the ASM we built can serve — for certain applications — as a screening model. The question of the suitability of the ASM for specific applications and specific averaging times will be considered in the Discussion and Conclusions section. For some applications, the ASM might be competitive with a detailed model.

Although a number of investigators have simulated mass-based concentrations in urban and near-road environments using various techniques, the number of studies that have included simulations of particle number or size-resolved particle number is much smaller. Two studies that did not include UFP modeling but were instructive because of their methods of nesting dispersion models within larger-scale airshed models were those of Cook and colleagues (2008) and Stein and colleagues (2007). These studies combined a dispersion model (such as the EPA's AERMOD) with high-resolution CMAQ (an air quality model). Similar approaches have also included stochastic personal time–activity data as well as comparisons with LUR (Isakov et al. 2009; Johnson et al. 2010). The Operational Street Pollution Model has been evaluated against a large database of gas-phase measurements but does not use aerosol dynamics. For several hundred locations around Copenhagen, Denmark, the r^2 for the modeling of monthly NO_2 concentrations ($n > 1200$) was 0.76 (Berkowicz et al. 2008).

Physical models of size-resolved aerosols combine dispersion models with aerosol-dynamics treatments of nucleation, evaporation, condensation, coagulation, deposition, and other processes. All aerosol models for near-roadway applications include simulations of dilution, which has a strong influence on concentrations.

Models treating UFP number concentrations were reviewed by Kumar and colleagues (2011). One of the earlier applications of dispersion modeling to UFPs was described by Pohjola and colleagues (2003), who simulated the first 25 seconds of tailpipe-to-roadway dispersion. Gidhagen and colleagues combined aerosol-dynamics models with computational fluid-dynamics (CFD) models and dispersion modeling to simulate a street canyon (Gidhagen et al. 2004a), a roadway tunnel (Gidhagen et al. 2003), a near-road environment (Gidhagen et al. 2004b), and a large urban area at 500-m resolution (Gidhagen et al. 2005). Gidhagen and colleagues (2005) compared model results with 10 days of measurement data. Capaldo and Pandis (2001) used a one-dimensional Lagrangian model to investigate processing downwind of diesel-emission locations. Another high-resolution modeling effort was the application of the GATOR simulation to the Los Angeles near-road environment by Jacobson and Seinfeld (2004). The GATOR simulation used an Eulerian framework at 15-m horizontal resolution and 5-m vertical resolution; however, the modeling period was less than 1 day, and evaluation was limited. The GATOR model explicitly tracks aerosol-mixing states and is very insightful about aerosol coagulation as a way of changing mixing states near roadways. Zhang and Wexler and colleagues also simulated the Los Angeles near-road environment using a 3D model with dispersion and aerosol physics, developed at the University of California at Davis, and investigated the impact of condensation and evaporation on the evolution of aerosol size distributions (Zhang and Wexler 2004; Zhang et al. 2004; Zhang et al. 2005). The model first developed by Zhang and Wexler has been further developed into a combined system for CFD and aerosol-dynamics simulation (Wang and Zhang 2009; Steffens et al. 2012). CFD models coupled with aerosol-dynamics models have also been used to simulate the near-vehicle wake in the initial stages of tailpipe-to-roadway dilution (Carpentieri et al. 2011) as well as the dispersion of aerosols in an industrial environment (Fossum et al. 2012). The ADCHEM model developed by Roldin and colleagues (2011) is a detailed Lagrangian model with extensive aerosol chemistry and physics components. It has been applied to study the aging of urban plumes, but its results have not been compared with actual urban size-resolved particle number data. MAT/AERO3, a similar Lagrangian model with detailed aerosol dynamics, has been developed and demonstrated (Ketzel and Berkowicz 2005). A coupled dispersion and aerosol-dynamics model was constructed and run for 14 hours for comparison with detailed upwind and downwind concentration data near a major road (Pohjola et al. 2007).

Although the evaluation of size-resolved models has been limited, the number of data sets appropriate for evaluation is increasing (e.g., Shi et al. 2001; McMurry and Woo 2002; Jones and Harrison 2006; Moore et al. 2009; McAuley et al. 2010; Asmi et al. 2011; Wang et al. 2011; and Padro-Martinez et al. 2012).

Reviews of aerosol models relevant to the current study include the HEI Panel on the Health Effects of Traffic-Related Air Pollution (2010), a review by Tiwary and colleagues (2011) focused on intersections, a review by Kumar and colleagues (2011) of size-resolved models used in urban settings, and a review by Knibbs and colleagues (2011) of exposure models used for commuter exposure.

Statistical models can also be used to predict number concentrations. Fruin and colleagues (2008) introduced a multiple regression model for the on-road and neighborhood number concentrations in Los Angeles. This has been expanded to include detailed study and empirical models for in-cab–on-road concentration ratios (Hudda et al. 2012). A generalized additive model was able to estimate hourly variations in particle number in Helsinki, Finland (within 150 m of an arterial road), with a coefficient of determination of 0.83 when trained with a long time series of measurements and meteorologic data (Clifford et al. 2011). Predictor variables included hour of day, day of week, day of year, temperature, rainfall, wind speed, wind direction, and insolation. Another study obtained a coefficient of determination of 0.67 for the same data set in Helsinki using an alternate statistical time-series approach (Molgaard et al. 2012). Multiple linear regression has been applied to second-by-second highway chase data with good modeling skill for particle number and particle size distribution (Aggarwal et al. 2012). In their review of UFP exposures of commuters, Knibbs and colleagues (2011) reported that the majority of studies to date have used multivariate models with meteorologic factors, traffic, or other pollutants as predictors.

For long-term average exposures to traffic-related pollutants, LUR is widely used and has been reported to compare favorably with other methods, including dispersion modeling, when applied with suitable training and predictor data. Typical R^2 values for North American applications (e.g., $PM_{2.5}$, NO_2, and carbon monoxide [CO]) range from 0.56 to 0.79 (HEI Panel on the Health Effects of Traffic-Related Air Pollution 2010). However, very few studies have applied LUR to particle number. Hoek and colleagues (2011) applied LUR to particle number at 50 locations around Amsterdam, the Netherlands. They used a single central monitor to account for time-varying background concentrations and an LUR model to account for the increment above background that included distance to the port area of the city, traffic intensity times inverse squared distance to road, and address density. They reported an R^2 value of 0.67. Fuller and colleagues (2012) applied a multivariate model for time-resolved UFP exposures at multiple sites around Boston, Massachusetts.

SPECIFIC AIMS

The overarching goal of the current study was to develop, evaluate, and apply a model (i.e., a computer simulation) of hourly size-resolved particle number (in the size range of 3 nm to 2.5 μm). Distinguishing features of the model included user-specified spatial resolution; use of the WRF meteorologic model for winds; use of a large database of road segments (referred to as links), including freeway ramps and local streets; and extensive model evaluation for extended periods (weeks to months) at several measurement sites. In the name selected for our simulation, the Aerosol Screening Model (ASM), the term "screening" indicates our preference for a computationally efficient model able to simulate long periods of time (e.g., weeks, months, or years) and to screen the effects of many parameters, such as traffic volume or emissions characteristics. These characteristics distinguish it from models that rely on high-resolution 3D fluid-dynamical simulation of winds; such models require large computational resources and are typically limited to smaller domains and shorter time periods. The term "screening" also reflects our desire to build a model that could be widely disseminated and that allows simple and quick source–receptor calculations with limited input data (such as the type of screening calculation needed to support a facility-siting decision). Although the model is classified as a screening model for the reasons listed above, it does yield significant detail in terms of its simulation of aerosol dynamics and its treatment of roadway emissions as area sources with link-specific and hour-specific fleet mix, vehicle speed, and traffic volume.

The study's specific aims are stated below and are discussed in more detail in the Discussion and Conclusions section:

- Develop a computationally efficient model for making 3D predictions of concentrations at several user-specified receptor locations, allowing for arbitrarily located sources (i.e., roads). Combine analytic dispersion equations and two-dimensional and 3D aerosol-dynamics calculations to model number concentrations at several receptors. This aim required the completion of the following supporting objectives:
  - Develop an emission-calculation subroutine for total emissions over a time step (including vertical distribution of particles) for parcels passing over irregularly shaped road segments.
  - Develop preprocessing software to convert geographic information systems (GIS)-based road locations, road traffic volumes, and road speed information into model-ready formats for domains of 100 km^2 and larger.
  - Identify meteorologic fields from the WRF model or from observations for simulations.
  - Identify and implement a size-dependent deposition subroutine.
  - Create harmonized emission factors considering multiple published studies for particle sizes from 3 to 500 nm (where SMPS-based data sources were available) and for sizes from 0.5 to 10 μm using other sources. To the extent possible, account for inlet and sampler losses, engine type, vehicle size, and engine load.
- Evaluate the model by comparing its estimates with concentrations measured in California's Los Angeles and Riverside counties as part of HCMS (Moore et al. 2009) and CHAPS (Delfino et al. 2008).
- Evaluate the sensitivity of the model outputs and of the computational costs to design choices made about aerosol-dynamical processes and meteorologic data selection.

As the project evolved from proposal to implementation, a number of aspects of model development not included in the original proposal were identified and completed. Several objectives from the original proposal were not completed or were only partially completed. In most cases, these remain desirable to undertake as future work.

METHODS

STUDY DESIGN

The study was designed to develop, evaluate, and demonstrate a near-road physically based exposure model. From the beginning of the study, the team's focus was on the development of a model whose estimates could be compared with field measurements made by condensation particle counter (CPC) and scanning mobility particle sizer (SMPS). These instruments are widely used, sensitive to UFPs, and record data at 1-second (CPC) and ~2-minute (SMPS) time scales. High-resolution data like these are typically averaged to 1-hour data for summary reporting, archiving of field measurements, and comparison with models. One-hour time resolution is also commonly used for meteorologic and criteria-air-quality-monitoring data.

The model design also reflected a desire to have a large data set for model evaluation. Some near-road models are validated only for short periods, are evaluated against an average of monitored data, or are evaluated at one or a few sites. We felt strongly that a wider variety of locations was needed to better evaluate the model and to prevent the

model's being tuned to apparent good performance by comparing it against a small evaluation data set. HCMS and CHAPS both provided large data sets for evaluation. Even without using the entirety of the HCMS data, the current study's full evaluation data set included 11 locations, 365 days of paired model–observation data, and a 100-fold variation in nearby HDV traffic. The selection of the CHAPS data from the Los Angeles area for model evaluation, although providing a large data set, was not without its problems. First, there are many non-road sources of particles, particularly in the Long Beach area. Second, the area's weather is complex because of the Basin's topography and interactions with the Pacific Ocean.

Another important factor in the study design was the desire to demonstrate the use of the model for predicting both measured (e.g., particle count) and unmeasured (e.g., particle count from local HDV traffic) variables associated with an existing health study. The CHAPS study served this purpose. The long-term underlying motivation for development of a model such as the ASM was to be able to integrate data on health effects, measurements, and model predictions to develop new insights into associations between aerosol exposures and human health effects. As presented in the report, although the model demonstrated many aspects of skill, its ability to predict week-to-week variation in particle number at the CHAPS sites is somewhat limited. The aim of integrating models with data on health effects, therefore, has yet to be achieved.

An additional factor in the study design was the desire to create a model that had variable spatial resolution, motivated by the steep spatial gradients measured in the near-road environment. In the Lagrangian model framework, this means taking large steps in space and time if far from receptors and small steps when close to receptors. In the Eulerian model framework, it means having large grid cells when far from receptors and small grid cells when close to receptors.

Additional questions of interest to the team that guided the model design included (1) the effects of distant (> ~1 km) heavily trafficked roads and freeways versus the effects of nearby neighboring streets, (2) the effects of vehicle acceleration on emissions and concentrations, and (3) the relative effects of LDV and HDV engines. Because monitoring data used for the model evaluation was gathered from 2005 to 2007 and pre-dated the widespread use of advanced diesel technology and because the emissions framework lacked emission factors and traffic activity for advanced diesel technology, the model will need to be updated for predictions against more recent monitoring data.

Because roadway sources were of interest, the California Line Source Dispersion model (CALINE4) and its performance evaluation were examined in detail; components of CALINE4 were incorporated where appropriate.

The factors described above — the ability to simulate at hourly time resolution (for detailed evaluation), the ability to simulate thousands of receptor–hour combinations, variable spatial resolution, the ability to include neighboring streets as potential sources, and flexible emission factors — guided the model design and construction. The detailed model description, underlying assumptions, and rationale for model component choices are continued in the following section.

MODEL DESCRIPTION

The ASM is a computational package for simulating hourly average concentrations of traffic-derived aerosols and gases at receptor locations in areas where traffic influences on concentrations are substantial. The model structure is capable of including other emissions types, such as area and point sources, but has currently only been tested for traffic sources. The information flow of the ASM is shown in Figure 1.

For the study of UFP exposures and health effects, particle number and volume or mass size distribution are key parameters. The number size distribution quantifies the counts of particles at various sizes. Similarly, the volume or mass distribution quantifies the amount of particulate volume or mass as a function of particle diameter (Baron and Willeke 2001). In considering UFP exposures, often the distribution functions are integrated to report quantities in specific

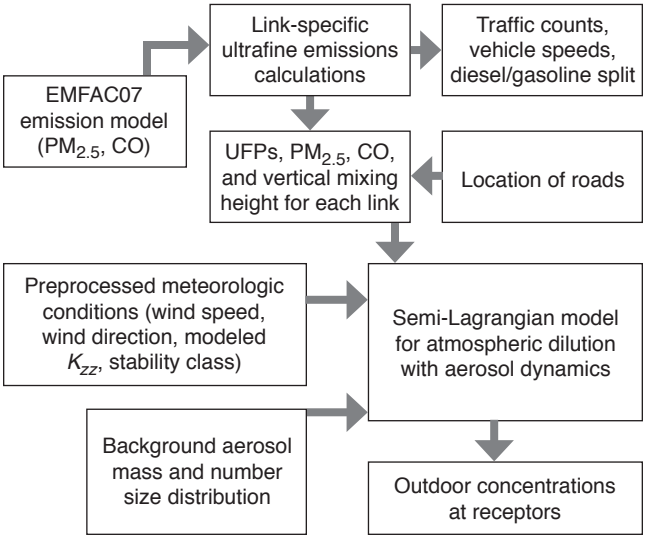

Figure 1. Information flow chart for the ASM.

size ranges, such as the aerosol number, mass, or volume in the size range of 10 to 100 nm. Because aerosol's microphysical properties of coagulation, evaporation, and condensation depend on absolute aerosol concentrations (and in some cases absolute gas-phase concentrations), additive techniques in which the impact of each source on each receptor is calculated individually and then summed are not suitable. To overcome this, we used a group of parcels in the simulation. The group of parcels moves with the wind and has a slab or wall configuration, as shown in Figure 2. The entire group of parcels moves in a uniform downwind direction (Lagrangian movement), and vertical and crosswind gradients are calculated by allowing diffusion between the parcels in the two latter directions. The overall height of the stack of parcels was set at 300 m. For most simulations, an 11-layer vertical configuration was used,

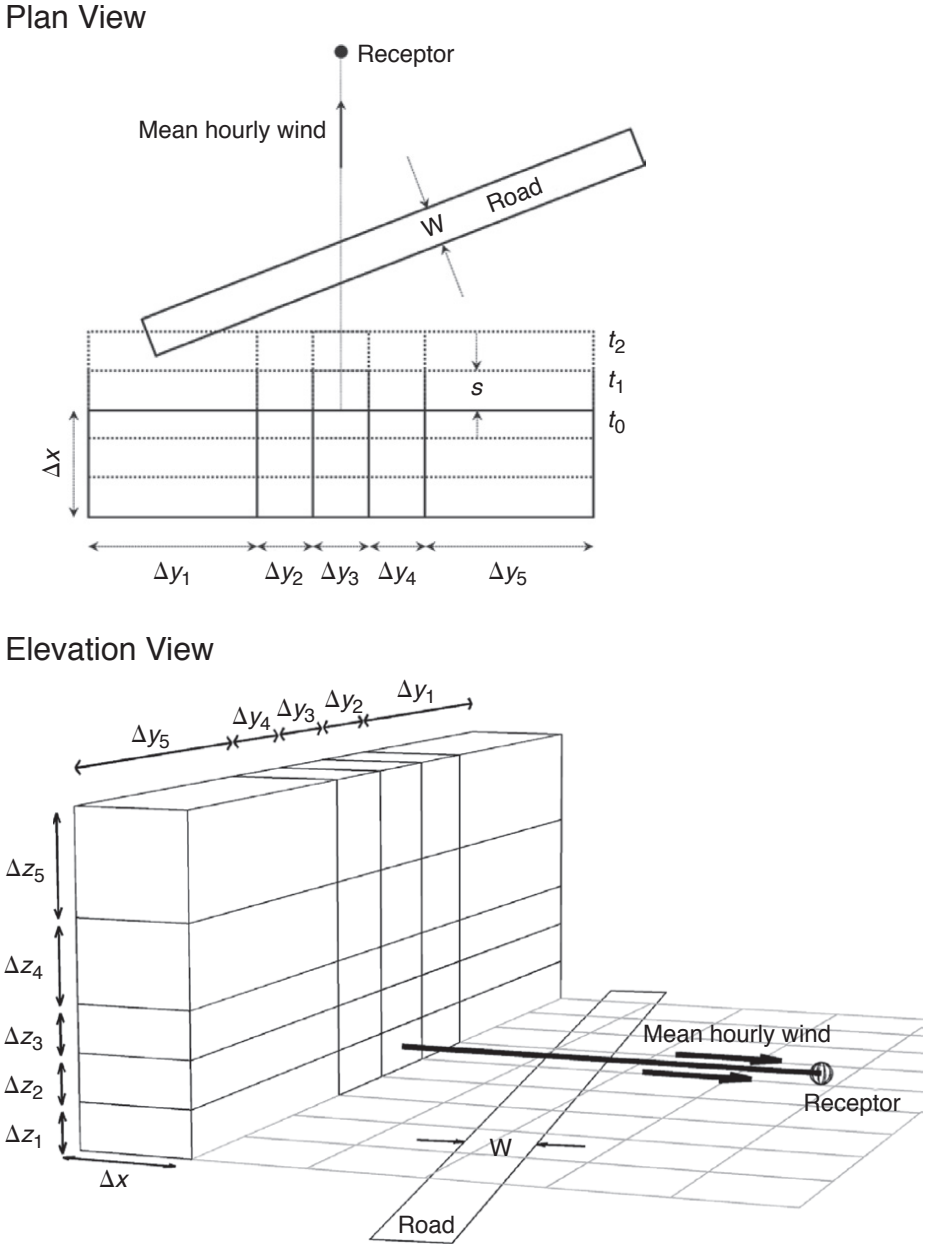

Figure 2. Two views of the geometry of air parcels as represented in the ASM. (Top) Detailed plan view shows a slab of parcels advancing distance *s* toward a receptor in time *t* and begins to overlap with a road, thus receiving emissions into the leftmost cell. (Bottom) Simplified 3D view showing air parcels advecting toward a road of width W and a receptor located 2 m above the surface. The first layer (Δz_1) of the air parcel is 4 m thick.

with the height at the top of each of the layers set at 4, 8, 12, 20, 28, 40, 70, 90, 120, 200, and 300 m, respectively. The ASM uses a fixed sectional representation for aerosols. The model simulations use 50 size bins lognormally spaced from 1 nm to 10 μm. All parcels are assumed to move in the direction and speed of the mean hourly wind (from WRF at 10 m elevation above the surface). According to gradient-transfer theory (K-theory), particles exchange horizontally and vertically between parcels. The governing equations of the ASM are listed below. The model is adapted from an earlier model with a vertical stack of parcels (Capaldo et al. 1999; Capaldo and Pandis 2001). Each parcel's governing equation is

$$\frac{\partial n_i(v,\, y, z, t)}{\partial t} =$$
$$\frac{\partial}{\partial z}\left(K_{zz}(z)\frac{\partial n(v, y, z, t)}{\partial z}\right) + \frac{\partial}{\partial y}\left(K_{yy}\frac{\partial n(v, y, z, t)}{\partial y}\right) - R(v,t)$$
$$+ \frac{1}{2}\int_0^v K(v-q,\, q)n(v-q, z, t)n(q, z, t)dq$$
$$- n(v,\, z,\, t)\int_0^\infty K(q, v)n(q, z, t)dq + E_i(v, z, t), \qquad (1)$$

where n is the number concentration distribution in parcel i, t is time, v is particle size, and y and z represent the crosswind and elevations positions. The first and second terms on the right-hand side of the equation represent vertical and horizontal turbulent dispersion to adjacent parcels. For the parcels at the lateral and top boundary of the slab of parcels, a zero-flux boundary condition is assumed, meaning there is no dispersion to the outside of the slab of parcels. The third term — $R(v,t)$ — is removal via deposition, which is only active in the lowest (surface-contacting) set of parcels. The fourth and fifth terms on the right-hand side represent coagulation, and the final term represents emission into a parcel. $K_{zz}(z)$ and K_{yy} are the vertical and horizontal (crosswind) eddy-diffusion coefficients, respectively. Dispersion in the downwind direction (the x direction) is assumed to be negligible. $K(q,v)$ is the coagulation-rate constant for particles of volumes q and v. $E_i(v,z,t)$ is the emission rate into parcel i.

Lagrangian models have important limitations. As implemented in this work, these limitations include the neglect of wind shear, the neglect of vertical advection, the neglect of horizontal transport in the crosswind direction at lateral boundaries, sensitivity to initial conditions, and the neglect of dispersion in the downwind direction (Liu and Seinfeld 1975; Russell and Dennis 2000). Although the errors associated with many of these limitations were minimized in this study by the short travel times (1 hour) of the parcels, they can still be significant. Furthermore, the size and direction of the errors can be variable and difficult to quantify.

Meteorologic Data Inputs

The WRF model is a community-based mesoscale numerical weather-prediction system designed for both operational forecasting and atmospheric research. The National Center for Atmospheric Research develops and distributes the WRF model. In the current study, version 3.1 of the model (Advanced Research WRF version 3.1, *www.mmm.ucar.edu/wrf/users/wrfv3.1/wrf_model.html*) was used to simulate the meteorologic variables needed for pollutant dispersion. This version of the WRF model supports fully compressible nonhydrostatic equations with a hydrostatic option, contains complete Coriolis and curvature terms, and supports two-way nesting with multiple nests and nest levels.

Two one-way nested subgrids were used for the meteorologic simulations. The larger domain encompassed all of California at 12-km resolution with 61 east–west grid cells (732 km) and 49 north–south grid cells (588 km). The smaller domain encompassed the South Coast Air Basin at 4-km resolution with 85 east–west grid cells (340 km) and 88 north–south grid cells (352 km). North America Regional Reanalysis 3-hour data were used for the WRF preprocessing system to generate boundary and initial conditions. Observational nudging was used to increase agreement between the WRF model and measured wind speed and direction (*www.mmm.ucar.edu/wrf/users/wrfv2/How_to_run_obs_fdda.html*). Measured hourly wind speed, wind direction, temperature, and pressure were retrieved from 11 National Weather Service (NWS) sites (*www.ncdc.noaa.gov/oa/climate/stationlocator.html*) in the study area and converted to a format suitable for observational-nudging input. Wind direction, wind speed, and temperature in the surface layer were nudged. Lambert conformal coordinates were used. Key WRF model settings for this study were the Monin–Obukhov surface layer scheme, the unified Noah land-surface model, and Mellor–Yamada–Janjic (Eta model) turbulent kinetic energy (TKE) boundary-layer physics. The WRF model's namelist used in the study is shown in Appendix C (available on the Web at *www.healtheffects.org*). EPA recommendations were followed for running the WRF model with one spin-up day and five model-simulation days. For vertical layering, a 29-level terrain-following hydrostatic Eta vertical grid was used, as recommended in the report of the Ozone Transport modeling committee (Baker et al. 2010), with a model top at 50 hectopascal and increased resolution in the planetary boundary layer and near the tropopause. The top of the first model layer was at ~20 m above the surface (with the exact

height depending on atmospheric pressure), with the result that the midpoint of the layer was at 10 m above ground level and corresponded to standard anemometer height.

Key inputs for the ASM were extracted from the WRF model. These included the 3D fields (position and time but not elevation) of Monin–Obukhov length, friction velocity, wind speed, and wind direction at 10 m — U10(x,y,t) and V10(x,y,t). They also included the four-dimensional field (position, elevation, and time) of K_{zz}, the vertical eddy diffusivity. K_{zz} values were taken from the EXCH_H variable of the WRF model and linearly interpolated to the vertical layers of the ASM model. K_{zz} parameterizes how quickly concentration gradients in the vertical dimension relax; it is found in equation 1.

The particle monitoring sites used in the HCMS were instrumented with weather stations. Davis 181 Vantage Pro2 or Pro2 Plus weather stations (Davis Instruments, Hayward, CA) were installed at each site, except LA1, where data were collected by an existing weather station. Weather data included wind speed, wind direction, wind gust, temperature, relative humidity, and precipitation (Moore et al. 2009).

Although stability classifications were not used in the final ASM (except in the calculation of K_{yy}; see below), they were used for grouping periods for subsequent data analysis. The WRF Monin–Obhukov length (RMOL in the WRF model) was used according to the classification scheme found in Table 1 (Seinfeld and Pandis 2006).

Table 1. Determination of Stability Class from Monin–Obukhov Length (L)

Monin–Obukhov Length (m)	Stability Class
$-100 < L < 0$	Very unstable
$-10^5 \le L \le -100$	Unstable
$\|L\| > 10^5$	Neutral
$10 \le L \le 10^5$	Stable
$0 < L < 10$	Very stable

Parameterized Size-Resolved Dry Deposition

The ASM incorporated a size-resolved dry deposition parameterization from Feng (2008). The particle deposition velocity is calculated as a function of the Schmidt number and roughness Reynolds number:

$$V_d = u_* \left\{ Sc^{-0.6} + c_1 e^{-0.5[(\mathrm{Re}^* - c_2)/c_3]^2} + c_4 e^{-0.5[(\ln\tau^+ - \ln c_5)/c_6]^2} \right\}, \quad (2)$$

where c_1 = 0.0226, c_2 = 40,300, c_3 = 15,330, c_4 = 0.8947, c_5 = 18, c_6 = 1.7. Friction velocity is denoted by u_*, and Sc is the Schmidt number (υ/D), where υ is kinematic viscosity and D is a particle diffusion coefficient (defined in the section on coagulation, below). Re* is the roughness Reynolds number ($u_* z_o/\upsilon$), where z_o is the surface roughness length. τ^+ is given by ($\tau u_*^2/\upsilon$), where τ is the particle relaxation time. Re* is set to c_2 when it exceeds c_2 initially. Particle relaxation time is calculated from $\tau = \rho_p d_p^3 C_c/(18\mu)$, where ρ_p is the density of a particle with diameter d_p, C_c is the Cunningham slip correction factor, and μ is air viscosity. Hinds (1999) was used for the Cunningham slip correction factor,

$$C_c = 1 + \frac{2.52\lambda}{d_p} \quad (d_p > 0.1\ \mu\mathrm{m}) = 1 + \frac{\lambda}{d_p}\left[2.34 + 1.05\exp\left(-0.39\frac{d_p}{\lambda}\right)\right], \quad (3)$$

where λ is the mean free path of air. Because the ASM was applied for urban conditions, a surface roughness of 2 m was used (McRae et al. 1982).

Coagulation

Brownian coagulation can be an important factor in transforming atmospheric size distributions (Pohjola et al. 2003; Jacobson and Seinfeld 2004). The current study used Brownian coagulation of spherical particles, although fractal agglomerates have been shown to have enhanced coagulation (Rogak and Flagan 1992). Enhanced coagulation caused by van der Waals forces (Jacobson and Seinfeld 2004) was not considered in the current study. Kinematic coagulation (i.e., other than Brownian coagulation) is not important in the ultrafine aerosol range that was the focus for model evaluation in the current study. In the governing equation of the ASM (equation 1), the fourth and fifth terms are coagulation. The Fuchs form of the Brownian coagulation coefficient was used for the ASM with coagulation-rate and mass-conserving corrections (Fuchs 1964; Gaydos et al. 2005; Seinfeld and Pandis 2006).

Vertical and Horizontal Dispersion

Vertical and horizontal dispersion (the first and second terms of equation 1) were solved using K_{zz} values extracted hourly from the WRF meteorologic model used for the project. Both vertical and horizontal rates of exchange between

parcels were computed using a second-order central finite difference approximation. K_{yy} eddy diffusivities for unstable conditions were calculated from a semi-empirical expression (Seinfeld and Pandis 2006):

$$K_{yy} = 0.1Z^{4/3}(-\kappa L)^{-1/3}u_*, \quad (4)$$

where Z is the mixed-layer height (the field PBLH from the WRF model was used), κ is the von Karman constant (0.4), L is the Monin–Obhukov length (the field RMOL from the WRF model was used), and u_* is the friction velocity (the field UST from the WRF model was used). Any K_{yy} values in excess of 500 m^2/sec were coerced to 500 m^2/sec. The coercion of high values of K_{yy} was needed, as very large values of K_{yy} lead to very small solver time steps for diffusion. The value of the coerced limit (500 m^2/sec) was found in a number of dispersion modeling textbooks and papers, such as Liu and Seinfeld (1975), which give 500 m^2/sec as the upper limit on urban horizontal diffusivities. The value of the limit is also well above the typical unstable horizontal diffusivities (50–100 m^2/sec) cited by Seinfeld and Pandis (2006), and it is well above the mean of the very unstable hours in the modeled meteorologic data (155 m^2/sec) (Appendix D, Table D.1, available on the Web at *www.healtheffects.org*). The upper limit was only invoked in 367 out of 17,717 values, or 2.1%.

A minimum value of K_{yy} was calculated for all stability conditions as $K_{yy,\min} = (13.7\text{ m})u$, where u is the surface wind speed. This was determined as the value of $K_{yy,\min}$ to spread 10% of the mass of the diffusing plume to beyond 15° of the centerline (262 m away from centerline) after 1 km of downwind travel. This minimum was necessary because subhourly changes in wind direction were not otherwise accounted for. During neutral and stable conditions, $K_{yy,\min}$ was used for K_{yy}. Modeled wind speeds less than 0.1 m/sec were coerced to 0.1 m/sec. The exact specification of K_{yy} and its variation with meteorologic conditions (and height) are areas needing further refinement in the ASM and similar models.

Modeling Domains

Five modeling domains were used, all in the Los Angeles area. Figure 3 gives an overview of the areas. Within each domain, simulations can be used to determine concentrations at any receptor location in the domain and at any date and hour. Simulations were limited to locations and times when evaluation data were available. The Long Beach

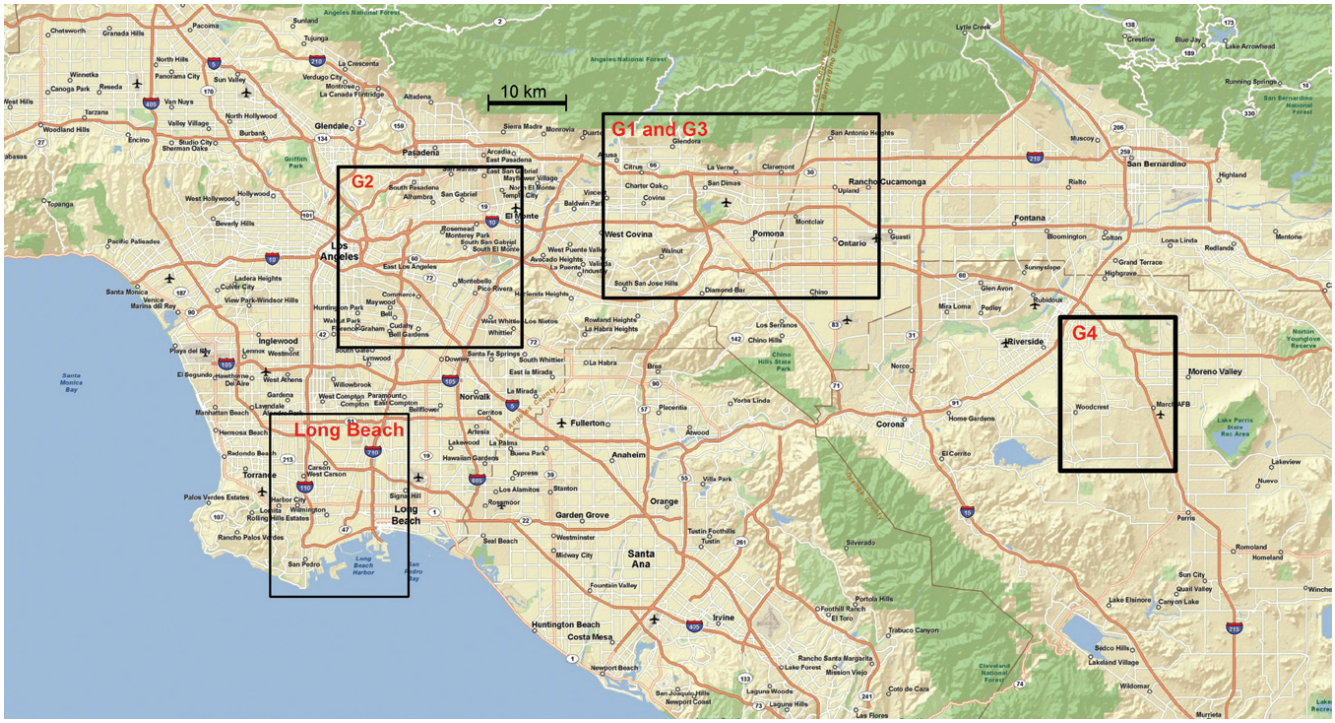

Figure 3. Map of the Los Angeles Basin, in California, showing the general locations of the HCMS (Long Beach) and CHAPS (G1 through G4) modeling domains used in the study. (Used by permission. Copyright © Esri, Tele Atlas.)

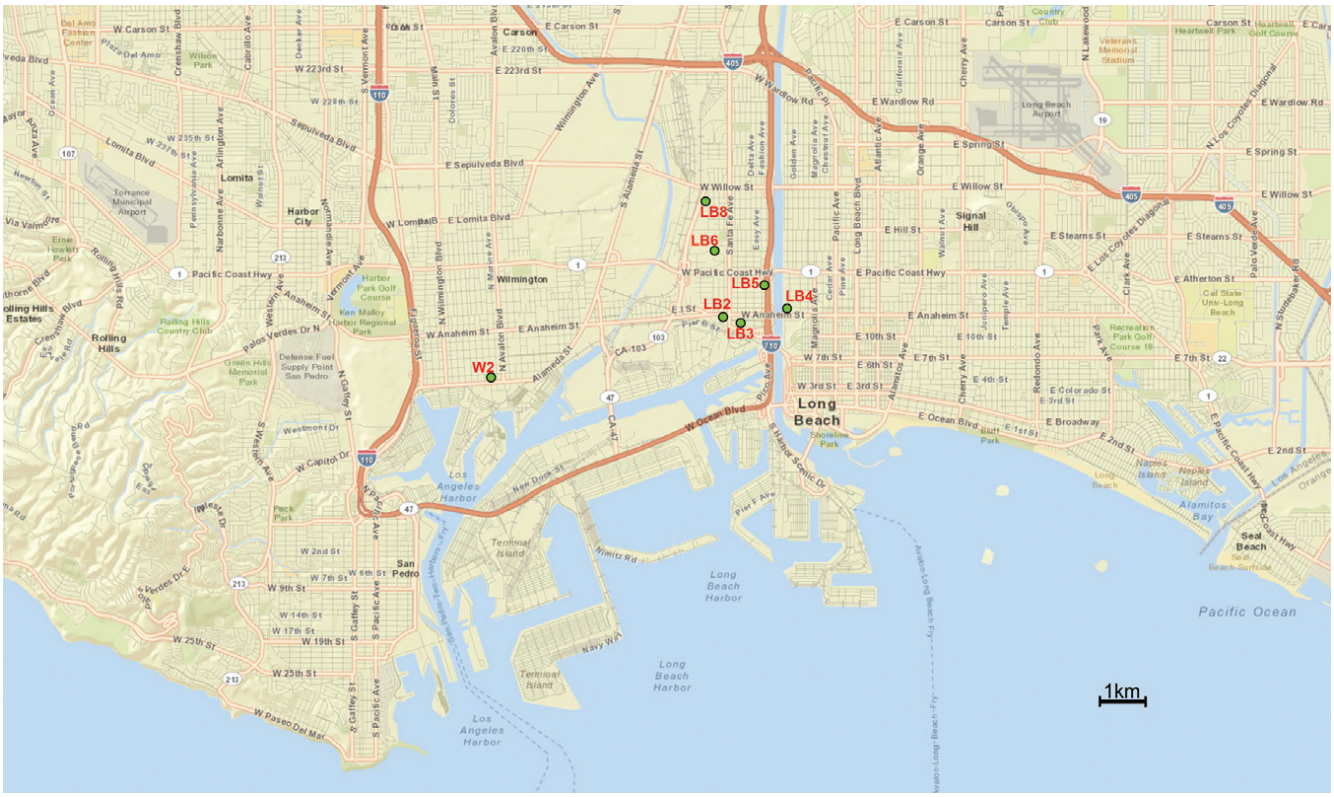

Figure 4. Map of the Long Beach area, in California, showing seven of the HCMS sampling sites (LB2 through LB8 and W2). (Used by permission. Copyright © Esri, Tele Atlas.)

domain was used for simulations to compare with measured data from the HCMS sampling sites. A map of the Long Beach domain is shown in Figure 4. Seven of the 14 HCMS sampling sites were used for evaluation, and the seven sites used are indicated in Figure 4. Each CHAPS (Delfino et al. 2008; Delfino et al. 2009) domain (G1 through G4) included one monitoring location that was used as the ASM receptor. Both the domains (where the road networks and emissions were considered) and the receptors are referred to as G1, G2, G3, and G4, respectively. Precise locations of the CHAPS sites are not given to maintain confidentiality, consistent with other CHAPS publications.

Road Network Data and Traffic Activity

Road location, width, and traffic volume are key inputs for the ASM. Our ultimate source of data on traffic activity was the Southern California Association of Governments (SCAG) travel-demand model. SCAG has two base travel-demand models (one for 2003 and one for 2008). SCAG reports annual average modeled traffic volumes (e.g., vehicles/hr on the modeled road links) for two types of vehicle classes (LDV and HDV) during four time periods: morning peak (6 to 9 AM), evening peak (3 to 7 PM), midday off-peak (9 AM to 3 PM), and midnight off-peak (7 PM to 6 AM). Traffic volumes in the SCAG database are not differentiated by either the day of the week or weekends versus weekdays. The SCAG database includes eight classes of road links (classes 1–8 in Table 2).

Geometric Processing of Road Link Database SCAG provided modeled traffic volume to our team in GIS format, and road coordinates were converted to Universal Transverse Mercator (UTM) coordinates using ArcGIS (ESRI, Redlands, CA). GeoWizard (ET Spatial Techniques, *www.ian-ko.com*) was used to process road coordinates into points with GIS information. A MATLAB script written at the University of Iowa (Roaduploader) served as the road preprocessor for the ASM; it aggregated the points into a road network (i.e., a list of road links with link-specific coordinates, dimensions, and traffic volume) in the areas of interest.

The Roaduploader script included the capability of adding the coordinates of class 9 roads using coordinates from StreetMap (ArcGIS, ESRI). Class 9 road traffic activity was

Table 2. Road Classes and Acceleration Fractions Used in the Current Study

SCAG/ Street-Map USA Road Class	ASM Road Class	Description[a]	Acceleration Fraction		Assumed Width (m)	Diurnal Profile	
			LDV	HDV		LDV	HDV
1	1	Freeway	0.06[b]	0.20[b]	12	c	d
2	2	High-occupancy-vehicle road	0.06[b]	0.20[b]	12	c	d
3	3	Expressway	0.06[b]	0.20[b]	12	c	d
4	4	Principal arterial	0.07	0.30	10	e	d
5	5	Minor arterial	0.07	0.30	6	e	d
6	6	Major collector	0.07	0.30	6	e	d
7	7	Minor collector	0.07	0.30	3	e	d
8	8	Ramp	0.24[f]	0.65[f]	3	c	d
9	9	Local, neighbor, rural	0.075	0.30	3	e	d
10	9	Cul-de-sac, traffic circle	0.075	0.30	3	e	d
11	9	Other minor access roads	0.075	0.30	3	e	d

[a] For more detailed definitions see *web.scag.ca.gov/modeling/pdf/MVS03/MVS03_Chap04.pdf.*

[b] If the speed on the road link was less than 48 mph, the highway was assumed to be experiencing some congestion and alternate acceleration fractions of 0.075 and 0.30 were used to reflect a higher probability of speed variation.

[c] Separate profiles for Monday–Thursday, Friday, Saturday, and Sunday (Funk et al. 2001).

[d] Separate profiles for Monday–Friday, Saturday, and Sunday (Funk et al. 2001).

[e] Separate profiles for weekday and weekend (Funk et al. 2001).

[f] If the speed on the road link was less than 30 mph, the arterial-collector acceleration fractions were used.

not available from any of the sources; an assumed traffic volume for these roads was set at 50% of the average for class 7 (minor collector) roads.

Additional Data Sources for Traffic Activity Diurnal patterns based on analysis of weight-in-motion road sensor data were used to enhance diurnal traffic profiles (Funk et al. 2001). Table 2 includes a column indicating which diurnal pattern was used for which road class, vehicle type, and day of the week.

Emissions

Gaseous Pollutants CO emission rates were calculated for use in the ASM. The emission rates of mobile sources were determined using factors such as vehicle engine type, age, velocity, acceleration, and fuel specifications. Three regulatory emission factor models are in extensive use: EMFAC, from the California Air Resources Board (*www.arb.ca.gov/msei/modeling.htm*); MOBILE6.2, from the EPA (*www.epa.gov/otaq/m6.htm*); and MOVES (*www.epa.gov/otaq/models/moves/index.htm*), another EPA model, released as a replacement for MOBILE6.2. EMFAC was specifically designed for California mobile source emissions and version 2007 was used in the current study. It produces mobile emissions summaries for various pollutants and technology classes in 69 geographic locations across the state. In this model, emission factors are a function of relative humidity, ambient temperature, and fleet mix. It includes geographically specific fleets for the years 1965 to 2020. Fleet-averaged 2007 emissions for CO for LDV in the South Coast Air Basin were calculated as a function of air temperature and speed and used in the ASM as a lookup table (see Appendix E, available on the Web at *www.healtheffects.org*).

Particle Emissions from Mobile Sources The ASM requires size-resolved particle emission factors to calculate the evolution of particle size distributions from sources to receptors. Although there have been many studies of size-resolved concentrations in urban, on-road, and near-road environments, fewer studies have reported size-resolved particle number emission factors (see 2011 review by Kumar and colleagues). Data from emissions studies using diluted engine exhaust are not appropriate for use in number-based UFP studies (but are more suitable for use in mass-based emissions studies), because (1) it is difficult to match tailpipe

emissions to roadway dilution processes experimentally and (2) these studies only capture emissions from a small number of engines. Accordingly, tunnel and chase studies with calculations of an emission factor were the preferred data sources for the ASM. Other types of emission factor measurements have been extensively reviewed (HEI Panel on the Health Effects of Traffic-Related Air Pollution 2010).

Kittelson and colleagues (2006a,b) reported size-resolved emission factors for diesel and spark-ignition vehicles based on on-road chase experiments using CPCs (3-nm size limit) and SMPS's (9-nm size limit). The chase experiments were performed in June and July 2002 on highways in Minneapolis, Minnesota. Size-resolved emissions for both cruising and acceleration on the highways were reported, as well as (via the chase experiments) the size distribution averaged over multiple vehicles (Johnson et al. 2005). The challenges of using the Minnesota emission factors were (1) the question of how applicable emission measurements made in summertime Minnesota in 2002 were to those made in Los Angeles in 2007, (2) the fairly substantial losses of particles less than 20 nm in size, (3) the large and variable differences in emission factors derived from CPC compared with SMPS methods, and (4) a 261-nm upper limit, which was well short of the 2.5- or 10-μm upper limit felt to be desirable in the ASM simulations.

The drawback of there being insufficient emissions data in the accumulation and coarse size ranges was dealt with by incorporating measurements from Geller and colleagues (2005) and Robert and colleagues (2007a,b). Geller and colleagues (2005) reported size-resolved emission factors (in six size intervals), including quasi-ultrafine mass (< 180 nm), from a tunnel study in California. Robert and colleagues (2007a,b) measured size-resolved mass (and size-resolved aerosol chemical composition) from numerous light-duty gasoline and heavy-duty diesel engines using chassis dynamometer techniques.

An alternate approach to using emission factors reported in chase and tunnel studies is to treat emission factors as an adjustable parameter or set of parameters and fit for optimal agreement with ambient measurements. Although this approach can lead to superior results compared with the training data set, it raises complications of generalizability to other locations and time periods and the possibility for compensation of bias in modeled processes other than emissions through changes in emissions. Our final size-resolved emission factors were prepared from these three data sources in the following four steps:

1. Combination into a merged size distribution;
2. Correction for SMPS losses using size-resolved instrument sampling efficiencies;
3. Extension of the size distribution to 1 nm using estimates of particle losses in on-road studies and differences between emission factors with a 3–5 nm lower size cutoff (often using CPC-based techniques) and emission factors with a 9–15 nm lower size cutoff (often using SMPS techniques); and
4. Correction for particle coagulation and deposition in the roadway environment so that sampling of the modeled on-road particle population with instrumentation free of particle loss would yield the emission factor from step 3.

The results of this four-step process are discussed below, in the Results section. Only the input size distributions are shown here, in Figure 5.

In step 1, the height of the number size distribution was allowed to vary in a fitting program while an objective function was minimized. Qualitatively, the objective function represented a departure from the Minnesota size distributions (Johnson et al. 2005), the measured mass distribution of Geller and colleagues (2005), and the fractional mass distribution of Robert and colleagues (2007a,b). Quantitatively, the objective function was

$$w_1 \sum_{i=1\ldots n} \left[\frac{N_i - N_{i,obs}}{N_{\max,obs}}\right]^2 + w_2 \sum_{i=1\ldots n} \left[\frac{V_i - V_{i,obs}}{V_{\max,obs}}\right]^2 + w_3 \sum_{j=1\ldots p} \left[\frac{M_j - M_{j,obs}}{M_{\max,obs}}\right]^2 + w_4 \sum_{i=2\ldots n} [\log_{10} N_i - \log_{10} N_{i-1}]^2 + w_5 \sum_{i=2\ldots n} [\log_{10} V_i - \log_{10} V_{i-1}]^2, \quad (5)$$

where the w's are weights, N_i is the height of the number distribution function in bin i, $N_{i,obs}$ is the measured height of the number distribution function in bin i, and $N_{\max,obs}$ is the maximum value of the measured number distribution function (which serves to normalize the error). V_i is the height of the volume distribution function in bin i, $V_{i,obs}$ is the measured height of the volume distribution function in bin i, and $V_{\max,obs}$ is the maximum value of the measured number distribution function. Data from Johnson and colleagues (2005) were used for $N_{i,obs}$ and $V_{i,obs}$. M_j is the mass calculated from particle size and effective density in size interval j (calculated using effective density to convert between mobility and aerodynamic mass), $M_{j,obs}$ is the mass observed in bin j, and $M_{\max,obs}$ is the mass in the most heavily loaded bin. The total mass was taken from Geller and colleagues (2005) and distributed by size according to Robert and

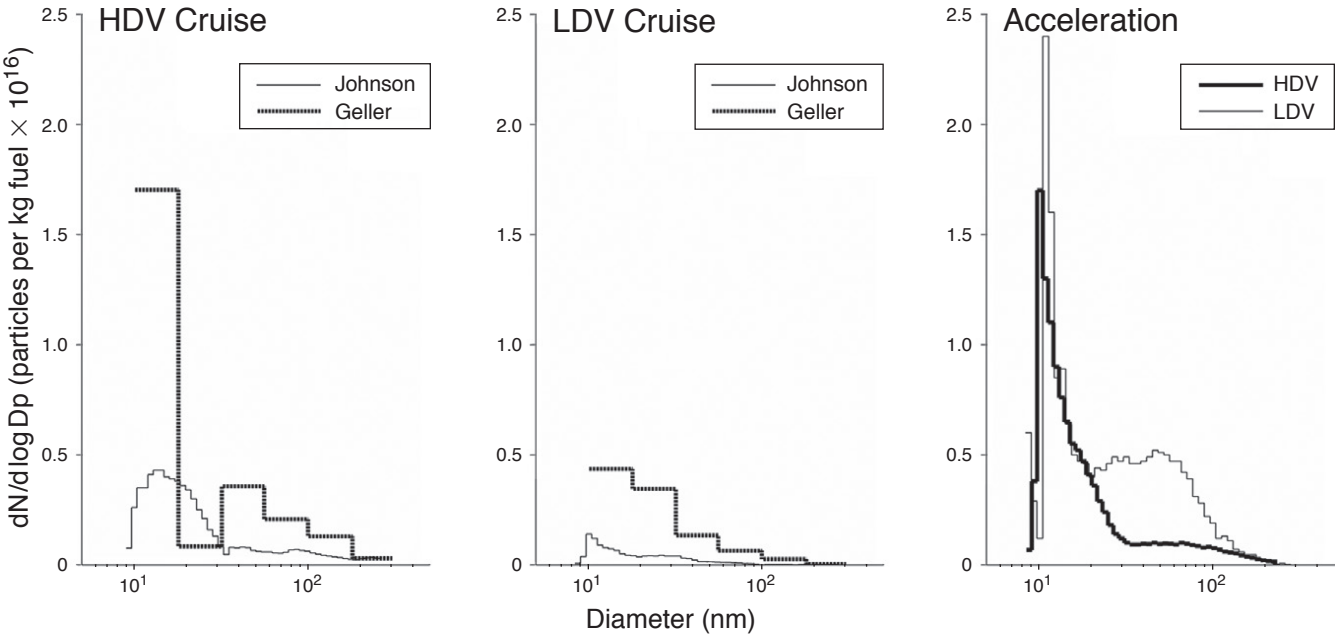

Figure 5. Size distributions used for the ASM's four input size distributions. (Left) HDV cruise size-resolved fuel-based emissions; (middle) LDV cruise size-resolved fuel-based emissions; and (right) both HDV and LDV on-road size-resolved fuel-based emissions from accelerating vehicles during a chase study (Johnson et al. 2005). Legend indicates source of data: Johnson et al. 2005 and Geller et al. 2005.

colleagues (2007a,b), together forming the $M_{j,obs}$ values. The fourth and fifth terms in the objective function are penalty functions for size distributions that change rapidly as a function of size. The values of the weights were $w_1 = 0.49$, $w_2 = 0.0025$, $w_3 = 0.0625$, and $w_4 = w_5 = 0.125$. Weights were chosen subjectively by trial and error based on visual inspection of the final number distribution, volume distribution, and sectional masses. Fitting was performed using the lsqnonlin function in MATLAB with nonnegativity constraints on the size distribution.

In step 2, the observed size distributions were divided by the size-dependent instrument sampling efficiencies to form loss-corrected size distributions. This was done because the size distributions used in step 1 were not corrected for SMPS and CPC sampling losses. The instrument sampling efficiency is the fraction of reported particles at a specific size divided by the atmospheric concentration at that size. Transmission efficiency through inlets and (mainly for SMPS instruments) diffusion losses in the instrument yield instrument sampling efficiencies of less than one. Values used in earlier work (Fissan et al. 1996; Ayala et al. 2003; Kittelson et al. 2006a) were applied to the distribution in step 2 (only at sizes greater than the lower instrument cutoff, which was 9 nm). The instrument sampling efficiencies used in this work are shown in Appendix A, and additional information about them can be found in the Evaluation Data section.

Step 3 in the development of model-ready emission factors was to account for the measurement of particles smaller than the lower size limit of the SMPS (9 nm) but measured in the on-road chase experiments by a 3-nm-limit CPC. A wide range of SMPS-to-CPC ratios can be found in Kittelson and colleagues (2006b). Such ratios are likely to be variable, depending on fleet, engine loads, fuel composition, emissions controls, and other factors. We used ratio values of 4, 3, 6, and 4 for LDV cruise, HDV cruise, LDV acceleration, and HDV acceleration, respectively. So the size-distribution function was increased in the size range of 1 to 10 nm by the amount necessary to achieve the assumed SMPS-to-CPC ratio, adjusting for losses in both instruments. The increase was uniform across all sizes, in recognition that the shape of the nuclei-mode size distribution is highly variable and (even on average) not known.

Step 4, the final adjustment to the input size distributions, accounted for losses caused by on-road deposition and coagulation. The basic principle is that if we sampled the on-road size distribution in the model and an emission factor is calculated using a conservative combustion tracer

influenced by dispersion but not by deposition, one should recover the CPC-to-SMPS ratio corrected size distributions (i.e., the emission factor after step 3). However, if the final adjustment for deposition and coagulation is omitted, the recovered size-resolved emission factors would be slightly different from those found after step 3 because of the deposition and coagulation that occur between the moment of emission and the moment of sampling. Even in an idealized environment, with a single 6-m-wide road and wind perpendicular to the road, emissions values from the upwind edge of the road are processed using Equation 1 for a few seconds before reaching the center of the road. The changes as a result of coagulation and deposition are likely to be small, but they are calculable in the modeling framework. To develop this adjustment, an idealized road with 10,000 vehicles per hour (assuming a 7% HDV fraction) was simulated under cruise and acceleration emissions conditions for four possible wind directions relative to the road (parallel, 45°, 90°, and 135°). For a given wind direction and traffic condition (e.g., cruise or acceleration), the known emitted size distribution (used in the model) was compared to the modeled size distribution at the inlet of on-road measurement equipment. Because of the short processing time between emission and sampling, the size distribution changes only slightly as a result of deposition and coagulation. A size-dependent correction factor can be developed from these simulations. We averaged the results from the four wind directions. This correction factor can be applied to the size distribution from step 3.

Acceleration Fraction As shown in Figure 5, the difference between the cruise and acceleration size-resolved input fractions is quite large. This difference is supported by numerous earlier observations (Maricq et al. 1999; Kittelson et al. 2004; Fruin et al. 2008) but is not well quantified. Furthermore, the definition of acceleration in an on-road experiment is difficult to apply to the highly aggregated traffic information used for the ASM (which includes average speed and road class but not variability in speed or information on stop lights, stop signs, or congestion). For the current study, acceleration fractions were chosen after preliminary sensitivity runs involving the CHAPS domains. For 48-hour simulations at the G1 site, concentrations were overpredicted on average and had excessive diurnal variation compared with measurements when an acceleration fraction of 0.5 was used, but number concentrations were similar to measured values when an acceleration fraction of 0.10 was used. The acceleration fractions for the lower-speed roads (classes 4–7 and 9) were therefore set to ~0.1. The HDV acceleration fractions were set higher than the LDV acceleration fractions because of a simple physical consideration: the power requirement to accelerate a vehicle is proportional to the rate of acceleration and the speed and mass of the vehicle. Because of this dependence on mass, for equal histories of velocity versus time, a heavier vehicle devotes a greater fraction of total energy to acceleration compared with other energy consumption modes (i.e., aerodynamic losses, drivetrain losses, tire friction, etc.). The ratio between heavy-duty and light-duty acceleration fractions and the ratio between the lower-speed roads (classes 4–7 and 9) and the highway and ramp road classes were established by a comparison of the energy required to overcome inertia as a function of link speed and vehicle weight. It should be stressed that the acceleration fractions were somewhat subjective and will require further constraint in the future.

Initial Mixing Assumptions

In a screening model such as the ASM, it is not feasible to simulate the tailpipe-to-roadway dilution process. Furthermore, on-road concentration estimates from a physics-based model such as the ASM can only be approximate without detailed consideration of the fluid dynamics of the roadway. However, because the roadway is the start of the dilution process, the ASM requires an assumed spatial distribution of the initial emissions at the roadway. The following assumptions were used in the ASM:

1. Tailpipe emissions are rapidly mixed in a predefined mixing zone.
2. Emissions are evenly mixed horizontally across the width of the road and are not mixed beyond the edge of the road (i.e., they must be carried beyond the edge of the road by horizontal diffusion, assuming the wind is not at a 90° angle to the road, and by advection with the wind).
3. Emissions are rapidly mixed into a predefined vertical distribution, meaning that a fraction of the emissions is mixed into each vertical layer.
4. Turbulence produced by vehicles can increase the height to which emissions are assumed to mix initially (see Assumption 3).

Assumption 3 is based on observations that roadway turbulence significantly mixes emissions. Baumer and colleagues (2005) found that motorway-induced turbulence reduced the concentrations of CO by 50% to 70%, NO by about 50%, and NO_2 by about 40%. Furthermore, Wang and Zhang (2009) found that this assumption improved results from a model based on areas near California freeways.

These four assumptions were built into the ASM using a vertical standard deviation $\sigma_{z,init}$, which is a parameter in an assumed initial vertical profile $C(z) = C(z = 0)\exp[-z^2/2(\sigma_{z,init})^2]$. $\sigma_{z,init}$ is calculated using a modified version of the initial mixing height assumed in the CALINE4 line dispersion model (Benson 1992). We used $\sigma_{z,init} = 1.5 + \mathrm{TR}/10[(E)_i/E_{\mathrm{CAL}}]^{0.25}$. Also used was H_{mix}, the height that contains 95% of the initial emissions, expressed as $1.96\sigma_{z,init}$. When emissions are distributed vertically, they are distributed up to the lowest layer that contains H_{mix}. This layer receives all particles that would go into higher layers according to the $C(z)$ function above. TR is the transit time of an air parcel across the line source, and 10 is an empirically determined factor based on field data from a near-road test (U.S. EPA 1976), which used a four-lane test road with a traffic volume of 1367 vehicles per hour per lane traveling at 50 mph. E_i is the turbulent roadway mixing energy from link i, and E_{CAL} is the turbulent roadway mixing energy from the GM/EPA experiment used for CALINE. This was still a crude treatment of a process that is very important for modeling on-road emissions, and further work is needed in this area, including greater use of the growing number of experimental studies of vertical distributions near roadways. The power 0.25 was based on calculations of the distance traveled by objects experiencing drag as a function of velocity squared. Increases in initial energy lead to changes in final position according to the 0.25 power of the initial kinetic energy. The travel time TR is given by $W/2/[u\sin(\phi)]$ when the wind angle ϕ is more than 45° relative to the roadway and $W/2[u\sin(45°)]$ when the wind angle is less than 45° relative to the roadway. Wind perpendicular to the roadway is ϕ of 90° and parallel to the roadway is 0°. Wind velocity is u. Di Sabatino and colleagues (2003) proposed that traffic-produced turbulence be parameterized by

$$\sigma^2 = \frac{(nC_d)^{2/3}V^2h^2}{(SA)^{2/3}}, \tag{6}$$

where σ is the magnitude of the turbulent velocity fluctuations, n is the vehicle density (i.e., vehicles per length of roadway), C_d is the drag coefficient, V is the vehicle velocity, h is the vehicle height, and SA is the vehicle surface area. For a mix of vehicles, the variables C_d, V, h, and SA are weighted averages of larger HDVs and of smaller LDVs [e.g., $V = V_{hd}f_{hd} + V_{ld}(1 - f_{hd})$, where f_{hd} is the fraction of HDVs]. n is not the weighted average of vehicle densities but rather the sum of the LDV and HDV densities. Based on Baumer and colleagues (2005), we used E_i as the motorway turbulent kinetic energy, expressed as $0.5\sigma^2$. Values of C_d and h were taken from Baumer and colleagues (2005) and were 0.9 and 3.5 m for HDVs, respectively, and 0.3 and 2.4 m for LDVs, respectively.

Parcel Dimensions, Step Sizes, and Variable-Width Parcels

The starting location of the slab of parcels is set to be 4000 m upwind from the receptor or, during low-wind-speed hours (less than 1.11 m/sec), an upwind distance equal to the wind-travel distance over a 1-hour period. The step size of the slab of parcels is initially large and is gradually decreased to a user-specified value of R_{min}, the minimum desired resolution of the simulation. The final 10 steps of the simulation are taken with step sizes of R_{min}. Step sizes ΔL decreased according to the formula

$$\Delta L = R_{\mathrm{min}} + \left(\frac{x - \Delta L}{x_{\mathrm{max}} - 10R_{\mathrm{min}}}\right)^{2/3}\left(\frac{Y}{3} - R_{\mathrm{min}}\right) \tag{7}$$

where x is the current distance to the receptor, x_{max} is the maximum distance to the receptor, and Y is the crosswind length of the slab of parcels. Initial step sizes are $Y/3$.

Initially, the slab of parcels is set to three parcels in the crosswind direction (Figure 2 shows an example with five parcels in the crosswind direction). In between any integration time steps, any vertical column of parcels can be subdivided into three equal-width parcels. This is done when additional resolution is needed in the crosswind direction, that is, when the mixing of sources at different distances from the plume centerline would lead to incorrect concentrations at the receptor. Both the large initial step sizes of Equation 7 and the subdivision of grid cells are ways to minimize the computational burden of the ASM calculation while simulating at high spatial resolution for sources close to the receptor. The maximum allowable parcel size in the crosswind dimension (Δy_{max}) is calculated as a function of distance from the plume centerline (y) and distance from the receptor (x) using a Gaussian plume equation. Δy_{max} is solved using Equation 8 as the size of parcel that, upon division into three parcels, would give a different mean concentration based on a point source on the plume centerline at distance x from the receptor:

$$\mathrm{TOL} = \frac{2}{3}\exp\left(-\frac{y^2}{2\sigma_y^2}\right) - \frac{1}{3}\exp\left(-\frac{(y + \Delta y_{\mathrm{max}})^2}{2\sigma_y^2}\right) - \frac{1}{3}\exp\left(-\frac{(y - \Delta y_{\mathrm{max}})^2}{2\sigma_y^2}\right), \tag{8}$$

where TOL is a tolerance (0.02 was used in the final simulations) such that the subdivision of a parcel of crosswind

dimension $3\Delta y_{max}$ into three parcels (each of crosswind dimension Δy_{max}) gives a fractional change of 0.02 in the predicted concentration at the receptor. The value 0.02 was determined after tests with values of 0.1 and 0.05 showed that the concentrations were sensitive to the initial number of crosswind parcels (a sensitivity that should have been removed by the parcel subdivision step). In equation 9, the crosswind plume dispersion, σ_y, is calculated as a function of distance from the receptor (x), minimum resolution (R_{min}), wind speed (u), and crosswind eddy diffusivity (K_{yy}):

$$\sigma_y = \sqrt{2K_{yy}\max(x,R_{min})/u}. \quad (9)$$

Large parcels are allowed in two cases, when the Lagrangian parcel has a long travel time remaining before hitting the receptor (large x/u) and when the parcel is far away from the plume centerline (large y). Division of parcels progresses most prominently at the centerline. A typical value of Δy_{max} from equations 8 and 9 is (for TOL = 0.02) 114 m at a distance of 1 km from the receptor. Additional examples of progressive subdivision are shown in the Results section. Alternate approaches include considering actual emissions in the parcel and the crosswind distribution of emissions within the parcel. These would add complexity to the algorithm but further limit the number of subdivisions.

Computation of Emissions into a Parcel During a Time Step

During each step of the model calculation, the slab of parcels advances ΔL toward the receptor as the equation for concentrations in each parcel and size bin is solved (equation 1). The emission term for equation 1 is calculated based on an overlap of parcels and roadways. Specifically, the average rate of particle emission (expressed as particles per time step) into a grid cell is needed. Even if there were a long time step in which a parcel started the time step far away from a road, crossed the road during the time step, and finished the time step across the road, the average rate of particle emission during the time step would be used. The equation for the average rate of particle emission into a parcel is

$$E = (EF)(CF)A\frac{\Delta x}{W}\frac{T}{\Delta L}, \quad (10)$$

where EF is an emission factor, CF is a conversion factor, Δx is the downwind parcel dimension, W is the road width, T is the traffic volume, and ΔL is the step size. A is the area of overlap between two polygons, one the roadway and the other a polygon swept out over the course of the time step as the leading edge of the parcel moves forward. Equation 11 restates equation 10 using units for clarity:

$$\text{particles/sec} = \frac{\text{particles}}{\text{kg fuel}}\frac{\text{kg fuel}}{\text{m traveled per vehicle}}\ \text{m}^2 \times \frac{\text{m}}{\text{m}}\frac{\text{vehicles/sec}}{\text{m}}. \quad (11)$$

The formula for the conversion factor CF is

$$CF = 2.35 \times 10^{-3}\,\rho/mpg, \quad (12)$$

where ρ is the fuel density in kg/L, mpg is the average vehicle fuel economy in miles per gallon. CF is expressed as kg/m-vehicle.

Background $PM_{2.5}$ Mass Concentrations and Size Distributions

The ASM requires a background size distribution to initialize the simulation. Because coagulation with the background aerosol is an important loss mechanism for UFPs, realistic values for the background size distribution are important. Background size distributions were developed using a two-step procedure. First, the coordinates of the start of the parcel were determined as described above, and a $PM_{2.5}$ mass estimate was developed for that location using EPA and IMPROVE hourly and daily monitor values and kriging (Sousan 2012). An assumed size distribution was used based on the $PM_{2.5}$ mass estimate. Several values of the assumed background size distribution for both particle number and particle volume are shown in Figure 6.

The distributions shown in the figure were created in four steps, as follows:

1. Measured number-weighted size distributions at the LB4 site in the wind direction with the lowest $PM_{2.5}$ (135°–180°) were averaged;
2. This average was fitted to three lognormal modes with mode positions of 23 nm, 46 nm, and 164 nm for particle number, based on previous ambient sampling in Los Angeles (Kim et al. 2002). The counts of the lognormal modes were 1812, 4189, and 427 particles/cm^3, respectively, and the log sigma mode widths were 0.25, 0.288, and 0.201, respectively. The distribution had a mass integral (derived from the volume distribution and assuming spherical particles of density 1.4) of 5.6 $\mu g/m^3$ $PM_{2.5}$.
3. To obtain masses less than 5.6 $\mu g/m^3$, this base distribution was decreased while maintaining its shape.
4. To obtain initial masses greater than 5.6 $\mu g/m^3$, the distribution was aged (i.e., subjected to condensation and coagulation) while a continuous source of the smallest mode (the 23-nm mode) was added.

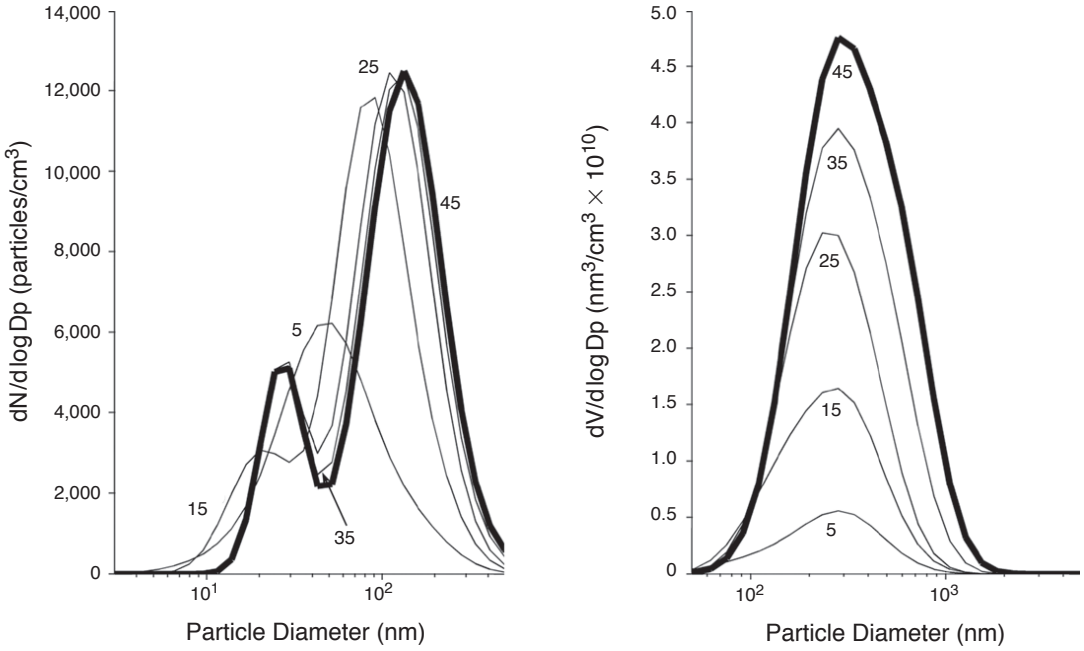

Figure 6. Assumed background size distributions for a range of $PM_{2.5}$ mass concentrations from 5 to 45 μg/m^3, shown (left) as particle counts and (right) as particle volumes.

EVALUATION DATA

Data Sources

To evaluate the performance of the ASM, HCMS data were used (Krudysz et al. 2009; Moore et al. 2009). In HCMS, particle number and particle size distribution were measured at 14 monitoring sites in Long Beach from mid-February to mid-December 2007 to investigate diurnal, seasonal, and spatial patterns of particle concentrations. Total number concentrations varied by a factor of up to 10 (from less than 10,000/cm^3 to 90,000/cm^3 for hourly averages calculated by month). Figure 4 shows the locations of HCMS sites used for evaluation. SMPS instruments were selectively deployed in three or four sites at a time for several weeks. CPC data from all sites were available for April, October, and September of 2007. The CPC instrument (model 3022A, TSI) used for HCMS had a manufacturer-reported 50% sampling cutoff at 7 nm. The SMPS data from HCMS is available to a minimum size of 14 nm. Receptor locations used in our modeling runs (most of which corresponded to the HCMS sampling locations in Long Beach) are listed in Table 3.

CPC measurements taken during CHAPS (Polidori et al. 2007; Delfino et al. 2008) were also used for model evaluation. The general locations of the CHAPS sites are shown in Figure 3. The modeling runs to be discussed in the Results section are listed in Table 4.

Particle-Loss Assumptions and Instrument Comparison

Particle-sampling losses in inlet tubing and inside instruments at particle sizes of less than 20 nm require consideration both in measurement studies and in comparison of simulations to observations. HCMS, for example, used two methods to measure particle number. One method used SMPS's, which combine a differential mobility analyzer with a CPC to measure the size distribution in size bins, usually with resolution of 64 channels per lognormal decade (i.e., 64 channels between 10 and 100 nm, 64 channels between 100 and 1000 nm, etc.). Total number concentration (in a wide size range) can be calculated from SMPS data by summing the concentrations in all size bins. HCMS's SMPS data were reported for a particle size range of 14.1 to 736.5 nm. The method to measure particle number used in HCMS was direct particle counts by means of CPC with a lower size limit of 7 nm and an upper size limit determined by inlet efficiency and other instrument parameters (usually about 2 μm). The number of particles above this upper size limit is usually negligible compared with the overall uncertainty in the instrument. Because of their wider size range, CPCs collocated with SMPS's tend to have higher

Table 3. Receptor Locations in the Modeling Runs of the Current Study[a]

Receptor[b]	Domain	Latitude	Longitude	UTM *x* (m)	UTM *y* (m)
W2	Long Beach	33.7711	−118.2644	382,915	3,737,496
LB2	Long Beach	33.7825	−118.2169	387,337	3,738,706
LB3	Long Beach	33.7817	−118.2136	387,636	3,738,610
LB4	Long Beach	33.7836	−118.2036	388,565	3,738,812
LB5	Long Beach	33.7878	−118.2081	388,159	3,739,281
LB6	Long Beach	33.7931	−118.2186	387,188	3,739,878
LB8	Long Beach	33.8025	−118.2200	387,072	3,740,927

[a] Locations given using Universal Transverse Mercator (UTM) coordinate system.
[b] Of the 11 sites used for model evaluation, the locations of 4 sites (G1, G2, G3, and G4) cannot be described because of confidentiality agreements.

Table 4. Periods for Long Beach and CHAPS Receptor Simulations

Simulation Case Code	Date	Receptor	Duration (hours)	Evaluation Data
Long Beach				
Sept	9/1–9/15/2007		355	Hourly SMPS measurements
Run01_LB4_Sept		LB4		
Run02_LB5_Sept		LB5		
Run03_W2_Sept		W2		
May	5/1–5/15/2007		336	Hourly SMPS measurements
Run04_LB2_May		LB2		
Run05_LB3_May		LB3		
Run06_W2_May		W2		
Oct	10/1–10/13/2007		305	1-min CPC measurements averaged to 1 hour
Run07_LB4_Oct		LB4		
Run08_LB5_Oct		LB5		
Run09_LB6_Oct		LB6		
Run10_LB8_Oct		LB8		
Run11_W2_Oct		W2		
CHAPS				Hourly CPC counts, OC, EC, and CO
Run01_G1	10/16–12/08/2005	G1	1098	
Run02_G2	8/20–10/13/2005	G2	1313	
Run03_G2	1/1–2/16/2006	G2	1121	
Run04_G3	7/2–8/17/2006	G3	1121	
Run05_G3	10/15–11/30/2006	G3	1121	
Run06_G4	8/20–10/13/2006	G4	1313	
Run07_G4	1/01–2/15/2007	G4	1097	

total particle counts than those of the SMPS's. Furthermore, losses of UFPs in SMPS's can be appreciable, and SMPS concentrations are more uncertain that those of CPCs because of the uncertain charging fractions and more complex flow systems of SMPS's.

As a result of this comparison of the two types of instruments, we assumed some diffusional particle losses based on the equations of Baron and Willeke (2001). For CPCs, we assumed a 2-m inlet tubing with a flow rate of 1.5 L/min and an inner tubing diameter of 6.4 mm. For SMPS's, we again assumed the diffusional particle-loss equations of Baron and Willeke (2001) and adjusted the residence time for agreement with reported losses (Kittelson et al. 2006a). Our assumed instrument sampling efficiencies can be found in Appendix A. In brief, CPC sampling efficiencies were assumed to be 62% at 5 nm, 82% at 10 nm, 92% at 20 nm, and 97% at 50 nm, and SMPS sampling efficiencies were assumed to be 15% at 10 nm, 54% at 20 nm, and 82% at 50 nm.

COMPUTATIONAL HARDWARE AND SOFTWARE

The ASM model was written in MATLAB and run on several Linux workstations. The two main workstations for the development and running of the ASM were an eight-core workstation with Intel Xeon 3.0 GHz processors and 16 GB RAM and a two-core workstation with 2.67 GHz Intel processors and 4 GB RAM. The WRF model was also run on these and similar Linux workstations. The operating system was openSUSE 11.3 (x86_64). The computationally demanding processes of calculating the overlap between two polygons and of calculating the derivatives of equation 1 were performed as C or Fortran subroutines. For geometric overlap and search algorithms (search algorithms were sometimes used in postprocessing and visualization), subroutines from the MATLAB central file exchange were used (i.e., Polygon Clipper [Holz 2006] and kdtree [Michael 2008]). The derivative function for equation 1 was written in Fortran and compiled using the g95 compiler (GCC v4.0.3 and g95 v0.92, June 24, 2009) and linked to MATLAB using the mex (MATLAB executable) command. MATLAB versions 7.12.0 (R2011a) and 7.8.0 (R2009a) are both compatible with the ASM and its pre- and postprocessing scripts.

STATISTICAL METHODS AND DATA ANALYSIS

The ASM was evaluated mainly by comparing pairs of model estimates and measured data. Both hourly and daily (24-hour average from midnight to midnight) values were used. Statistics used included the following (Emery et al. 2001):

Mean Bias (MB)

$$M_{MB} = \frac{1}{N}\sum_{i=1}^{N}(M_i - O_i) = \bar{M} - \bar{O} \tag{13}$$

Mean Error (ME)

$$M_{ME} = \frac{1}{N}\sum_{i=1}^{N}(|M_i - O_i|) \tag{14}$$

Mean Normalized Bias (NB)

$$M_{NB} = \frac{1}{N}\sum_{i=1}^{N}\frac{M_i - O_i}{O_i} \times 100\% \tag{15}$$

Mean Normalized Error (NE)

$$M_{NE} = \frac{1}{N}\sum_{i=1}^{N}\frac{|M_i - O_i|}{O_i} \times 100\% \tag{16}$$

Correlation Coefficient (r)

$$r = \frac{\sum_{i=1}^{N}(M_i - \bar{M})(O_i - \bar{O})}{\left[\sum_{i=1}^{N}(M_i - \bar{M})^2 \sum_{i=1}^{N}(O_i - \bar{O})^2\right]^{1/2}} \tag{17}$$

Root Mean Squared Error (RMSE)

$$\left[\frac{1}{N}\sum_{i=1}^{N}(M_i - O_i)^2\right]^{1/2} \tag{18}$$

Index of Agreement (IOA)

$$1 - \left[\frac{N \cdot RMSE^2}{\sum_{i=1}^{N}|M_i - \bar{O}| + |O_i - \bar{O}|}\right], \tag{19}$$

where N is the number of observation–model pairs, M_i and O_i are the ith pair of model and observation values, and the overbar symbol refers to the mean.

All statistical evaluations in this section are based on comparisons of paired hourly values. Additional evaluation was performed using conditional probability function plots (Kim and Hopke 2004).

Seven HCMS sites and all four CHAPS sites were used for our model evaluations. The evaluation periods ranged in duration from 77 to 1053 hours. The mean evaluation period was 448 hours (about 19 days). In general, for a complete model evaluation, sites are needed that vary in distance from roads and in other characteristics (e.g., surrounding land use, topography, and location within the Basin), and the evaluations should stretch across several months of a

given season. Our model evaluation was balanced across a variety of months representing both the Basin's cooler, wetter period (November through March) and its warmer, drier period (June through October). A weakness of the evaluation was that background sites were not evaluated. All of the sampled sites were affected to some degree by roadways. Additional sample data reflecting regional pollution but not local (e.g., within 4 km) port or roadway pollution would be a useful evaluation tool.

RESULTS

PREPROCESSING AND TRAFFIC ACTIVITY

Construction of Model-Ready Road Links

The process of converting the GIS-based road links into an array of rectangular road segments for the model resulted in large arrays. The Long Beach road array contained 18,334 road segments; the road arrays of the domains including the G1 through G4 sites contained between 63,577 and 88,850 segments; the increase in segments was caused by the inclusion of class 9 roads. Figure 7 shows a closer view of the Long Beach domain and the monitoring sites used for the evaluation of the ASM.

The Long Beach domain included only road classes 1 through 8 and therefore did not have streets smaller than the collector level. For the CHAPS simulations, class 9 roads were included, and the finer level of streets can be seen in Figure 8, which shows a central portion of the G2 domain.

Because the domains were large (400 km^2) compared with the areas swept out by the parcels during a time step (~1 km^2 or smaller), an efficient way of searching for road–parcel overlap was needed. For this purpose, a catalog of road segments was made using a 500-m overlay on top of the larger grid, and only the roads within 500 or 1000 m of the parcels were searched during any given time step.

As an example of the information available for the modeling and analysis process, descriptive statistics for roadways in the G1 domain can be found in Table 5. The majority of the links were associated with class 9 roadways. According to the SCAG traffic-demand model (and our assumption about the relative traffic volume on collector and local streets), the majority (67%) of vehicle travel was on roadway classes 1, 2, 3, or 8 (freeway, high-occupancy-vehicle road, expressway, and ramp road classes, respectively). The remainder of the traffic volume was on arterial (28%), collector (1%), and local (4%) streets. A more detailed set of descriptive statistics for the roads of the G1 domain can be found in Appendix F (available on the Web at *www.healtheffects.org*).

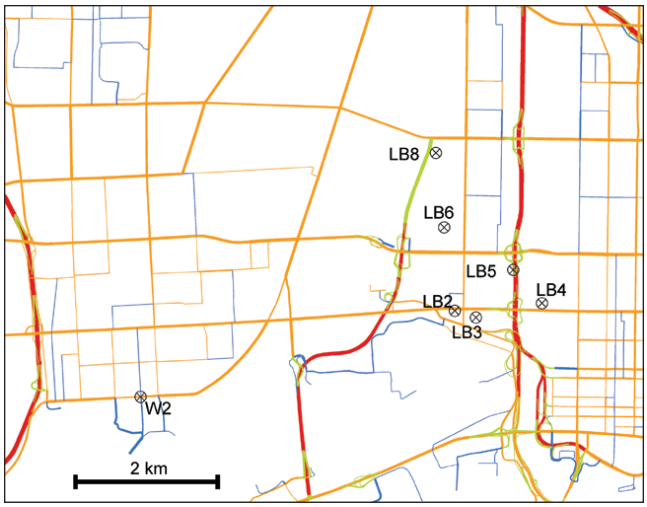

Figure 7. The ASM's representation of street segments as sources in the Long Beach domain, showing the seven sites used to evaluate the model. Segment color indicates road class. Highways (classes 1–3) are red; arterials (classes 4 and 5) are orange; collectors (classes 6 and 7) are blue; and ramps (class 8) are green. Segment widths indicate traffic volume for noon on a weekday: Wider segments have higher traffic volumes. Narrower segments have lower traffic volumes.

The accuracy of the road locations (taken from GIS databases and processed into straight segments by Roaduploader) was checked for the receptor closest to a roadway (LB5). Measuring from the coordinates of Moore and colleagues (2009) to the ramp edge using the Google Earth measurement tool gave a result of 21 m to the edge of the ramp and 28 m to the center of the southbound freeway. In the ASM representation of this area, the distances were 14 and 24 m, respectively. Road widths are associated with road class in the ASM, which might have contributed to these differences.

Application of Detailed Diurnal Profiles to the SCAG Traffic-Demand Model

The SCAG database of traffic volumes included eight diurnal traffic-activity levels for each road in classes 1 through 8 — that is, morning peak, midday, afternoon peak, and evening traffic during weekdays for LDV and HDV vehicles, respectively. Our preliminary modeling results showed a strong resemblance between predicted pollutant concentrations and the SCAG diurnal profile, although the sharp increase at 6 AM and sharp decrease at 7 PM were not typically reflected in the measured aerosol number concentrations. In addition, because the SCAG database did not include weekend traffic volumes, hourly diurnal profiles

Figure 8. The ASM's representation of street segments as sources in the CHAPS G2 domain. Segment color indicates road class. Highways (classes 1 to 3) are red; arterials (classes 4 and 5) are orange; collectors (classes 6 and 7) are blue; ramps (class 8) are green; local streets (class 9) are black. Segment widths indicate traffic volume for noon on a weekday: Wider segments have higher traffic volumes. Narrower segments have fewer than 50 vehicles per hour.

Table 5. Road-Level Descriptive Statistics for the G1 Domain

Road Class / Variable[a]	Number of Links	Distance (Summed over all links)	Total V-km/day (% of total)	Simple Average[b]	Vehicle-km Weighted Average[c]
1. Freeway	1,189	145	12,924,588 (56%)		
Speed (mph)				51.5	45.7
Traffic volume (vehicles/day)				93,100	95,469
HDV fraction (%)				13.5	12.0
2. High-occupancy-vehicle road	780	101	1,488,283 (6.5%)		
Speed (mph)				54.8	45.4
Traffic volume (vehicles/day)				14,546	16,854
HDV fraction (%)				0	0
3. Expressway	13	6	264,201 (1.1%)		
Speed (mph)				22.5	21.6
Traffic volume (vehicles/day)				44,620	43,542
HDV fraction (%)				11.3	10.0
4. Principal arterial	1,940	193	3,880,841 (17%)		
Speed (mph)				33.9	30.9
Traffic volume (vehicles/day)				19,170	25,475
HDV fraction (%)				3.1	3.0
5. Minor arterial	3,156	330	2,471,814 (11%)		
Speed (mph)				32.5	30.2
Traffic volume (vehicles/day)				9,350	12,160
HDV fraction (%)				2.6	2.7
6. Major collector	405	40	108,105 (0.5%)		
Speed (mph)				31.3	26.8
Traffic volume (vehicles/day)				2,738	6,791
HDV fraction (%)				2.5	2.1
7. Minor collector	45	3	1,862 (<0.1%)		
Speed (mph)				24.0	24.6
Traffic volume (vehicles/day)				840	788
HDV fraction (%)				1.9	1.9
8. Ramp	3,118	107	1,016,339 (4.4%)		
Speed (mph)				26.0	24.5
Traffic volume (vehicles/day)				7,611	18,295
HDV fraction (%)				5.6	7.6
9. Local, neighborhood, rural	51,174	2,210	837,777 (3.6%)		
Speed (mph)				17.0	17.0
Traffic volume (vehicles/day)				379	379
HDV fraction (%)				2.8	2.8
Total	61,820	3,135	22,993,809		

[a] Traffic volumes for classes 1–3 reflect only one direction of travel. Total volume on a freeway may be the sum of two directions of class 1 and two directions of class 2 links.

[b] Simulation average is $(1/N)\sum_{i=1}^{N} x_i$, where x expresses speed, traffic volume, or HDV fraction when we have a value for that property of each of N links ($i = 1 \ldots N$).

[c] Vehicle-km weighted average is $(1/\sum_{i=1}^{N} TV_i\, l_i)\sum_{i=1}^{N} x_i TV_i\, l_i$, where x expresses velocity (speed), traffic volume, or HDV fraction; TV_i is traffic volume on link i (vehicles/day); and l_i is the length of link i (km).

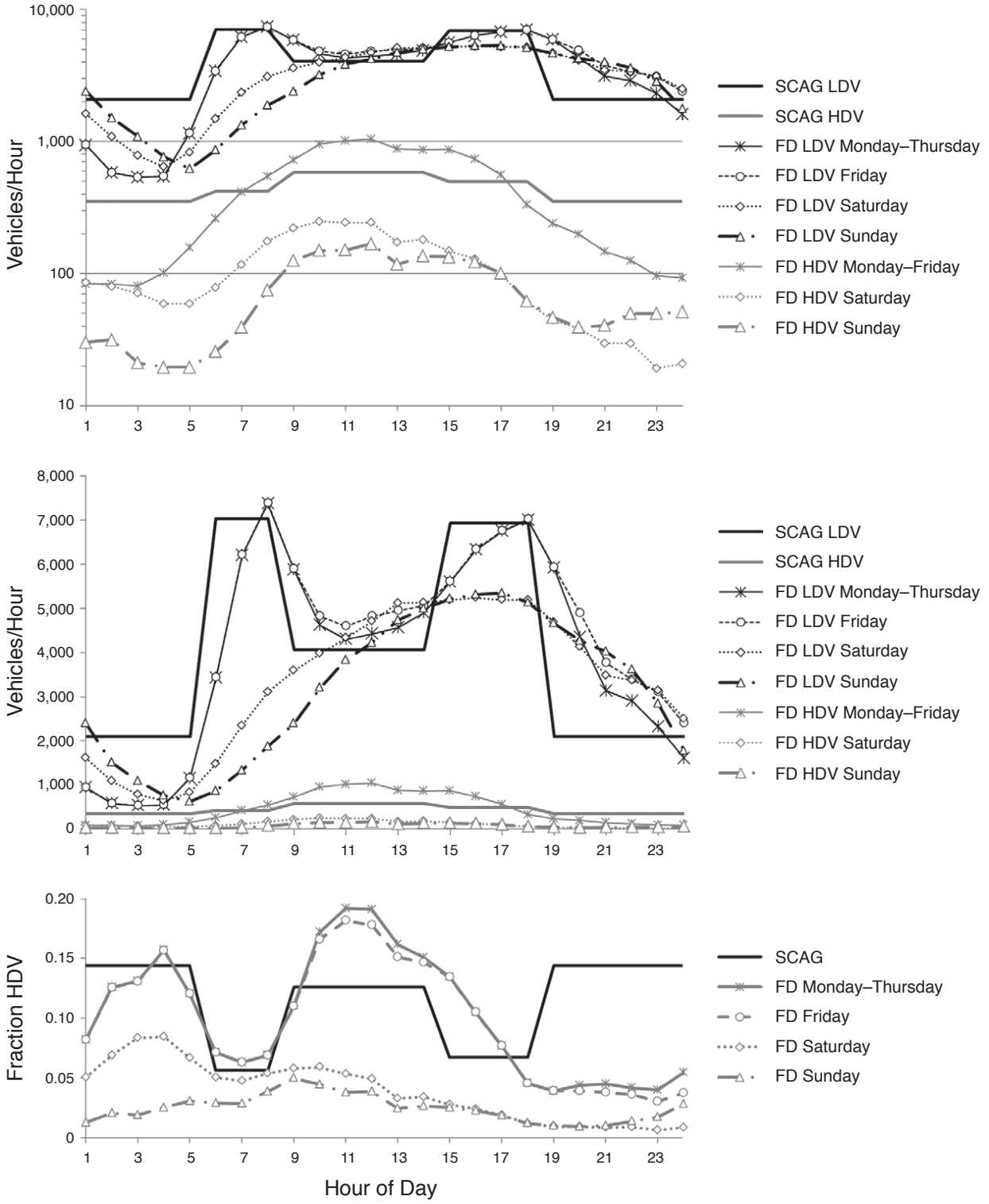

Figure 9. Sample of hourly traffic volume profiles by day of the week at (top) log and (middle) linear scales and showing (bottom) the fraction of HDVs, comparing SCAG modeled diurnal traffic profiles with the final diurnal (FD) traffic volumes used for the ASM runs.

and ratios were taken from a Los Angeles–specific analysis of hourly traffic counts by Funk and colleagues (2001). Figure 9 shows the SCAG diurnal profiles and the final day-of-the-week diurnal profiles used in the ASM, which were based on the SCAG weekday link volume, with hourly variations and weekday-to-weekend ratios forced to match those reported by Funk and colleagues (2001). LDV traffic was day specific (separate profiles were used for Monday–Thursday, Friday, Saturday, and Sunday) and HDV traffic had separate profiles for Monday–Friday, Saturday, and Sunday. The advantage of this modification to the input data was that the transitions from peak to off-peak were more realistic. The disadvantage was that an analysis based on a small number of roads was applied to all road links in the domain. Furthermore, the LDV and HDV diurnal profiles taken from freeways in Long Beach were applied as far away as Riverside, where the actual profiles were likely different. Specifically, on freeways carrying interstate truck traffic (as opposed to Long Beach port traffic), the diurnal variation in HDV traffic is not as pronounced; Long Beach HDV traffic has a diurnal variation (peak-to-minimum ratio) of a factor of 10. It must be stressed that the resulting hourly traffic estimates do not reflect day-to-day variability other than the day-of-week average variability in the diurnal profiles reported by Funk and colleagues (2001). Daily variations in traffic volume, timing, fleet composition, acceleration fractions, and speeds are not reflected in the approach used for the ASM. Such variations have myriad causes, including inclement weather, work schedules (e.g., holidays), road construction, and accidents.

DESCRIPTION OF EVALUATION AND INPUT DATA

Characteristics of Receptor Sites Based on Traffic Activity and Other Sources

By counting traffic activity (vehicle-km per day) as a function of direction, distance, and time of day, one can generate a detailed picture of local traffic at each measurement (and modeling) site. Figure 10 summarizes our analysis of traffic activity; details of traffic activity by direction, distance, and road class can be found in Appendix G (available on

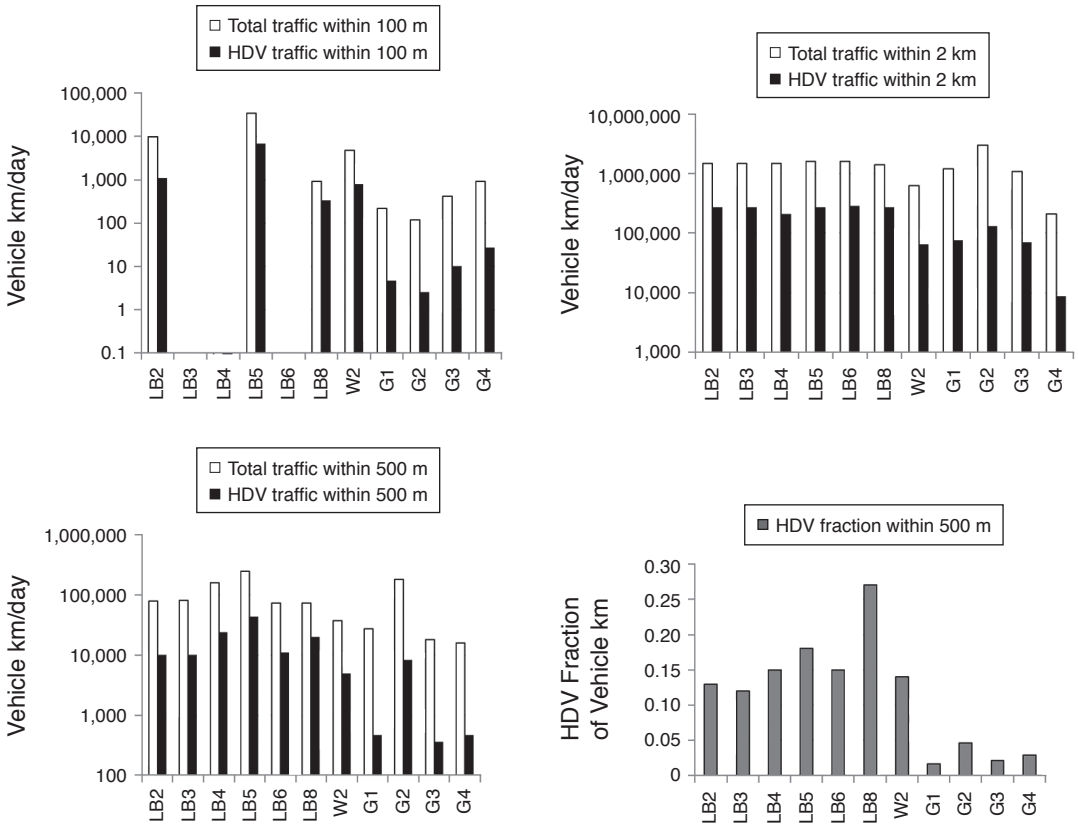

Figure 10. Traffic activity within 100 m, 500 m, and 2 km of a site and as the HDV fraction of vehicle-km within 500 m of a site. Note that the *y*-axis scales differ.

the Web at *www.healtheffects.org*). Figure 10 shows that the 11 sites provided excellent variation in conditions for model testing. The LB5 site, which is within 30 m of Interstate 710 (I-710), had the heaviest traffic. When ranking sites by traffic volume within 500 m of a receptor, the LB4 site had the next heaviest traffic. It is within 150 m of an arterial street (Anaheim Street) and within 500 m of I-710. LB4 and LB5 are in a commercial–industrial area. Port of Long Beach sources, including port vehicles and ships, were not included in the emissions modeled by the ASM. Port emissions could affect results at LB4 and LB5, especially with winds from the south or southwest. The closest boundary of the port to these sites is about 1 km away. Similarly, railway emissions were not included in the ASM. Railway emissions could affect results at LB4 and LB5 if winds are from the south, southwest, or west. The closest approach of railways to these sites is about 800 m.

The LB8 site had the next highest traffic volume; it is within 100 m of the Terminal Island Freeway. According to the SCAG database, it is exposed to a very high percentage of HDVs, with a mean of more than 40% when the wind was from the west. Land use to the east of the LB8 site is residential. However, for all other directions, there are particle sources that were not represented in the model, including rail, intermodal freight, port, and petrochemical operations. Specifically, to the north are rail lines and intermodal freight operations; to the west are rail lines (nearest is 180 m away), intermodal freight operations, and petrochemical facilities (nearest is 1.3 km); and to the south is the Port of Long Beach (at a distance of about 3 km).

LB2, LB3, and LB6 were next in order of traffic volume and have very similar magnitudes of both total and HDV traffic within 500 m. Of these three sites, LB2 has an arterial road (Anaheim Street) within 100 m, whereas LB3 and LB6 are more distant from major roads. LB2 and LB3 are quite close to one another (~310 m apart), the principal difference being the distance from Anaheim Street. LB2 and LB3 are both influenced by the port (which lies 250 m to the south and southwest) and have a railway running to the southwest at a distance of approximately 200 m. LB6 is relatively far from arterial streets. Highway 1 is about 350 m to the south. LB6 is potentially influenced by the port (2 km to the south and southwest), railways (the nearest is 600 m to the west), and petrochemical and intermodal freight operations (to the west, northwest, and north), with some activities within 1 km.

The Long Beach W2 site is the farthest to the south of the sites used in our study and is thus the one potentially most influenced by port or industrial activities. Only with winds from the north or northwest would W2 be primarily influenced by the traffic sources considered in the ASM. W2 is very close to the junction of an arterial and a collector street, but the streets have lower traffic volume than the other arterials near LB4 and LB2 (according to the SCAG traffic-demand-model volumes). However, for winds from the east, south, or west, W2 would be exposed to port emissions. A petrochemical facility is within 2 km to the west. The large corridor of intermodal freight, petrochemical facilities, and railways that potentially influences LB6 and LB8 lies to the northeast of W2.

The CHAPS sites G1 through G4 had much lower HDV vehicle fractions within 500 m (all less than 0.05) compared with the Long Beach sites, which had fractions greater than 0.10. With the exception of G2, the contrast with the Long Beach sites is striking. The Long Beach sites had overall traffic within 500 m of 107,700 vehicle-km per day, whereas the overall traffic within 500 m for G1, G3, and G4 averaged 20,300 vehicle-km per day (G2 had 180,000 vehicle-km per day). Ordering the CHAPS sites by traffic within 100 m showed that G4 > G3 > G1 > G2. However, when ordering the sites by traffic within 500 m, the order was exactly reversed, with G2 > G1 > G3 > G4. These orderings do not consider wind direction and are uncertain because of the approximate nature of the assumed traffic volumes on the class 9 roads. G2 and G3 had variation in the amount of nearby traffic depending on wind direction; G1 and G4 were more evenly surrounded by roads. G1 and G3 had some unmodeled combustion sources (e.g., airports and rail transport) within 2 km. G2 and G4 did not have any obvious unmodeled sources within that radius.

Characterization of Sites by Meteorologic Data

A detailed comparison of modeled and measured winds at the LB4 and LB5 sites was performed using NWS data for observational nudging, output from the WRF model (after observational nudging), and meteorologic data gathered at these locations by the original group of researchers at the University of Southern California (USC) that conducted the HCMS. Several weather stations were used for the observational nudging, but the only station in the area of the was the Long Beach Airport NWS observation station, located about 6 km from the LB4 and LB5 sites.

The general pattern in Long Beach in September 2007 was of weak onshore (south to north) winds from about midnight until about 11 AM. This onshore wind was most consistent during the early morning hours (5 to 6 AM) and affected peak concentrations during the morning peak travel period (which often were higher than during the afternoon travel period because of winds favorable for dispersion in the afternoon. An offshore (north to south) wind typically developed by the early afternoon. Wind speeds peaked between 1 and 5 PM.

Wind roses for LB5, comparing 24-hour, day, and night wind speeds and wind directions, are shown in Figure 11.

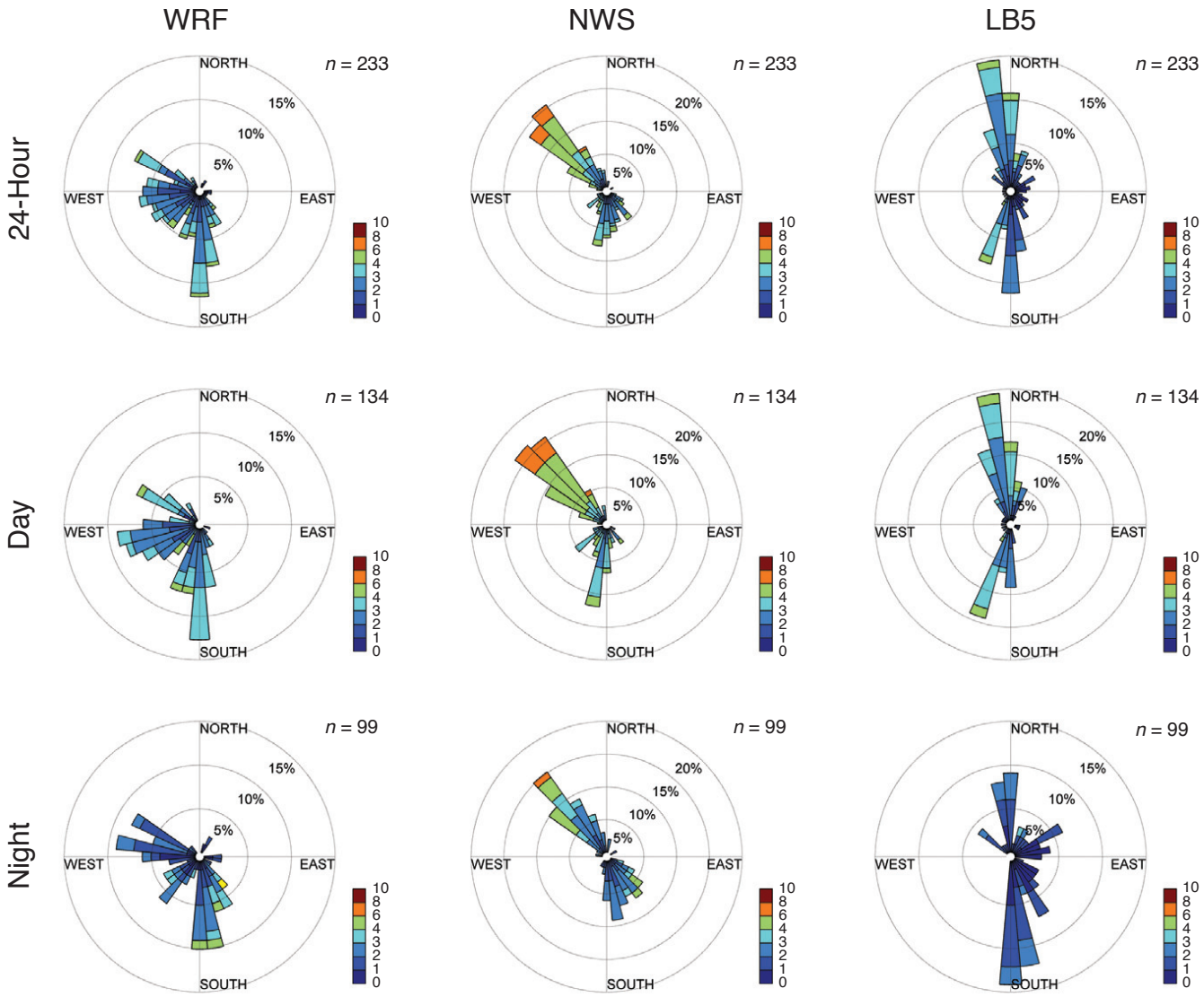

Figure 11. Wind roses for the LB5 site from three data sources, comparing (top row) 24-hour, (middle row) day (6 AM to 6 PM), and (bottom row) night (7 PM to 5 AM) wind speeds and directions. Data are for September 2007 from (left column) the WRF model after observational nudging, (middle column) the NWS weather station at Long Beach Airport, and (right column) the observations at LB5 (Moore et al. 2009). Colors indicate wind velocities in m/sec. Note that the wind-direction percentage scales differ.

Wind roses for LB4 are shown in Appendix H (available on the Web at *www.healtheffects.org*). There are significant differences between the WRF model, the NWS observations, and the USC observations; they are consistent with the quantitative comparisons discussed below.

Appendix D (available on the Web at *www.healtheffects.org*) includes vertical profiles of modeled K_{zz} (Figure D.2) and descriptive statistics on meteorologic variables as a function of WRF-model stability class and time of day (Table D.1). In some cases the average modeled meteorologic data for specific stability conditions was used as the meteorologic data for test simulations (e.g., the calculation of on-road losses below was made using the average modeled meteorologic data for the unstable low-wind-speed condition) (Table D.1).

Comparing WRF modeled data for the LB5 site with NWS Long Beach Airport data for September 2007 using hourly paired statistics, the mean model bias was −26°, and the mean model error was 65°. The IOA was 0.58, and the RMSE in wind direction was 87°. The WRF mean wind speed was 2.34 m/sec, whereas the NWS mean (paired to the same hours) was 3.24 m/sec. The wind speed IOA and RMSE were 0.43 and 1.91 m/sec, respectively, compared with the NWS data. Agreement between modeled wind directions using WRF data and the USC group's data was poor, with an IOA of 0.43 and an RMSE of 138°. The USC group's mean observed wind speed at LB5 was 1.71 m/sec (lower than the WRF model result, which, paired to the same hours, was 2.34 m/sec). The Davis 181 Vantage Pro2 or Pro2 Plus weather-station measurements used by the USC group might have disagreed with NWS measurements because of differences in anemometer height and limitations in the Davis instruments in direction and speed indicators at low wind speeds. The NWS anemometer is 10 m above the ground; the anemometer used by the USC group was lower. The WRF wind-speed estimates were at an elevation of 10 m.

Comparing WRF modeled data for the LB4 site and NWS Long Beach Airport data for September 2007 gave results identical to those for the LB5 comparison because the WRF data were the same (LB4 was in the same 1-km grid cell) and the NWS station was the same. Agreement between the WRF-modeled wind directions and the USC-group–measured wind directions was poor, with an IOA of 0.42 and an RMSE of 117°. The USC group's mean observed wind speed at LB4 was 1.36 (lower than that of the WRF data, which, paired to the same hours, was 2.34 m/sec). The IOA between NWS- and USC-group–measured wind directions was 0.67 at LB4 and 0.55 at LB5.

These results can be compared with the model-performance benchmarks of Emery and colleagues (2001) for good model performance. For wind speed, the benchmarks are 0.6 for IOA and 2.0 m/sec for RMSE. Using hourly statistics of the NWS data for comparison, the WRF modeled wind speed had an IOA of 0.43 (compared with the benchmark of 0.6) and an RMSE of 1.91 m/sec (compared with the benchmark of 2.0 m/sec). The wind direction had a gross mean error of 65° (compared with a benchmark of 20°). In other words, the wind-direction agreement between model and measurements was poor; the wind speed skill was somewhat better in terms of RMSE than of IOA.

Descriptive and Directional Statistics for Measured Particle Number

Descriptive statistics for particle number concentrations are summarized in Table 6. Directional statistics for the dependence of the particle number concentrations on wind direction is plotted for a subset of the measurements in Figure 12 using conditional probability function plots. These plots show the fraction of hours with wind in a specific directional bin that exceeded a given concentration threshold. Each plot has three thresholds, corresponding to the median, 75th, and 90th percentile concentration measurement. This type of plot normalizes for the unequal number of hours of wind from various directions. The plots in Figure 12 are perhaps surprising for their lack of directional patterns. In the plot for LB5 in September, there is some indication that high concentrations are favored when winds are from the northeast (LB5 is less than 30 m to the west of I-710), but the pattern is not as strong in the plot for LB5 in October. LB4 has an arterial road 150 m to the south, but concentrations are not elevated above the median when winds are from the south. The plot for LB4 shows elevated concentrations with winds from the west, but this is a rare occurrence, as the wind rose in Appendix H shows. The plot for LB8 also shows a tendency toward high concentrations when winds are from the west, which corresponds to the direction of the Terminal Island freeway and nonroadway sources.

Figure 13 shows the mean measured particle number concentration at each site versus HDV traffic volume within 500 m, which was more strongly correlated with particle number concentrations than was total vehicular traffic volume or traffic volumes within 100 m of the sites. The figure shows that the concentrations measured by CPC were higher than those measured by SMPS, as expected because of the particle size limits of the instruments. Furthermore, there was a general trend toward increased concentrations as HDV traffic volumes increased. Concentrations at W2 and LB6 were somewhat high and concentrations at LB4 were somewhat low when considered in this manner.

Table 6. Descriptive Statistics on Measured Particle Number Concentration[a]

Simulation Run	Instrument[b]	Hours (*n*)	Mean	SD	Minimum	Percentile							Maximum	Mean	
						5th	10th	25th	50th	75th	90th	95th		Daytime/ Nighttime	Weekday/ Weekend
LB4_Sept	a	394	12,703	7,091	1,039	2,880	4,319	7,601	11,794	16,794	22,036	27,143	35,723	1.71	0.98
LB5_Sept	a	393	29,830	17,714	2,560	8,281	10,922	16,490	26,682	38,278	50,631	59,093	116,474	1.62	1.17
W2_Sept	a	341	13,889	8,465	1,606	2,706	3,312	6,714	13,278	19,176	25,910	29,616	47,855	1.02	1.00
LB2_May	b	79	13,110	5,749	5,276	6,015	7,427	8,659	11,337	16,661	21,254	23,792	33,701	1.17	—[c]
LB3_May	b	161	16,000	9,094	3,843	6,036	6,788	9,760	13,740	21,079	27,226	31,699	57,011	1.03	1.00
W2_May	b	182	13,475	7,819	2,493	4,302	5,247	7,905	11,913	16,948	23,170	29,504	44,469	1.34	1.06
LB4_Oct	b	744	22,491	10,893	1,804	7,895	9,789	13,527	20,930	30,512	37,225	41,815	66,350	1.46	1.19
LB5_Oct	b	744	41,345	23,510	7,766	13,067	16,401	23,579	35,165	55,973	74,963	86,616	144,335	1.05	1.45
LB6_Oct	b	733	26,347	12,995	4,715	10,847	12,896	17,411	23,739	32,380	42,793	51,167	93,506	1.50	1.31
LB8_Oct	b	606	25,288	11,679	339	9,344	12,345	16,799	23,217	32,021	41,349	46,983	71,408	1.47	1.34
W2_Oct	b	744	26,569	15,773	3,350	8,117	10,371	14,573	22,500	35,397	48,784	57,011	103,310	1.39	1.30
Run01G1	b	1,119	13,542	5,499	2,649	5,890	7,394	9,739	12,607	16,417	20,348	23,416	44,523	1.03	1.17
Run02G2	b	821	13,757	6,091	738	5,336	7,021	9,563	12,898	17,141	22,329	24,766	61,001	1.11	1.07
Run03G2	b	1,008	22,989	9,050	3,525	9,109	11,692	16,732	22,483	29,097	33,959	38,493	62,588	0.90	1.24
Run04G3	b	650	6,225	3,414	723	1,509	1,917	3,457	6,079	8,253	10,715	12,369	17,916	1.21	1.17
Run05G3	b	904	12,663	6,327	1,808	4,957	6,208	8,061	11,334	16,184	20,868	24,940	44,222	1.21	1.18
Run06G4	b	972	6,689	2,096	1,265	2,731	3,854	5,561	6,951	7,946	8,745	9,589	22,630	1.03	1.11
Run07G4	b	867	9,256	4,518	1,741	3,238	4,375	6,012	8,245	12,150	15,333	17,244	33,061	0.91	1.11

[a] Data expressed as particle number/cm^3, hourly averages. See Table 4 for sampling periods. SD indicates standard deviation.

[b] Instrument a is an SMPS system with a lower size cut of 14 nm; Instrument b is a CPC with a 50% detection efficiency at 7 nm.

[c] No weekend data samples included.

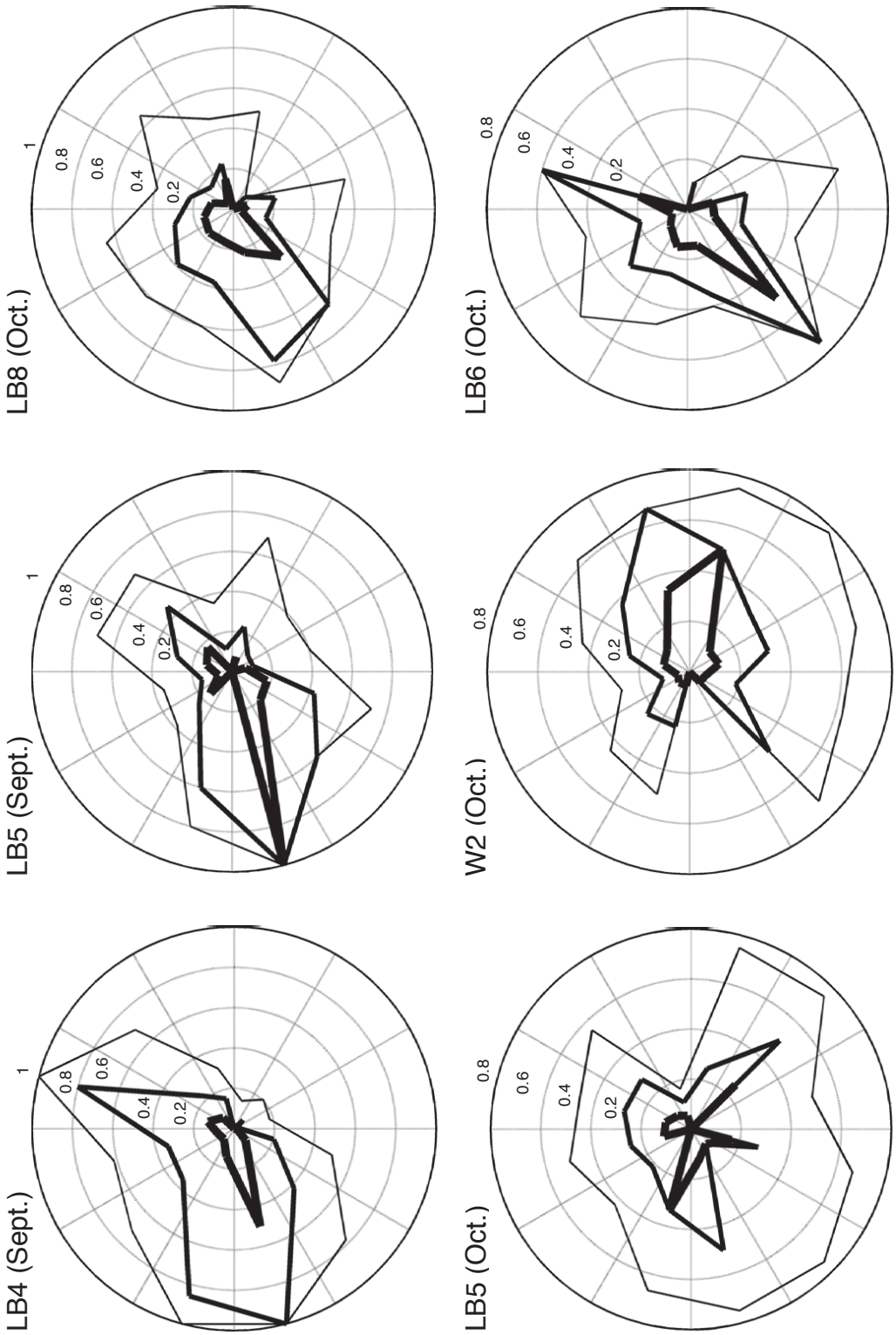

Figure 12. Conditional probability plots of measured data for selected sites and months in the USC data set, showing the dependence of particle number concentrations on wind direction. The distance of a plot line from the center of the plot indicates the conditional probability — ranging from zero at the center to 0.8 or 1 at the circumference — of the wind from a given direction yielding a particle concentration that exceeded a given concentration threshold (north is at the top of each plot). The thin lines show the results of using the sample median concentration as the threshold, the medium-thick lines show the 75th percentile as the threshold, and the thick lines show the 90th percentile as the threshold. The median, 75th percentile, and 90th percentile thresholds (in particles/cm^3) are 12,000, 17,000, and 27,000, respectively, for the LB4 site in September 2007; 26,000, 38,000, and 50,000 for LB5 in September 2007; 20,000, 29,000, and 40,000 for LB8 in October 2007; 35,000, 56,000, and 75,000 for LB5 in October 2007; 22,500, 35,000, and 48,000 for W2 in October 2007; and 22,500, 32,000, and 43,000 for LB6 in October 2007.

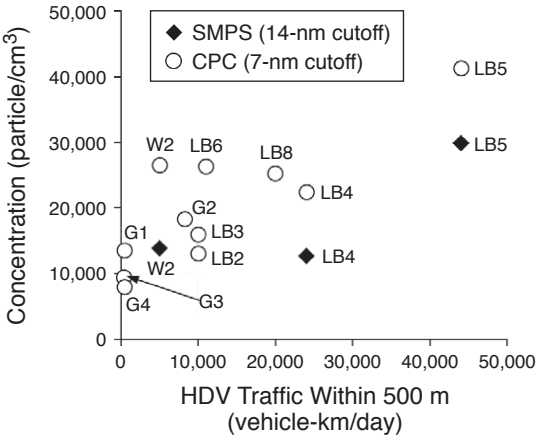

Figure 13. Measured mean particle concentrations at each site versus HDV traffic volume within 500 m of the site.

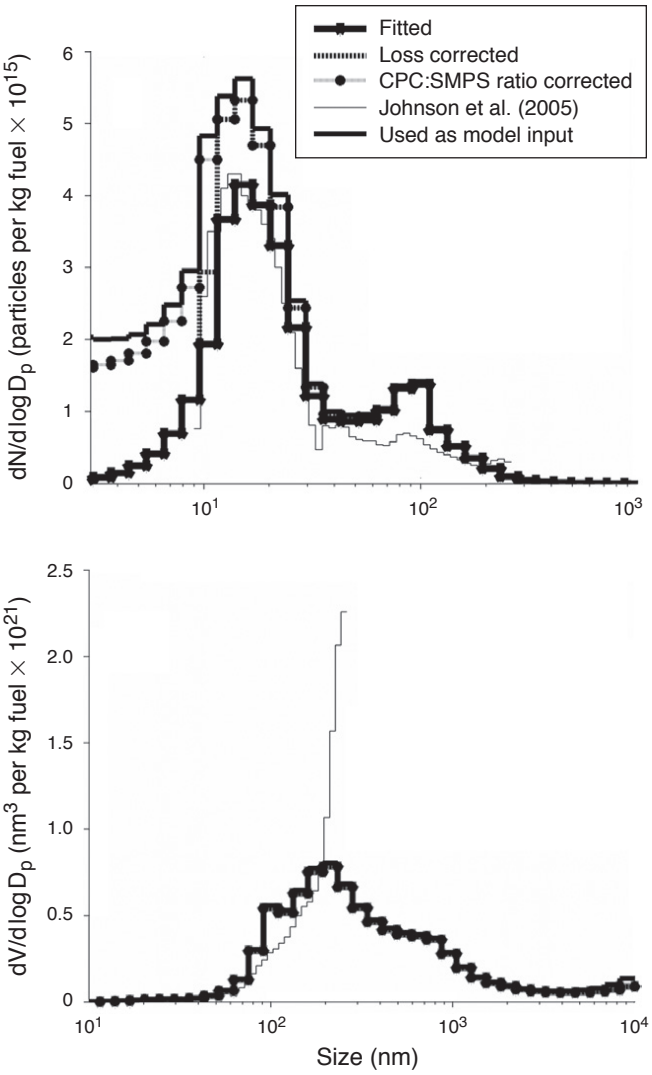

Figure 14. Input HDV cruise (top) number size distributions and (bottom) volume distributions, showing the curves at various stages of preprocessing, as described in the text, including the final model-ready curve used as the model input.

DEVELOPMENT OF MODEL-READY EMISSION FACTOR FOR SIZE-RESOLVED VEHICLE EMISSIONS

As discussed in the Methods section, the size-resolved fuel-based emission factors shown in Figure 5 were converted to model-ready emission factors in four steps.

Figure 14 and Figure 15 show size distributions for HDV and LDV, respectively. The "Fitted" curve shows the size distributions after step 1 (i.e., after combination of multiple input distributions by minimization of equation 5). The "Loss Corrected" curve shows the size distributions after step 2. (The instrument sampling efficiencies used in this study are graphed in Appendix A). The "CPC:SMPS Ratio Corrected" curve shows the size distribution after step 3 (i.e., after the application of assumed CPC-to-SMPS ratios of 4, 3, 6, and 4, which were within the ranges reported by Kittelson and colleagues [2006a,b]) for LDV cruise, HDV cruise, LDV acceleration, and HDV acceleration, respectively. The "Used as Model Input" curve shows the size distribution after step 4.

The correction factor (for the cruise mode) attributable to on-road coagulation and deposition losses (step 4) varied depending on the angle of the wind relative to the road and the particle size. At the small end of the particle size distribution, the loss processes are coagulation and deposition; at the 10-μm end of the distribution, the loss process is deposition. In the case of winds at 90°, the correction factors had a minimum of 1.01, were less than 1.1 for particles from 2.5 nm to 4.7 μm, and were 1.35 and 1.32 at the extreme particle sizes of 1 nm and 10 μm, respectively. In the case of winds parallel to the road, the correction factor was larger — it was 2.22 and 1.96 at the extreme particles sizes of 1 nm and 10 μm, respectively. The correction decreased at intermediate sizes, was less than 1.1 for particles larger than 11 nm and smaller than 2.2 μm, and had a minimum value of 1.04 at around 340 nm. The correction factors for the acceleration mode were slightly larger. This final correction for on-road losses was very small compared with the overall uncertainty in the emission factor and can be neglected in future work.

Table 7 shows emission factors for the four input size distributions (LDV cruise, HDV cruise, LDV acceleration, and HDV acceleration) for various lower size limits and assumed sampling losses. Sampling losses, if not corrected

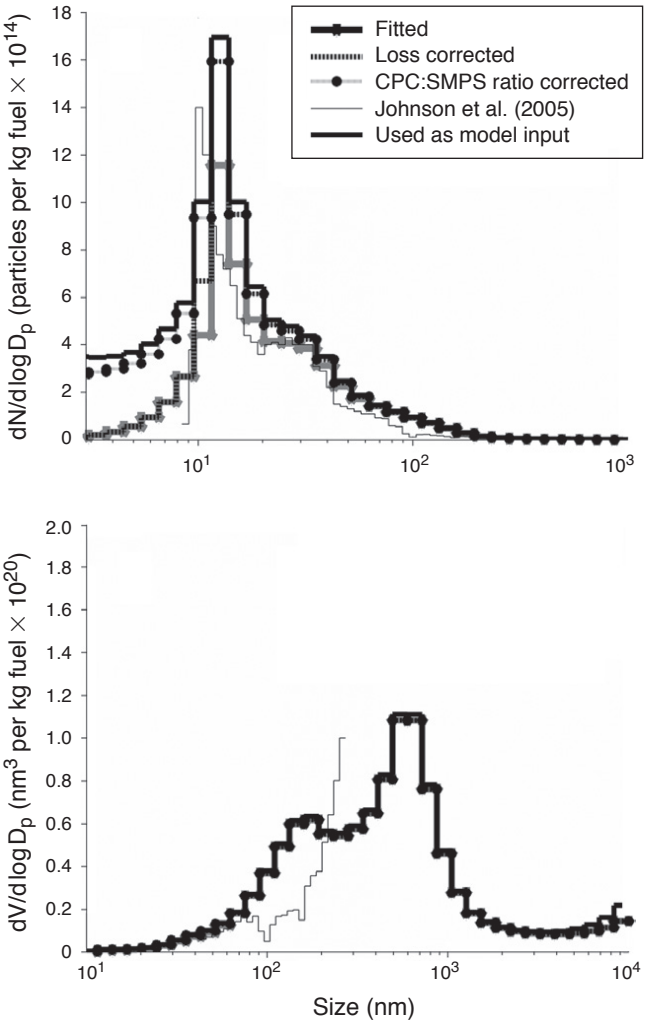

Figure 15. Input LDV cruise (top) number size distributions and (bottom) volume distributions, showing the curves at various stages of preprocessing, as described in the text, including the final model-ready curve used as the model input. Note that the *y*-axis scales differ from those of Figure 14.

Table 7. Emission Factors as a Function of Size Cutoff[a]

Variable and Size Range (nm) / Assumed Instrument Sampling Losses[b]	Cruise		Acceleration	
	LDV	HDV	LDV	HDV
Number[c] 3–10,000				
None	1.64	7.02	26.87	17.12
CPC	1.36	6.04	20.65	14.50
SMPS	0.46	2.43	6.22	4.33
Number[c] 7–10,000				
None	1.41	6.47	17.42	16.47
CPC	1.23	5.72	15.27	14.12
SMPS	0.46	2.42	6.18	4.32
Number[c] 10–10,000				
None	1.01	4.91	13.21	8.61
CPC	0.91	4.44	11.88	7.66
SMPS	0.41	2.24	5.77	3.32
Number[c] 14–10,000				
None	0.39	2.45	5.42	2.91
CPC	0.36	2.31	5.16	2.73
SMPS	0.25	1.56	3.78	1.84
Volume[d] 3–2,500				
None	0.88	6.77	6.48	7.36
CPC	0.87	6.72	6.38	7.30
SMPS	0.83	6.40	5.81	6.90
Mass[e] 3–2,500				
None	123	948	907	1031

[a] Emission factors can be converted to a per vehicle-km basis by multiplying LDV emissions by 0.0888, and HDV emissions by 0.395. This conversion is based on an LDV fuel economy of 12 L/100 km and a fuel density of 0.74 kg/L. For HDV, it is based on a fuel economy of 47 L/100 km and a fuel density of 0.84 kg/L.

[b] Losses based on assumed size-dependent instrument sampling efficiencies as described in text and graphed in Appendix A.

[c] Number emission factors are expressed as 10^{-15} particles/kg fuel. Therefore, a value of 1 refers to 1×10^{15} particles per kg fuel.

[d] Volume emission factors are expressed as 10^{-20} nm^3/kg fuel.

[e] Mass emission factors are expressed as mg/kg fuel assuming spherical particles of specific gravity 1.4.

for, can substantially reduce recovered emission factors. For example, the HDV cruise emission factor at sizes greater than 7 nm derived from CPC sampling with a typical inlet and without loss correction is 88% of that which would be determined from loss-free conditions. The HDV cruise emission factor at the same cutoff diameter (7 nm) derived from SMPS sampling is 37% of the loss-free value under the assumed losses derived from Kittelson and colleagues (2006a). Assumed efficiency curves are in Appendix A.

Using the conversions from particle number/kg-fuel to particle number/vehicle-km shown in the footnote to the table, emission factors can be converted to this unit and compared with an extensive list of emission factors in a review by Kumar and colleagues (2011). Kumar and colleagues reported emission factors for fleet average, LDVs, and HDVs. The emission factors in the current study (using a 10-nm size cutoff and assuming no losses) for LDVs ranged from 0.9×10^{14} (cruise) to 12×10^{14} (acceleration) particle number/vehicle-km. For comparison with Kumar and colleagues (2011), we consider emission factors sampled under hypothetical loss-free conditions (or equivalently, emission factors recovered after correction for inlet transmission efficiency). For HDVs (using a 10-nm cutoff), the

emission factors ranged from 19×10^{14} (cruise) to 34×10^{14} (acceleration) particle number/vehicle-km. For comparison, the fleet average emission factors reviewed by Kumar and colleagues (2011), using a 10-nm cutoff, ranged from 0.31×10^{14} to 4.7×10^{14} particle number/vehicle-km, with a median of 2.0×10^{14}. In the current study, a fleet consisting of 92% LDVs with a 10% acceleration fraction would have an emission factor of 3.5×10^{14} particle number/vehicle-km. Fleet-averaged emission factors in the current study are therefore comparable with the median emission factor in Kumar and colleagues (2011). The HDV emission factors reported by Kumar and colleagues, using a 10- or 11-nm cutoff, ranged from 6.7×10^{14} to 22×10^{14} particle number/vehicle-km, with a median of 6.7×10^{14}. The HDV emission factor in the current study, with a 10% acceleration fraction, is 20×10^{14} particle number/vehicle-km. In other words, the 10-nm cutoff emission factor used in the current study is higher than the median value of 6.7×10^{14} from the review, and toward the high range. However, in the review by Kumar and colleagues (2011), it can be seen that emissions increase by a factor of ~10 when the lower particle size limit is just extended to 7 nm, reflecting a high particle concentration in the range of 7 to 10 nm for HDV studies. For gasoline-fueled LDVs (using emission factors with lower size limits, from 7 to 11 nm), emission factors ranged from 0.02×10^{14} to 1.3×10^{14} particle number/vehicle-km in Kumar and colleagues (2011) compared with 2.0×10^{14} particle number/vehicle-km (with a 10% acceleration fraction) in the current study. In other words, the number emission factor for gasoline-fueled vehicles in the current study (based on the study by Johnson and colleagues [2005] and especially on the very high acceleration size distribution for gasoline-fueled-vehicle emissions in that study; see Figure 5) was higher than the range reported by Kumar and colleagues. It is not clear to what extent the emission factors in Kumar and colleagues were corrected for instrument-sampling losses.

Maximum On-Road Concentrations

Once the emission factors such as those in Table 7 were available, calculation of the maximum modeled on-road concentrations was straightforward. Furthermore, because the calculation was simple enough to be done in a spreadsheet, it could provide a useful check of the simulation results.

By assuming that a parcel of air travels perpendicular to a roadway and is therefore able to accumulate emissions for a time equal to the wind speed divided by the road width, if an assumption is made about the vertical mixing height (H), then the well-mixed concentration can be determined by manipulation of equation 10:

$$C_{\text{road}} = \frac{(EF)(CF)(TV)}{uH}, \tag{20}$$

where C_{road} is the number concentration in the well-mixed roadway volume (in particle number/cm^3), EF is the emission factor, CF is the conversion factor given by equation 12, TV is traffic volume (vehicles/hr), u is wind speed (m/sec), and H is the assumed mixing height (m). Values of C_{road}/TV are plotted in Figure 16 using equation 20 and the emission factors in Table 7 for the 7-nm lower size cutoff and CPC diffusion losses. The acceleration fraction and HDV fraction influence EF. The mean of the LDV and HDV acceleration fractions (from the current study) were plotted together with the HDV fraction for I-710 and traffic volumes for I-710 at midday (from the current study) as well as for the midday traffic volume and HDV fraction for Interstate 405 (I-405) in Los Angeles (Zhu et al. 2002). The graphs in Figure 16 reflect the assumption that emissions are restricted to a layer from 0 to 4 m high. In the ASM

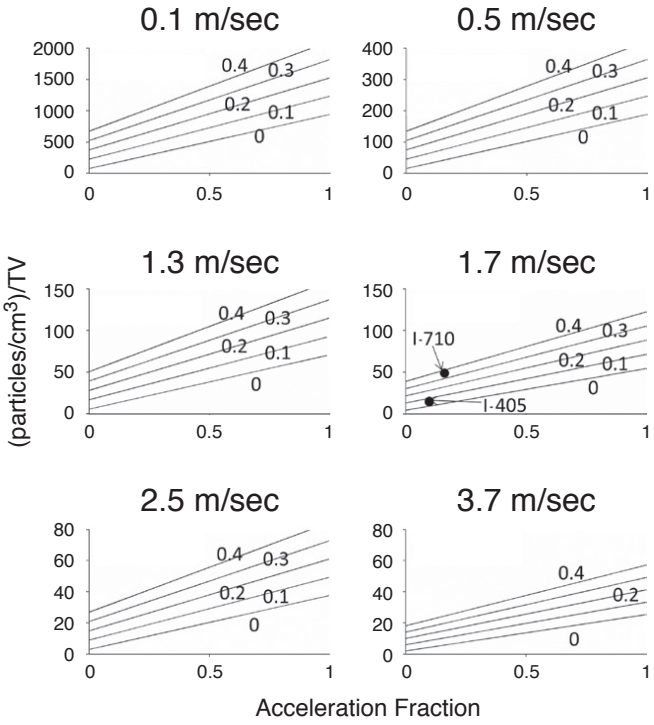

Figure 16. Normalized road-mixing-zone concentrations for winds (in m/sec) perpendicular to the roadway. Concentrations are for particles larger than 7 nm, with assumed modest diffusion losses. Mixing volume is assumed to be 4 m high, with width and length equal to the width of the road. The five lines in each graph represent the HDV fractions 0, 0.1, 0.2, 0.3, and 0.4. The two dots show the approximate positions of midday traffic volumes and HDV fractions reported for I-405 by Zhu and colleagues (2002) and for I-710 as calculated for the current study using the same assumed acceleration fractions. TV indicates traffic volume (in vehicles/hr). Note that the y-axis scales differ.

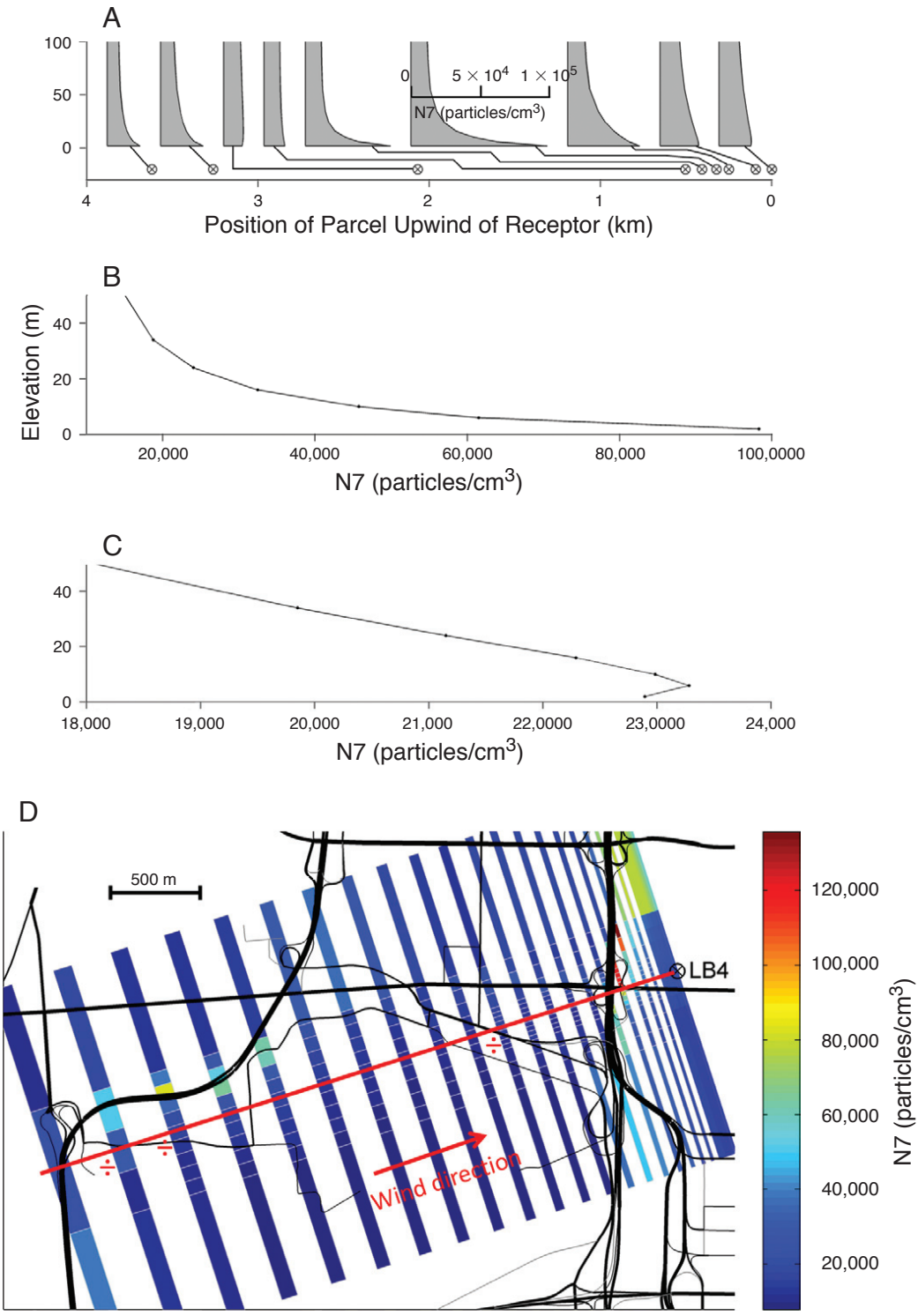

Figure 17. Examples of vertical profiles and surface-layer concentrations for particles greater than 7 nm (N7), as modeled by the ASM, for an unstable period at midday, when large gradients relax relatively quickly. (**A**) Vertical profiles to an elevation of 100 m for selected distances upwind of the LB4 receptor. (**B**) Vertical profile to an elevation of 50 m at 324 m upwind of LB4, where I-705 and Anaheim Street intersect. (**C**) Vertical profile at the LB4 receptor, where dry deposition to the surface has depleted the lowest model layer. (**D**) Plan view of the parcels' surface layers, with color-coded concentrations. The large model steps (initially almost 500 m long) decrease to 10 m in the final 100 m before reaching the receptor. The three red symbols (÷) indicate locations where parcels were subdivided in the crosswind direction for enhanced resolution.

model, the first model layer is also from 0 to 4 m high, the vertical distribution of the initial pollutants was calculated as described earlier in the Methods section, and 50% to 80% of the emissions were typically restricted to the first layer, depending on H_{mix}. None of the sites used in the current study were directly on a road, although the LB5 monitor was very close to I-710, and the LB2 and W2 monitors were close to arterial and collector streets. In Figure 16, two dots indicate the approximate positions of the measurements reported by Zhu and colleagues (2002) for I-405 and of the approximate traffic composition at noon on I-710. Actual model predictions for on-road concentrations can be lower (because of vertical mixing of the emissions into layers other than the first layer of the model, diffusion, coagulation, and deposition). They can also be higher than shown in Figure 16 if the wind is at an angle other than perpendicular to the roadway. Converting the *y*-axis value for I-405 to an on-road concentration gives about 17 (*y* position) × 13,000 (traffic volume), or 220,000/cm^3. Converting the value for I-710 to an on-road concentration gives about 45 (*y* position) × 10,000 (traffic volume), or 450,000/cm^3.

MODEL OUTPUT

Overview of Simulation Results

Example Outputs for Individual Hours Figure 17 shows both vertical profiles (panels A–C) and a plan view (panel D) of the full 4 km × 2.1 km path of travel for a slab of parcels for 1 hour at noon in September 2007. The operation of the model is perhaps best shown in the plan view. The model is initialized at the upwind boundary 4 km from the receptor using three parcels in the crosswind direction. Symbols (÷) indicate where the center column of parcels was divided into thirds to increase resolution in the crosswind direction. The model steps (initially almost 500 m) decrease to 10 m in the final 100 m before the receptor. Vertical profiles are shown at a variety of distances from the LB4 receptor (panel A), at the intersection of I-710 and Anaheim Street (panel B), and at the receptor (panel C). Because this area is rich in emission sources (roads), concentrations are elevated in the lowest model layers (< 50 m). However, concentrations at the surface layer itself are often slightly lower because of deposition, except when measured at or immediately after road intersections.

Another example of a plan view of modeling for 1 hour is shown in Figure 18, for a north-to-south flow (also at noon) affecting the LB5 receptor. The initial concentration (not shown) was 10,122/cm^3, and the final concentration simulated during

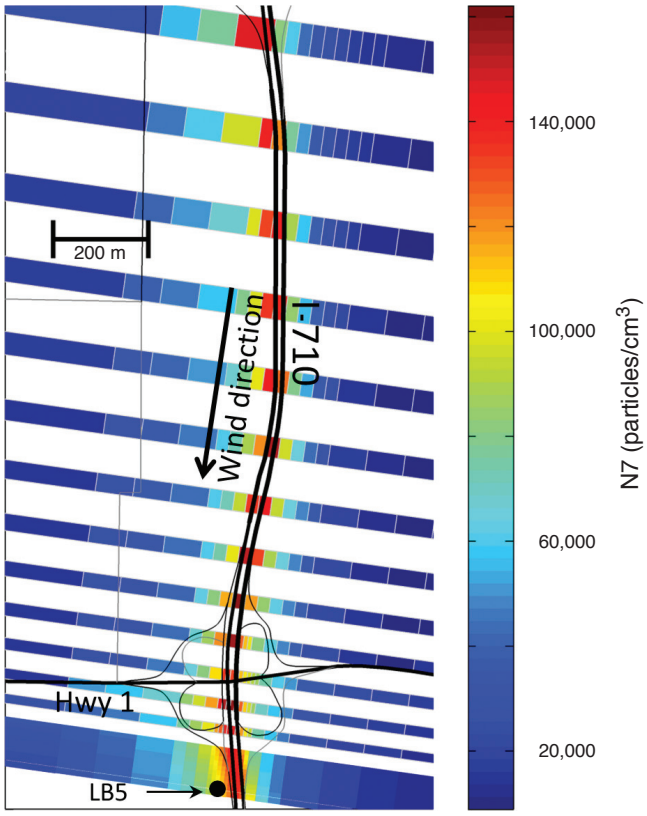

Figure 18. Plan view of the LB5 modeling domain as a slab of parcels advects for 1 hour toward the LB5 receptor from the north, parallel to I-710, during a typical afternoon offshore breeze. As the parcel approaches LB5, the step size decreases to 10 m, and the parcels are subdivided into smaller parcels with lateral dimensions of ~10 m, in an attempt to resolve the strong gradients (the simulation setting for the desired resolution in this run was 10 m at the receptor). The initial concentration (not shown) was 10,122 particles/cm^3; the final concentration at LB5 was 114,809 particles/cm^3 (for particles greater than 7 nm).

1 hour was 114,809/cm^3 (for particles > 7 nm [N7]). In the simulation, the slab of parcels advects toward the LB5 receptor from the north, parallel to I-710, during a typical afternoon offshore breeze. As the parcel approaches LB5, the step size decreases to 10 m, and the parcels are subdivided into smaller parcels with lateral dimensions of ~10 m in an attempt to resolve the strong gradients (the setting for desired resolution in this simulation was 10 m at the receptor).

A 1-hour time resolution was used in all simulations and observation data. For model assessment, these data were also calculated as average diurnal cycles and 24-hour averages. All statistics based on the 24-hour average period were actually based on averaging of any 24-hour period with 16 or more hours of model–observation paired hours.

Assessment of Overall Performance Simulations were performed for the time periods and monitoring locations shown in Table 4. Overall performance was charted using five types of plots: (1) scatterplots of 24-hour number concentration averages, (2) plots the average diurnal cycle of total number concentrations, (3) 3D plots (also referred to as colorplots) graphing the mean diurnal pattern in the size distribution, (4) size distribution plots showing either the number- or volume-weighted size distribution at specific times, and (5) conditional probability function plots based on modeled data. Tabular performance statistics for the AMS model are shown in Table 8 and Table 9. The overall scatterplots of the 24-hour modeled particle number and 24-hour measured particle number for the 11 simulation cases (each case is the combination of a time period and monitor designation) are shown in Figure 19, together with a 1:1 line (black), 1.6:1 lines (blue), and 2:1 lines (orange). Long Beach simulations are shown in the figure by month; CHAPS simulations are shown by year. The original model goal was for 90% of the 24-hour modeled concentrations to fall within the 1.6:1 envelope. Of the 365 concentrations, 255 (70%) met this 1.6:1 criterion; 85% fell within the 2:1 envelope. Performance by this metric was better at the CHAPS sites than at the Long Beach sites (for which the percentages were 48% and 69%, respectively). Modeled CPC concentrations were adjusted downward, assuming diffusional losses in 2 m of tubing at 1-L/min flow. A key feature of Figure 19 is the better agreement found when the comparison was made with a 7-nm cutoff (i.e., the cutoff for CPC-based measurements, such as those for the October Long Beach simulations in the figure [top] and all points for CHAPS [bottom]) than with the 14-nm

Table 8. Model Skill Statistics Based on Paired Hourly Concentrations[a]

	Model Mean[b]							Mean of $N7_{model}/N7_{meas}$			Count[c]	
Simulation Run	All Hours	Hours with Measurements	Measured Mean	*R*	IOA	RMSE	*n*	Daytime	Night	All Hours	Within 3.2:1	Within 4:1
LB4_Sept	8,686	8,687	13,103	0.18	0.46	8,485	355	0.68	1.28	0.95	321	341
LB5_Sept	14,255	14,255	30,597	0.00	0.42	26,536	355	0.51	0.75	0.62	228	253
W2_Sept	8,695	8,679	14,112	−0.03	0.41	11,016	305	1.05	1.15	1.1	242	272
LB2_May	7,644	7,336	13,280	−0.15	0.38	9,072	77	0.51	0.86	0.67	62	68
LB3_May	6,681	6,131	16,135	0.12	0.43	13,500	159	0.41	0.6	0.49	107	129
W2_May	7,350	6,910	13,797	−0.10	0.38	11,211	180	0.51	0.98	0.72	135	158
LB4_Oct	17,544	17,545	24,426	0.25	0.54	15,151	305	0.71	1.09	0.88	273	292
LB5_Oct	31,797	31,798	41,423	0.07	0.43	34,929	305	0.96	1.16	1.05	217	245
LB6_Oct	11,559	11,435	26,582	0.04	0.43	22,177	294	0.41	0.7	0.54	199	236
LB8_Oct	16,153	16,489	24,316	0.22	0.51	14,814	286	0.74	0.94	0.83	264	275
W2_Oct	17,750	17,750	25,299	0.02	0.4	20,725	305	0.72	1.33	0.99	232	262
R01_G1	9,692	9,802	13,476	0.33	0.56	7,125	1,053	0.77	0.83	0.8	996	1,034
R02_G2	12,404	12,358	13,757	0.07	0.41	8,934	821	1.03	1.19	1.11	773	801
R03_G2	19,524	19,929	22,989	0.35	0.53	16,743	1,008	0.92	0.9	0.91	910	963
R04_G3	7,199	7,148	6,225	0.00	0.3	4,228	650	1.49	2.11	1.78	576	596
R05_G3	8,955	9,247	12,663	0.29	0.54	7,373	904	0.77	1	0.88	845	881
R06_G4	7,088	7,173	6,689	0.09	0.39	2,540	972	1.23	1.23	1.23	937	956
R07_G4	6,639	6,646	9,256	0.25	0.49	5,246	867	0.96	0.77	0.88	794	826
Total							9,201				8,111 (88%)	8,588 (93%)

[a] A larger collection of modeled–measured comparison statistics can be found in Appendix B.

[b] Modeled values are number concentrations in units of particle number/cm^3. These are the modeled values with 14-nm cutoff (N14) (for comparison to SMPS measurements) or the modeled values with 7-nm cutoff (N7) (for comparison to CPC measurements). Modeled N7 concentrations are corrected downward to account for modest instrument losses. N14 is not adjusted.

[c] These values refer to the count of cases where the modeled value is within a factor of 3.2 or 4 of a measured value, respectively.

Table 9. Model Skill Statistics Based on Paired 24-Hour Concentrations[a,b,c]

Simulation Run	*r*	IOA	RMSE	*n*	Count[d] Within 1.6:1	Count[d] Within 2:1
LB4_Sept	0.54	0.53	5,719	15	6	13
LB5_Sept	0.17	0.41	18,470	15	4	6
W2_Sept	0.24	0.42	6,417	12	6	9
LB2_May	−0.11	0.42	5,904	3	2	2
LB3_May	0.18	0.37	11,724	7	0	2
W2_May	0.04	0.35	6,670	7	3	3
LB4_Oct	0.60	0.61	8,812	13	9	11
LB5_Oct	0.38	0.54	14,574	13	9	12
LB6_Oct	0.21	0.41	16,407	12	3	5
LB8_Oct	0.66	0.57	9,029	12	9	11
W2_Oct	0.48	0.40	9,521	13	8	10
R01_G1	0.47	0.53	4,738	43	34	40
R02_G2	0.18	0.47	4,461	31	25	31
R03_G2	0.57	0.68	5,547	41	35	41
R04_G3	−0.11	0.26	2,642	21	17	18
R05_G3	0.13	0.43	4,630	35	25	33
R06_G4	0.03	0.36	1,459	36	33	35
R07_G4	0.42	0.53	3,228	36	27	30
All 24-hour periods	0.76	0.79	7,554	365	255 (70%)	312 (85%)

[a] A more comprehensive table of statistics can be found in Appendix B.

[b] Modeled values are number concentrations in units of particle number/cm^3. These are the modeled values with 14-nm cutoff (N14) (for comparison to SMPS measurements) or the modeled values with 7-nm cutoff (N7) (for comparison to CPC measurements). Modeled N7 concentrations are corrected downward to account for modest instrument losses. N14 is not adjusted.

[c] Statistics are based on the paired midnight-to-midnight hours with 16 or more paired hours in the 24-hour period.

[d] These values refer to the count of cases where the modeled value is within a factor of 1.6 or 2.0 of a measured value, respectively.

cutoff for SMPS-based measurements. A second feature of the figure is that the model, when its results fail to fall within the 1.6:1 envelope, typically underestimates the particle concentration. Given that particle sources from new particle formation and non-road sources were excluded from the current model, this is probably the correct direction in which to err.

Although not shown graphically, performance of modeled hourly concentrations compared with the originally established performance goals for hourly model–measurement comparisons are shown in Table 8 for particles bigger than 7 nm or 14 nm. At the outset of the study, we estimated that hourly concentrations were more difficult to simulate (than 24-hour concentrations) by a factor of about two, mainly as a result of uncertainty and unmodeled variability in emissions, traffic, and weather. Therefore, one performance goal was to simulate hourly concentrations to within a factor of 3.2 for 90% of the simulation hours. Overall, 8111 of 9201 simulated hours (88%) fell within this 3.2:1 envelope, and 93% of hours fell within a 4:1 envelope. Performance based on this metric was better for the CHAPS sites (93% and 97% within the 3.2:1 and 4:1 envelopes, respectively) than for the Long Beach sites (78% and 87% within the 3.2:1 and 4:1 envelopes, respectively). The poorest performances by this metric were for LB5, LB3, and LB6. Because near-road contributions can be relatively small compared with background concentrations, this performance metric was a fairly weak measure of model skill. Tables of simulation results for all the statistical parameters listed in the Statistical Methods and Data Analysis section can be found in Appendix B. These were prepared for 1-hour averaging, 24-hour averaging, and the evaluation of mean concentrations for each simulation.

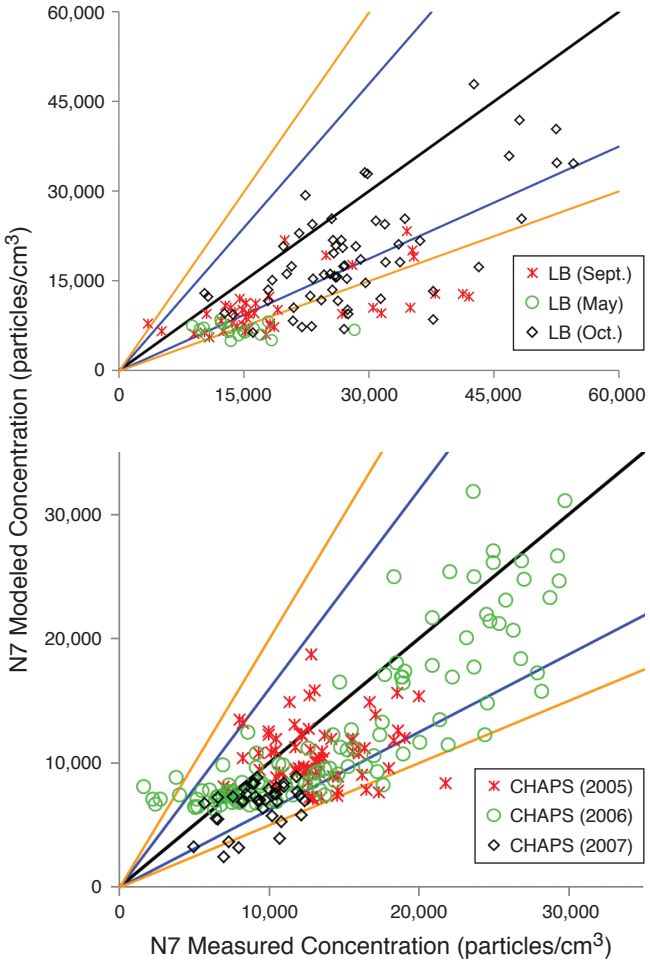

Figure 19. Scatterplots of 24-hour-averaged modeled and measured concentrations (in particles/cm^3 for particles greater than 7 nm [N7]) for all model runs, showing (top) the Long Beach (LB) runs by simulation month and (bottom) the CHAPS runs by simulation year. The 1:1 line (black) and the 1.6:1 (blue) and 2:1 (orange) lines indicate the concentrations that fell within these criteria. Months included in simulation years are August through December for 2005; January, February, July, August, October, and November for 2006; and January and February for 2007. Modeled CPC concentrations have been adjusted downward to reflect assumed diffusion sampling losses in 2 m of inlet tubing at a flow rate of 1 L/min.

The averaging across sizes and times involved in the 24-hour averaged scatterplot (Figure 19) did not adequately probe the model skill; a more detailed investigation of the model skill in predicting diurnal patterns and particle size is helpful. Figures 20 through 22 show diurnal patterns of particle number (including modeled and measured data) for many of the modeled sites. Figure 20 shows data based on SMPS measurements, using a 14-nm cutoff. For LB2 and LB3 simulations for May 2007, the comparison of modeled and measured particle number indicates that the model underpredicted particles > 14 nm during the morning peak travel time (5 to 10 AM), had insufficient variability in model concentrations, and, especially at LB3, had excessively low concentrations at night. The periods of underprediction at LB2 and LB3 corresponded to periods of observed onshore wind (i.e., from the south and from the port), which occur from about midnight until about 11 AM, when the offshore breeze is established (at least in the observed September weather). Figure 20 also shows diurnal profiles for LB4 and LB5 for September 2007; these again show model underprediction. The profiles for the LB4 site show some model overprediction at 10 PM to midnight, suggesting overly stagnant conditions in the model. The 5 to 9 AM particle increases were captured in the model qualitatively but not with nearly enough numbers of particles. After 10 AM at LB4, the model underpredicted at midday, when conditions became very favorable for dilution, and there were no secondary sources of particles and no prospect for photochemical growth of primary emission particles less than 14 nm to sizes greater than 14 nm.

Figure 21 shows comparisons of diurnal profiles in the CPC-based measurement model at four Long Beach sites (LB4, LB5, LB6, and LB8) (using a 7-nm cutoff) in October. The issue of model underprediction was not as evident as it was in Figure 20. Particle concentration trends till about 9 AM and after 9 PM were predicted fairly well at all the sites, whereas predicted midday concentrations were low at LB4, LB6, and LB8.

Figure 22 shows comparisons of diurnal profiles from the model with CPC-based measurements from the CHAPS sites G1 (November), G2 (September and January), G3 (July and November), and G4 (September and January). Qualitatively, the diurnal profiles and overall concentrations were predicted with more skill at the CHAPS sites than at the Long Beach sites (shown in Figure 21). For G2, the site with the highest traffic density, the model predicted a greater peak travel hour contribution than the measured values showed. At the remaining sites, the mean concentrations and diurnal profiles were predicted well in comparison with those of the Long Beach sites. Comparison of the values for G3 in July and November is interesting. The measured diurnal pattern was stronger in November; the modeled values matched this pattern. Also, in July the model predicted very little variability in afternoon particle concentrations. A low sample count was investigated as a potential cause of this lack of variability and ruled out — each box of Figure 22 represents on average of 46 days of data. The cause for the low variability in the afternoon modeled concentrations in the warm-season simulations for G3 was in fact caused by a combination of insufficient variability in the background number concentration, coupled with limited impact of traffic on particle

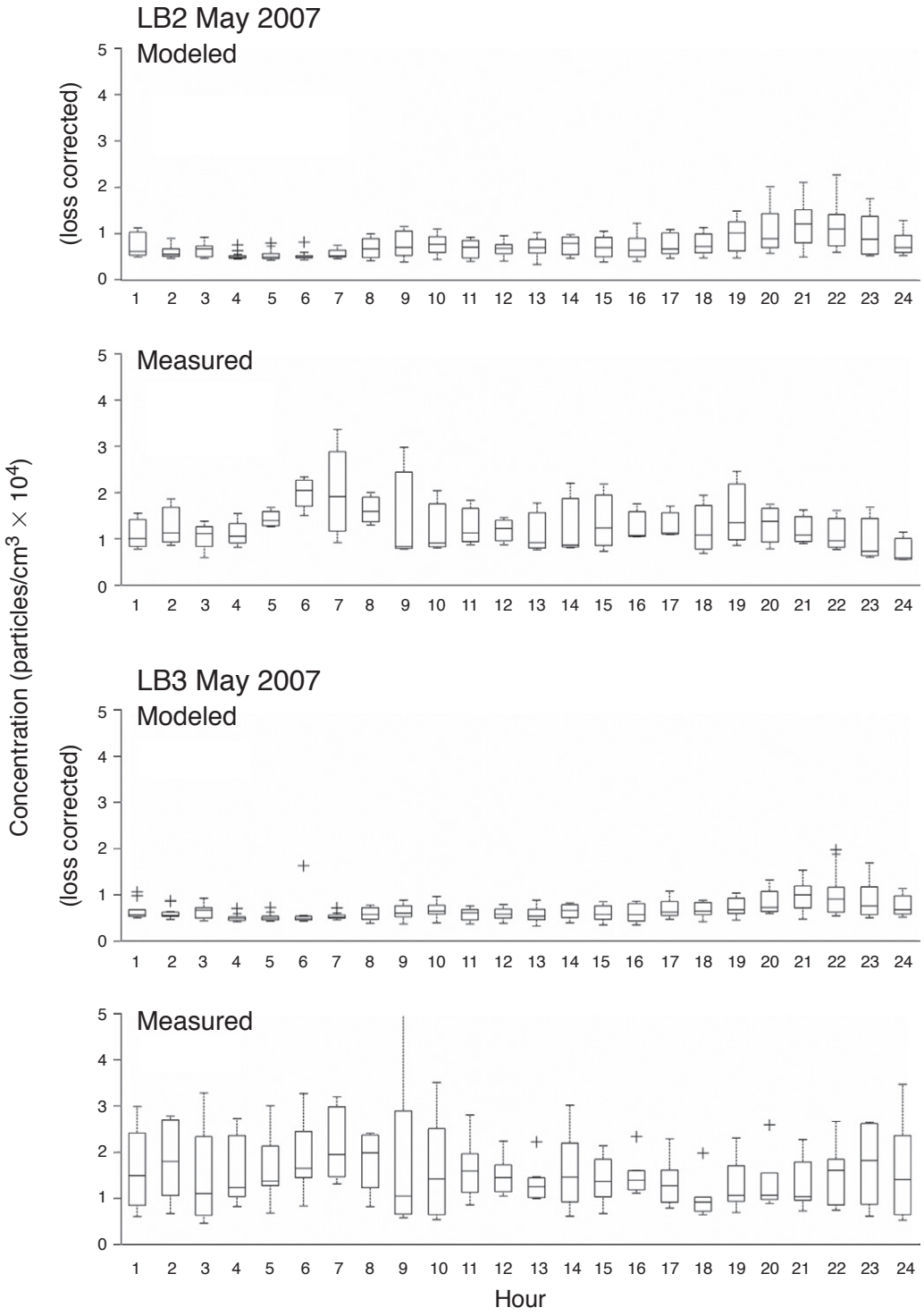

(*Figure continues on next page*)

Figure 20. Comparison of diurnal patterns in modeled and measured particle number concentrations (for particles greater than 14 nm) at LB2 and LB3 for May 2007 and LB4 and LB5 for September 2007. Boxes denote 25th percentile to 75th percentile of values, with central horizontal line as the median; whiskers extend vertically to the most extreme points within 1.5 interquartile range of the 25th and 75th percentile values, respectively. Outliers (beyond the whiskers) are plotted with + symbols.

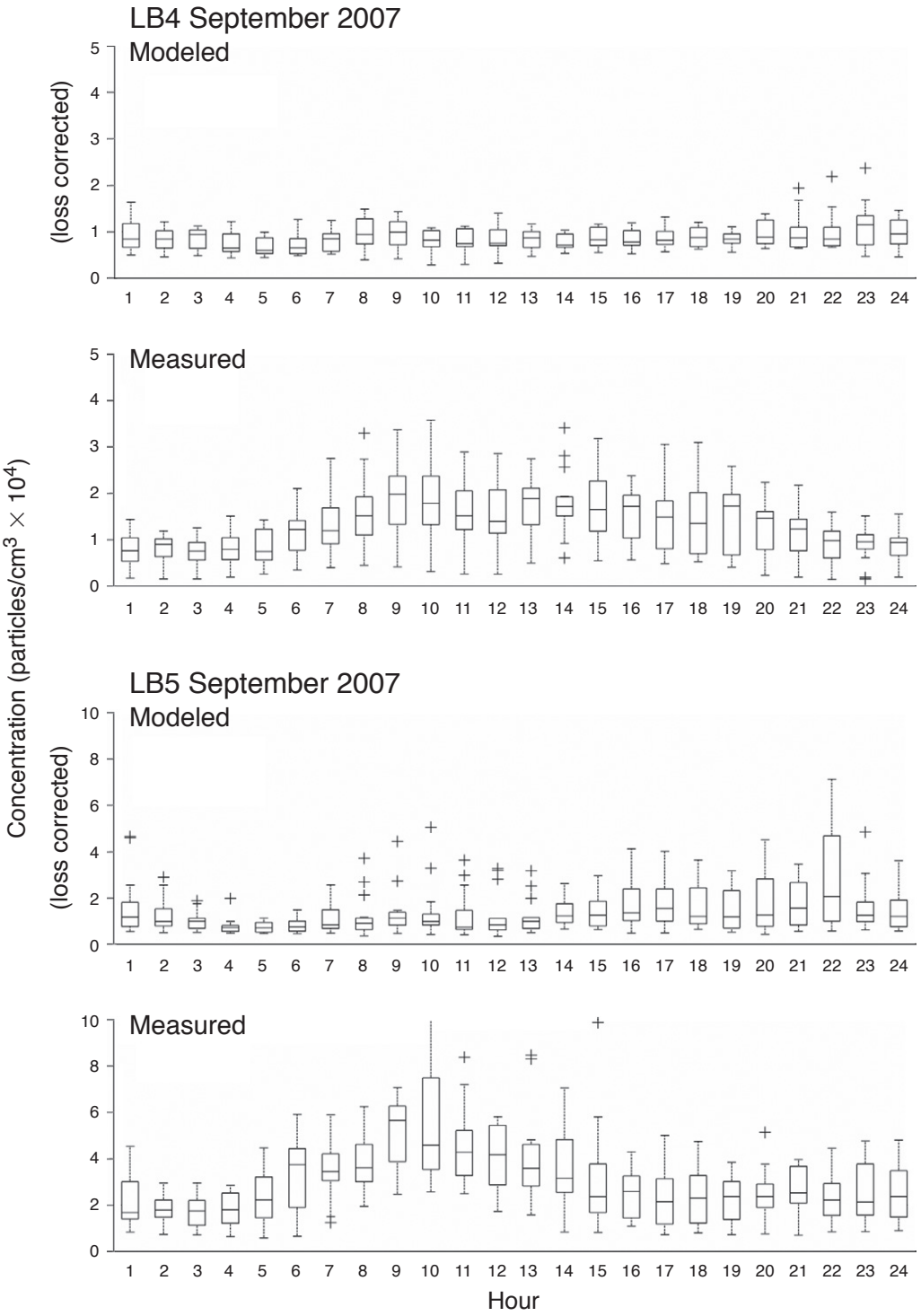

Figure 20 (*Continued*).

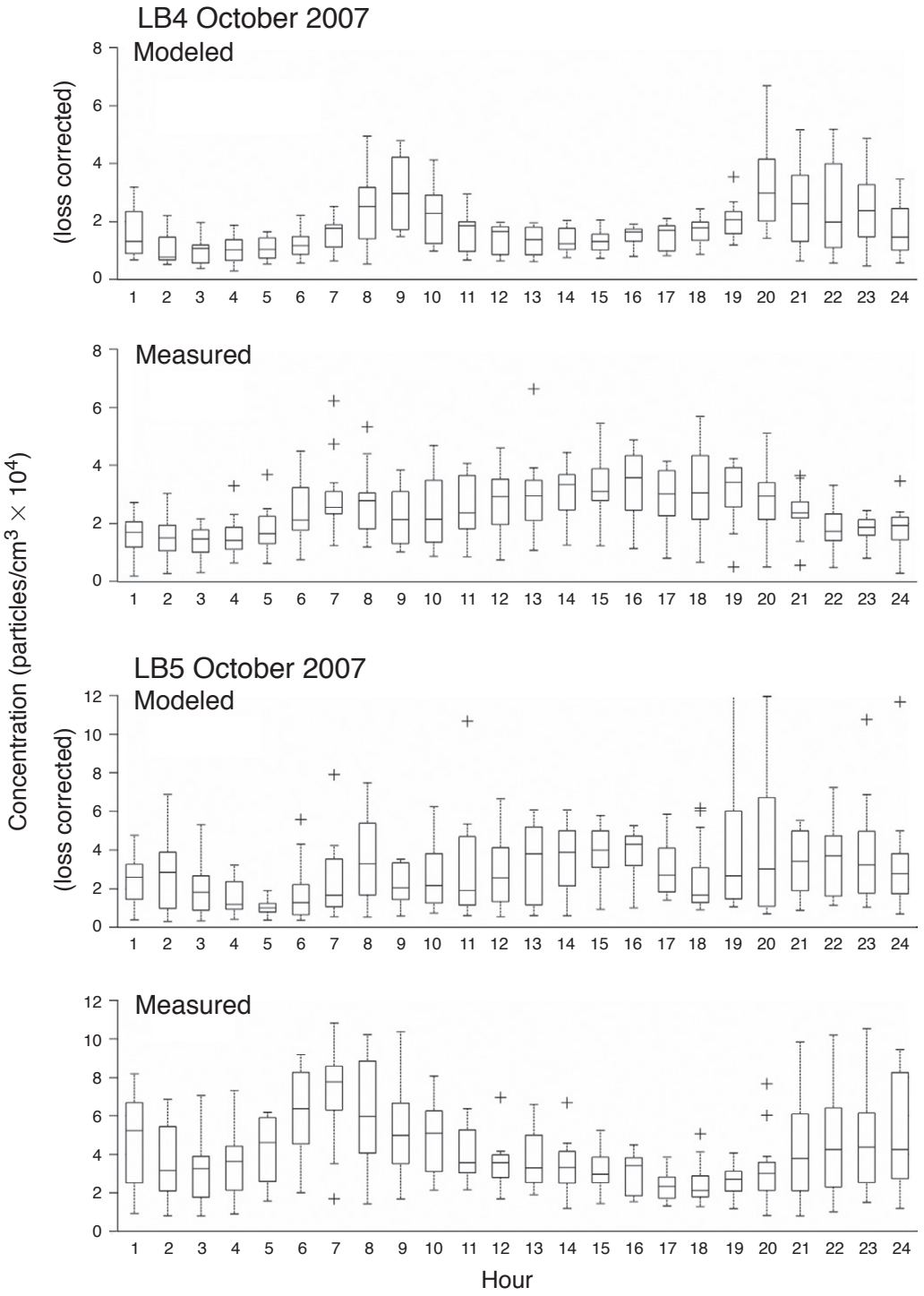

(*Figure continues on next page*)

Figure 21. Comparison of diurnal patterns in modeled and measured particle number concentrations (for particles greater than 7 nm) at LB4, LB5, LB6, and LB8 for October 2007. Modeled particle concentrations have been adjusted downward to reflect assumed diffusion sampling losses in 2 m of inlet tubing at a flow rate of 1 L/min. See caption of Figure 20 for details of boxplots.

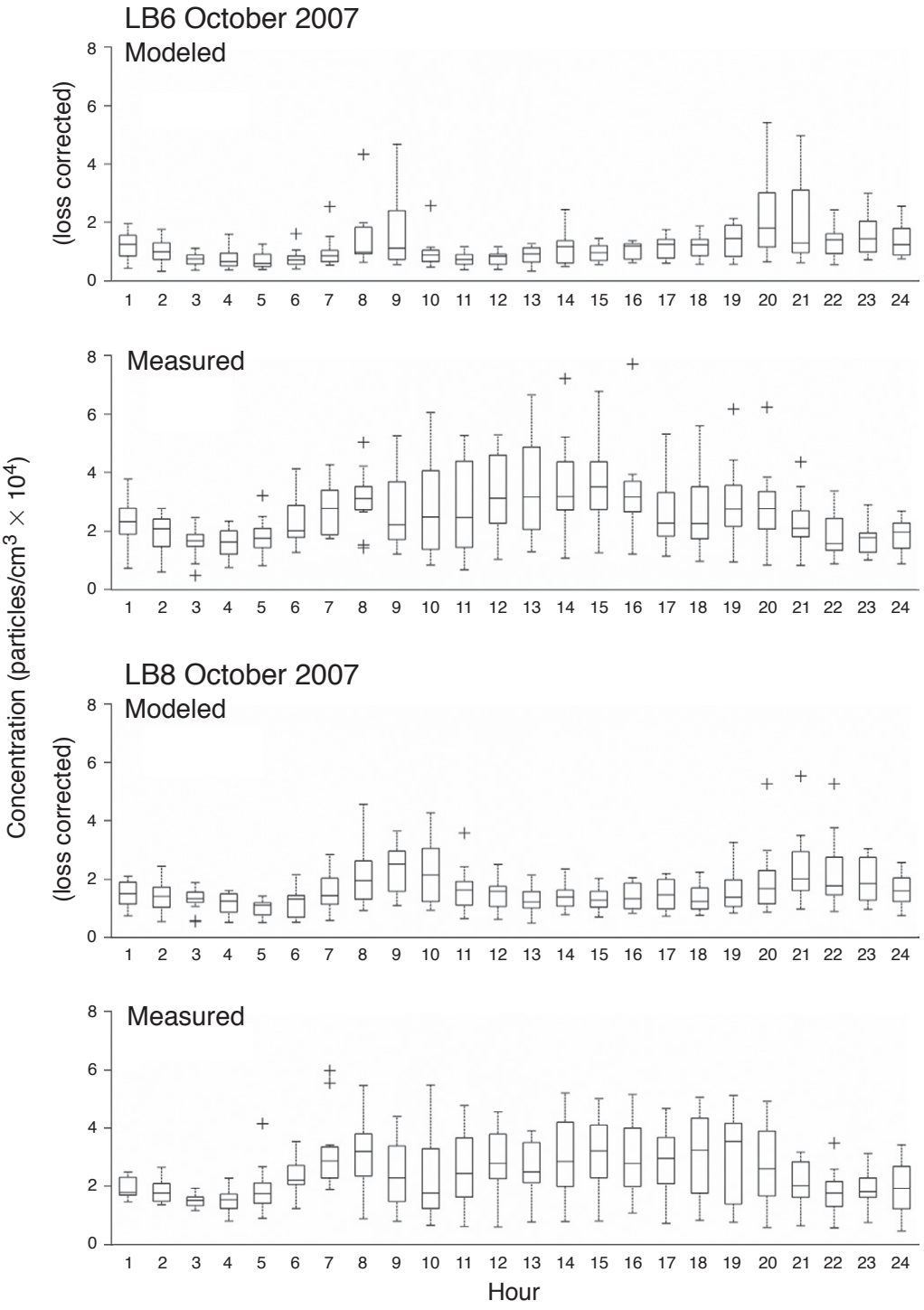

Figure 21 (*Continued*).

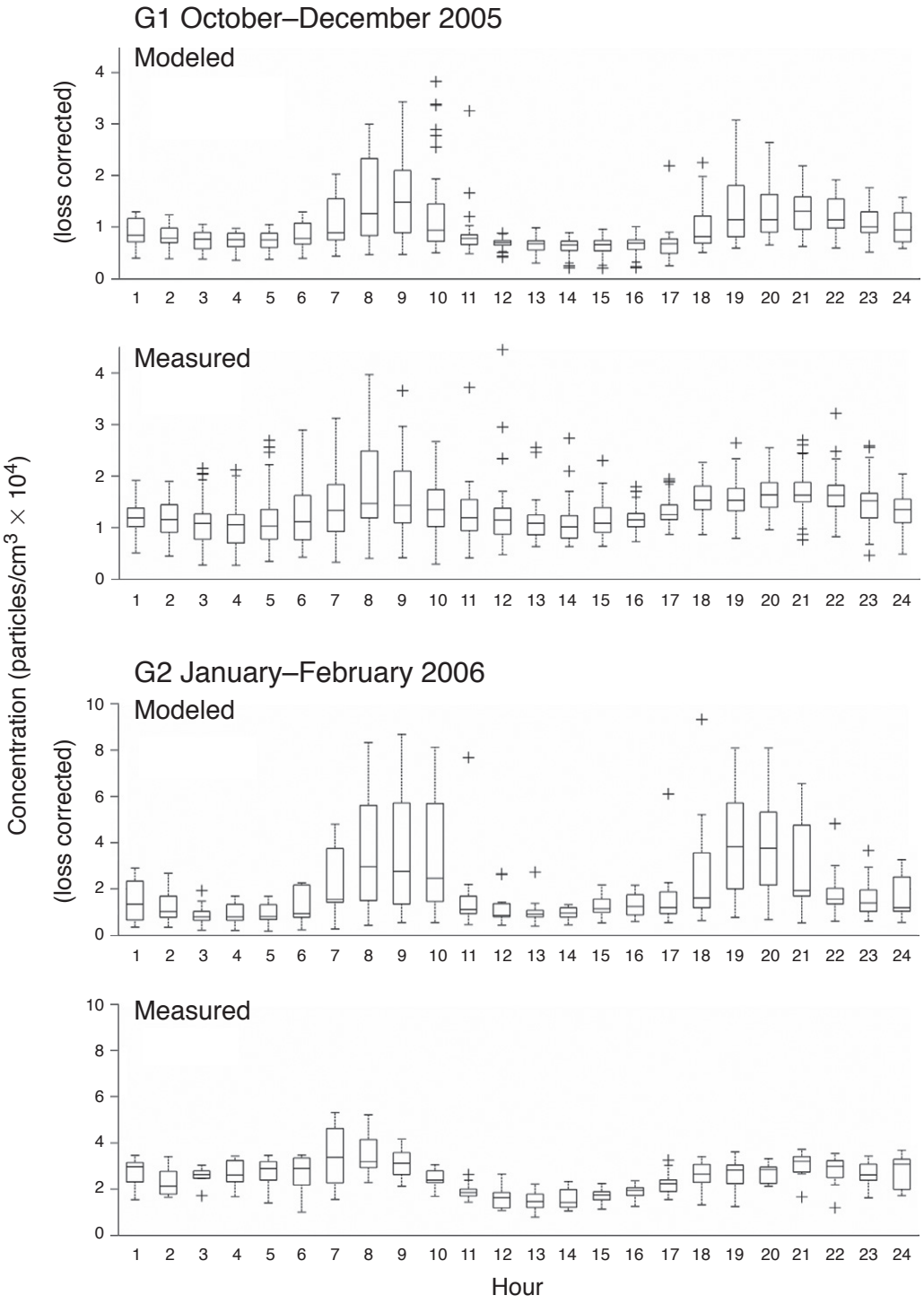

(*Figure continues on next two pages*)

Figure 22. Comparison of diurnal patterns in modeled and measured particle number concentrations (for particles greater than 7 nm) at G1, G2, G3, and G4. Time periods range from 2005 to 2007 and are indicated on figure. Modeled particle concentrations have been adjusted downward to reflect assumed diffusion sampling losses in 2 m of inlet tubing at a flow rate of 1 L/min. See caption of Figure 20 for details of boxplots.

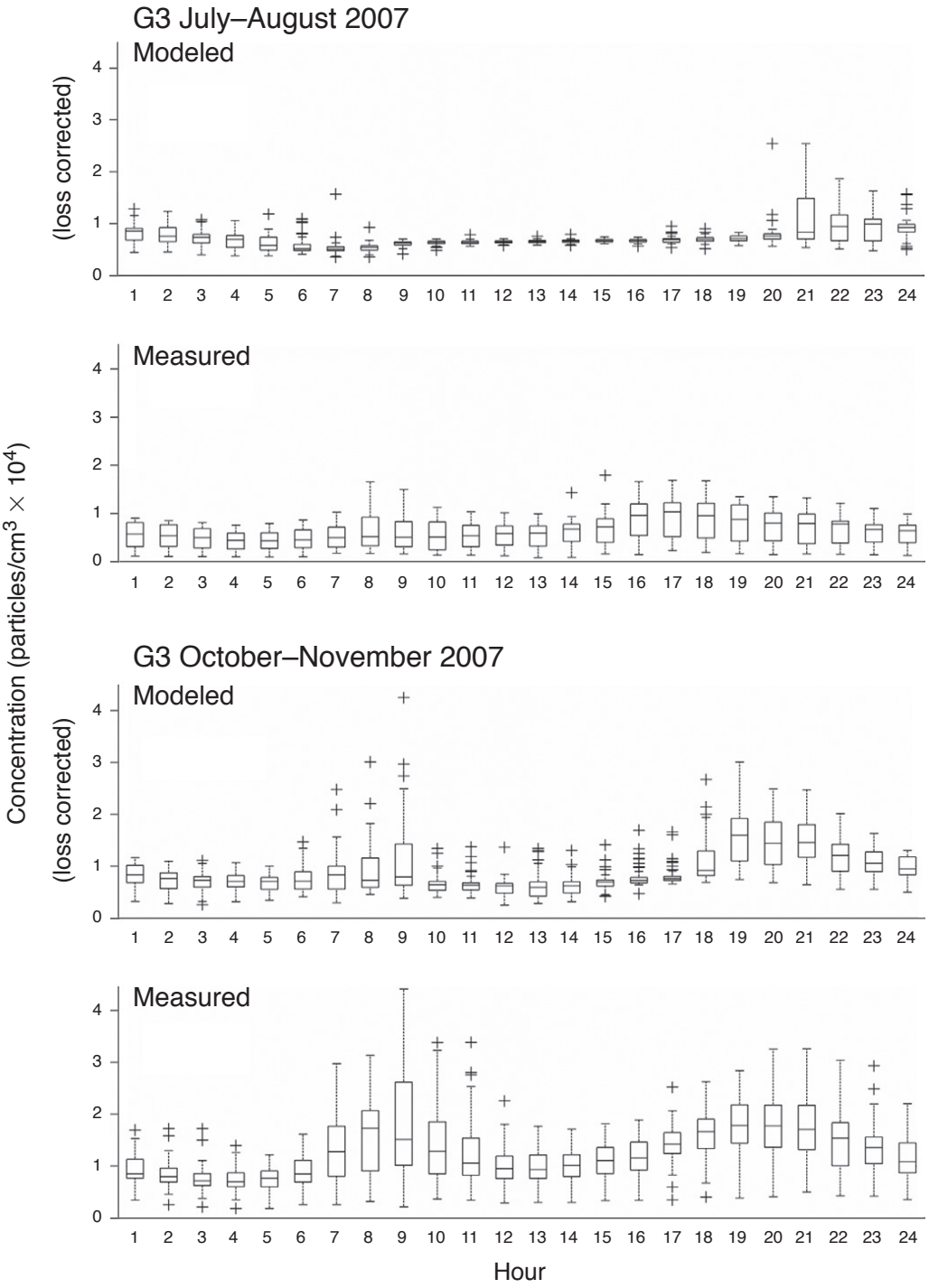

(*Figure continues on next page*)

Figure 22 (*Continued*).

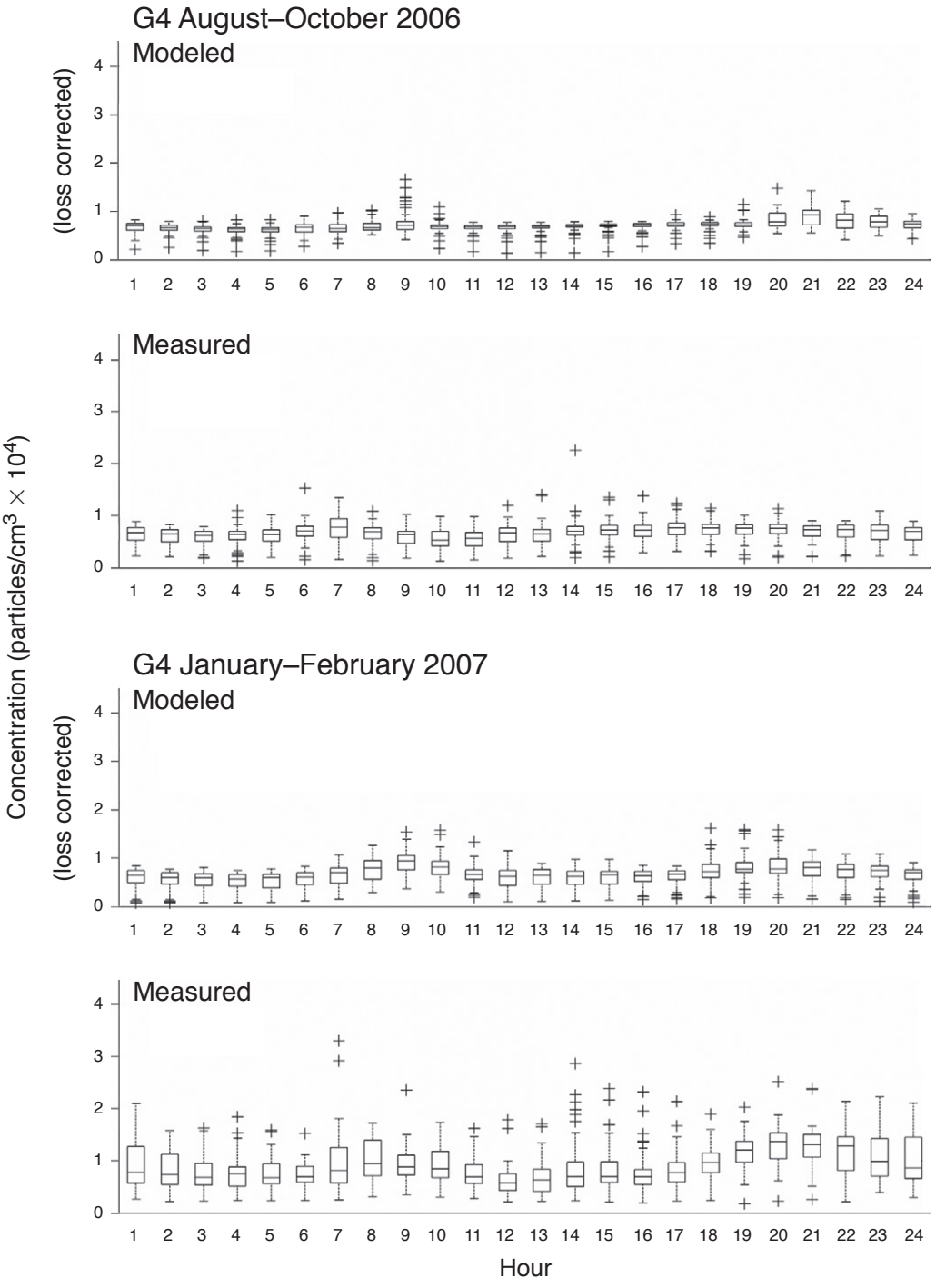

Figure 22 (*Continued*).

number in the afternoon (averaging 610/cm^3 and 1456/cm^3 for N7 particles above background at 2 PM in the warm- and cold-season simulations, respectively).

Additional Materials 1 (available on the HEI Web site at *www.healtheffects.org*) shows colorplots of measured particle number size distributions for the LB4 site averaged as a function of time of day and particle size across all paired modeled and measured hours. Both linear and log scales are shown, and the color scale was set for maximum visualization of the distribution. The peak color, for example, corresponds to the peak measured size distribution, which was at 24 nm at 2 PM at 30,010/cm^3. The key feature in the measured size distribution was an increase in particle number in a broad range of sizes from about 20 to 90 nm during the morning rush hour, which is characterized by south and southwesterly winds and low wind speeds — ideal for transporting particles from Anaheim Street, the port, and class 1 roads, including I-710, located to the south and southwest of the receptor. The transition in the size distribution at noon was probably related to the shift to an afternoon offshore wind, which is suitable for transporting particles from freeways, arterials, and local streets (both near and far from LB4) located to the north of the site.

Additional Materials 2 (available on the HEI Web site at *www.healtheffects.org*) shows colorplots of particle number size distributions for the LB4 site, comparing the average observed size distribution, modeled size distribution including particle losses, and modeled size distribution without particle losses. Concentrations greater than the measured maximum (30,010/cm^3) are all represented by the same deep red color. The colorplot for the model shows that the simulation lacked several qualitative features that would be desirable in a highly skilled simulation. First, the increase in accumulation-mode particles (100–500 nm) from 6 AM to 12 noon is not reproduced well, suggesting insufficient emissions in this size range or too much dilution. Second, the modeled distribution is bimodal, with modes at about 14 nm and 80 nm, whereas the measured distribution is unimodal (on average), with a single peak between 20 and 40 nm. Finally, the qualitative difference between morning and afternoon in the observations was not reproduced in the model.

Additional Materials 3 (available on the HEI Web site at *www.healtheffects.org*) shows colorplots of measured particle number size distributions for the LB5 site in September 2007. The colorplots shown are not for individual days but have been averaged across all model–observation pairs with SMPS data. Concentrations are scaled so that the color scale saturates at the observed maximum, which is 77,090/cm^3, occurred at 9 AM, and was for 20-nm particles. The LB5 observations were more variable from hour to hour than the LB4 observations, and clear morning and afternoon distributions (as seen in Additional Materials 1) were not as apparent. The variability compared with that of the LB4 site might have to do with the sensitivity of concentrations' detailed flow patterns and the nature of the switch from southerly to northerly winds in late morning. In other words, the exact details of how this shift occurs might cause variability in the morning concentrations.

Additional Materials 4 (available on the HEI Web site at *www.healtheffects.org*) shows colorplots of measured and modeled particle number size distributions for the LB5 site. Additional Materials 3 and 4 both show the underpredictions of the model in a wide range of sizes, from 14 to 500 nm range. Furthermore, the observed pattern has more in common with the diurnal pattern of the HDV fraction (Figure 9), whereas the model is more balanced between the influence of HDV and LDV.

Figure 23 and Figure 24 show modeled and measured number volume size distributions for the LB4 and LB5 sites at 3 AM, 7 AM, 12 noon, and 7 PM, providing some quantitative data corresponding to those times as portrayed in the colorplots. Like Additional Materials 2, they show that the model underpredicts at particle sizes greater than 14 nm during many time periods. The importance of and uncertainties introduced by losses of particles with diameters less than 20 nm and, more significantly, less than 10 nm are highlighted by Figure 23. The improved agreement when using a diameter greater than 7 nm can be explained, because the model compensates for the underprediction of particles with diameters greater than 14 nm with a large peak in the 7–14-nm range. This peak is consistent with the Minnesota on-road measurements (Kittelson et al. 2006a,b), but the near-road measurements in Long Beach as graphed in Figure 23 suggest that, either through atmospheric processing or because of different fleet mixes and operating conditions, the peak associated with traffic is more broadly spread. At the Long Beach sites (LB4 and LB5), the size distribution of particles smaller than 14 nm was not measured; therefore, the consistency of the large peak at 7 nm in the emission factors (Figures 14 and 15) for the ASM model with observations is difficult to assess. The higher instrumental number concentration readings using CPCs at LB4 and LB5 versus SMPS measurements (Table 6) provide evidence of a substantial particle population between 7 and 14 nm, but quantitative assessment of the size distribution for particles smaller than 14 nm is not feasible with the evaluation data chosen from Long Beach.

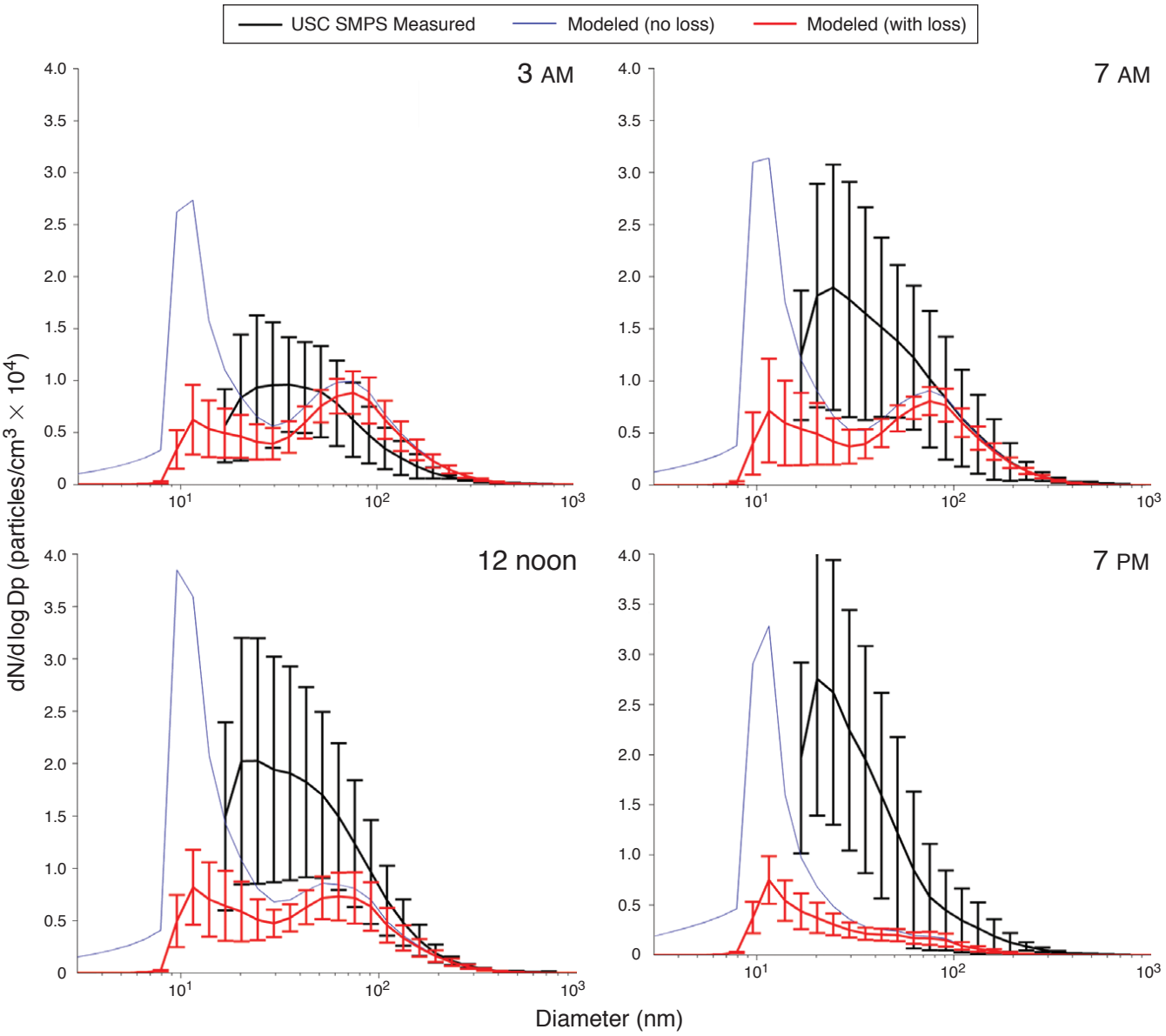

Figure 23. Comparison of modeled and measured number size distributions for the LB4 site at four selected times of day, averaged during the period September 1–15, 2007. Error bars correspond to one standard deviation.

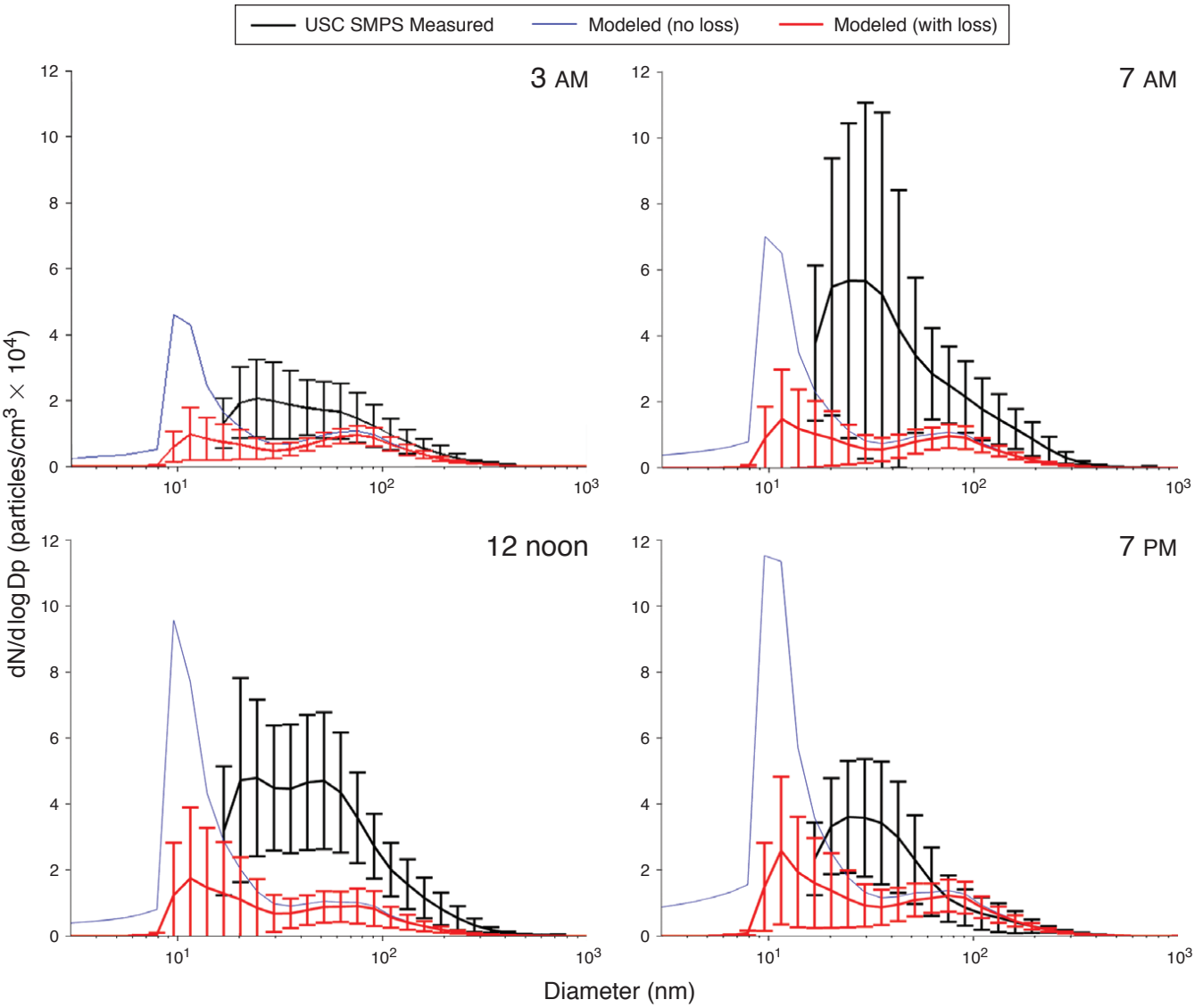

Figure 24. Comparison of modeled and measured number size distributions for the LB5 site at four selected times of day, averaged during the period September 1–15, 2007. Error bars correspond to one standard deviation.

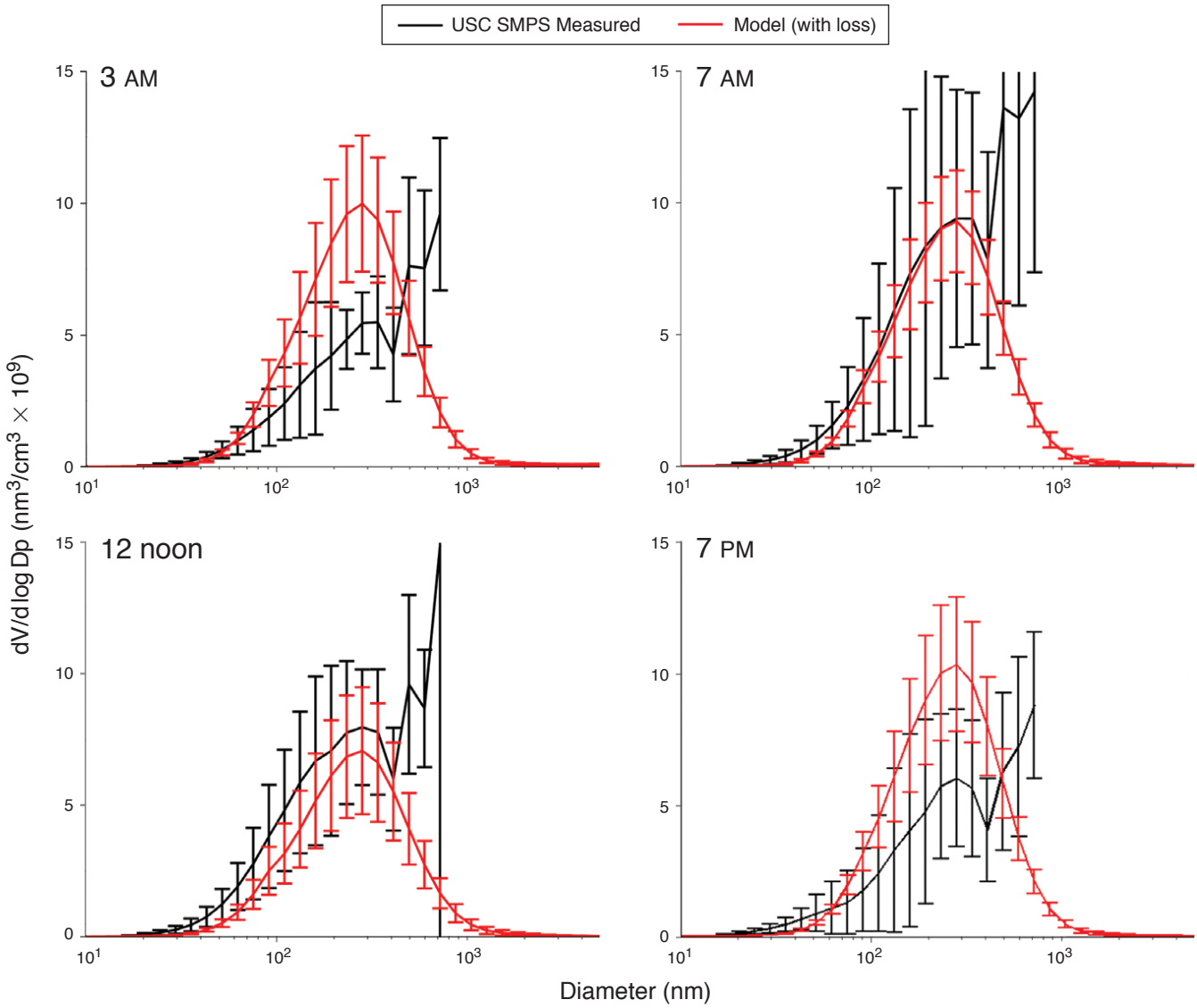

Figure 25. Comparison of modeled and measured volume size distributions for the LB4 site at four selected times of day, averaged during the period September 1–15, 2007. Error bars correspond to one standard deviation.

Modeled volume size distributions are compared to measured volume size distributions in Figure 25 (LB4) and Figure 26 (LB5). The LB4 volume size distribution matches the observation mode, which occurs between 200 and 400 nm, but overpredicts particle volume at night (3 AM and 7 PM). The observations indicate a possible second mode in the volume distribution (increasing values of the volume distribution beginning at 400 nm), which is not captured by the model. This disagreement in the volume distribution at sizes greater than 400 nm is not a major concern for two reasons. First, the current ASM model does not model coarse particles other than those in the background size distribution (Figure 6) and those in vehicle emissions (Figures 14 and 15). Second, SMPS measurements alone are a weak constraint on the volume size distribution at sizes greater than 500 nm (Khlystov et al. 2004).

The LB5 volume distributions are consistent with the conclusions drawn from the analysis of number distributions (Figure 24 and Additional Materials 4 available on the Web at *www.healtheffects.org*) — that the ASM model underpredicts particles larger than 14 nm during periods of the highest HDV influence.

Figure 27 shows modeled conditional probability plots of modeled number concentrations relative to wind direction

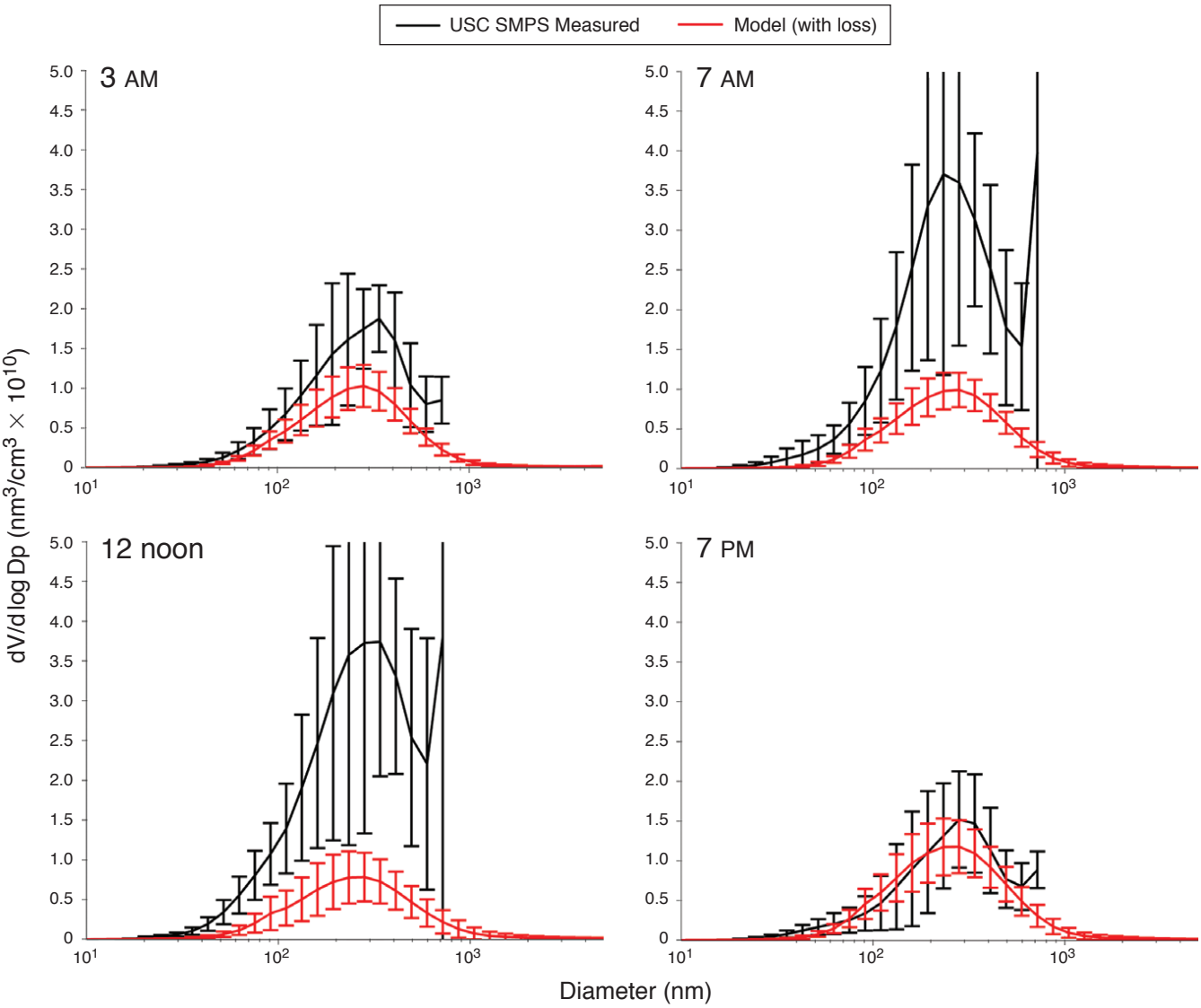

Figure 26. Comparison of modeled and measured volume size distributions for the LB5 at four selected times of day, averaged during the period September 1–15, 2007. Error bars correspond to one standard deviation.

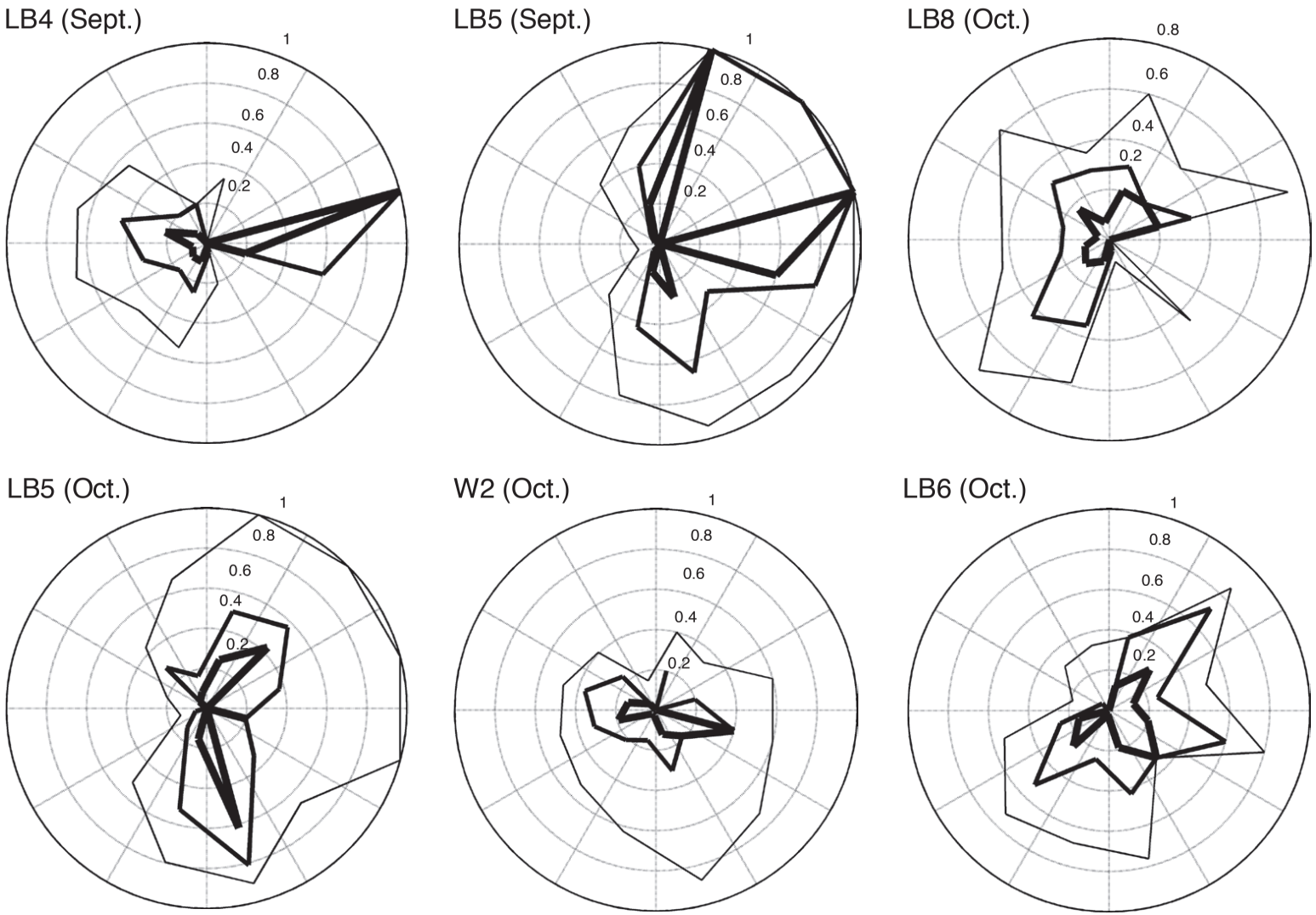

Figure 27. Conditional probability plots of modeled data for the sites and months for which measured data were given in Figure 12, showing the dependence of particle number concentrations on wind direction. Again, north is at the top. The distance of a plot line from the center of the plot indicates the conditional probability — ranging from zero at the center to 0.8 or 1 at the circumference — of the wind from a given direction yielding a particle concentration that exceeded a given concentration threshold. The thin lines show the results of using the sample median concentration as the threshold, the medium-thick lines show the 75th percentile as the threshold, and the thick lines show the 90th percentile as the threshold. Threshold values are the same as those of Figure 12.

for sites and times corresponding to those of the measured conditional probability plots shown in Figure 12. Some features — such as the peak concentrations at LB4 and LB8 that occur when the wind is from the west — can be seen in both figures. However, there are several differences. One, for example, is that the modeled LB5 plot — which looks as expected, given the model assumptions — shows increased concentrations with winds from the north or south, parallel to I-710, and increased concentrations for all winds from the east (because of I-710), whereas the measured LB5 plot does not have this sort of structure and even shows peak concentrations during times when the wind is from the west. This difference might reflect difficulties in measuring wind direction during calm periods near a freeway or it might indicate that the wake of the highway extends to the measurement site and mixes particles there regardless of the wind direction. The measured conditional probability plots for the W2 and LB6 sites have features that are consistent with the influence of port emissions.

Impact of Using Measured Meteorologic Data

One-week simulations were repeated for LB4 and LB5 using measured wind speed and direction (together with other meteorologic input parameters from the WRF model). The results of these simulations were inconclusive. Although specific time periods showed improved agreement, overall performance statistics showed mixed results. For LB4, the modeled mean N14 number concentration decreased by 13% as the frequency of west winds (bringing particles from I-710) decreased. The modeled mean for N14 was already low; accordingly the error and bias statistics deteriorated somewhat while the IOA improved slightly. For LB5, the decrease in the frequency of west winds and the increase in the frequency of north and south winds that resulted from using measured wind direction increased the mean modeled particle concentration and improved the performance statistics based on model bias (e.g., the mean normalized bias changed from −0.28 to 0.004), but decreased IOA slightly.

Sensitivity Calculations

As an example of the ability of the ASM model to quantify sensitivity of concentrations to emissions, tests were performed of the sensitivity of each receptor to LDV traffic, HDV traffic, and road class. Sensitivity was quantified as the fractional reduction in concentration divided by the fractional reduction in emissions. Sensitivity calculations were made by changing the emission variable (e.g., a simulation made with a 20% reduction in base-case emissions) and comparing this with the base-case simulation. A sensitivity value of 1 means that a 20% emission reduction resulted in a 20% concentration reduction; a sensitivity value of 0.1 means that a 20% emission reduction resulted in a 2% concentration reduction. More specific sensitivity cases where emissions are perturbed as a function of time, location, or other factors can be simulated with the ASM depending on the specific project need. Sensitivity to model settings, weather, and aerosol size distributions is also easily calculated using the ASM.

As shown in Figure 28, the sensitivity of modeled overall particle number (for particles above the 7-nm cutoff) to all types of traffic ranged from 0.87 at the most traffic-affected site to 0.28 at the least traffic-affected site. The figure also shows the sensitivity of the increment above background for these particles. The sensitivity of modeled particle volume is shown in Figure 29; the sensitivity of modeled particle volume ranged from 0.01 (G3 and G4) to 0.32 (LB5). The influences of LDV emissions versus HDV emissions on concentrations are shown in Figure 30 (for number concentration) and in Figure 31 (for particle volume).

The sensitivity simulations shown in Figures 28 through 31 suggest that HDV and freeway or arterial traffic had a greater influence on modeled particle number and traffic-induced particle mass at the Long Beach sites than did LDV or other road types. At the more residential CHAPS sites, conversely, LDV and local traffic had a greater influence on modeled particle number; freeway emissions had the greatest influence on traffic-induced particle mass and LDV and HDV were both influential.

Model Time Series Suitable for Evaluation Against CHAPS Health Endpoints

Figure 32 shows a 45-day model time series of the above-background particle concentrations (for particles above the 7-nm cutoff) and particle volumes (for particles below 2.5 μm) at the G1 receptor. A strong diurnal pattern is evident for both particle number and volume. The 24-hour running average shows much less temporal variability. A weekday–weekend signal in the model is apparent. Similar time series were calculated for all receptor sites, representing the modeled estimates of the impact of on-road emissions within 4 km of the receptor. Time series with other variables, such as concentrations corrected for particle losses or concentrations within specific size intervals, can also be calculated.

Model Runtimes

Using the CHAPS-domain mode simulations for benchmarking, a 1-hour simulation at one receptor required 11.4 seconds on average on our 8-core workstation. Times were somewhat longer on the 2-core workstation. Scaling this to a simulation of hourly concentrations for one month at one

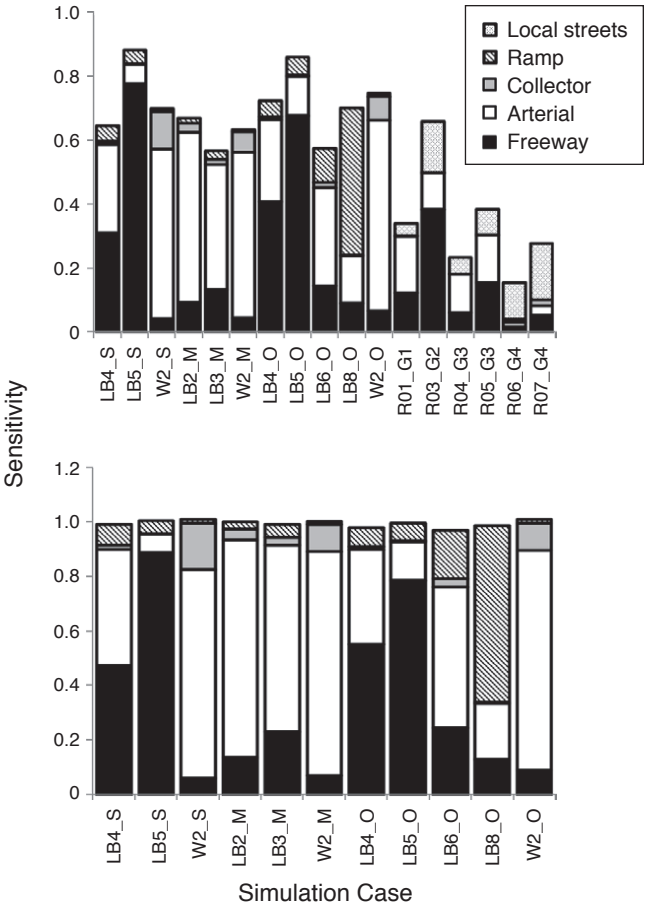

Figure 28. The sensitivity to various types of traffic of (top) modeled particle number concentrations (for particles greater than 7 nm) and of (bottom) the increment of these concentrations above background, caused by vehicle emissions within 4 km of the receptor. Sensitivity is measured as the fractional reduction in concentrations divided by the fractional reduction in road-class-specific emissions (e.g., a sensitivity value of 1 [top] would indicate that a 20% emissions reduction resulted in a 20% concentration reduction of the modeled concentration). Sensitivities (bottom) apportion the above-background increment in particle number to the different emission types within 4 km of the receptor. A sensitivity value of 1 (bottom) occurs when a 20% emissions reduction resulted in a 20% reduction in the increment of particle number concentration above a background-only case with no local traffic emissions. For the Long Beach simulations (sites LB2 through LB6, LB8, and W2), emissions from freeways (road classes 1 through 3) were treated as separate from emissions from ramps (class 8), and emissions from local roads were not included. For the CHAPS simulations (sites G1 through G4), local roads were included, and ramps were included with freeways. The sensitivity analyses were based on a 168-hour (1-week) simulation period. Each bar is for a different site/time period combination (see Table 6 for more details about sites and simulation time periods).

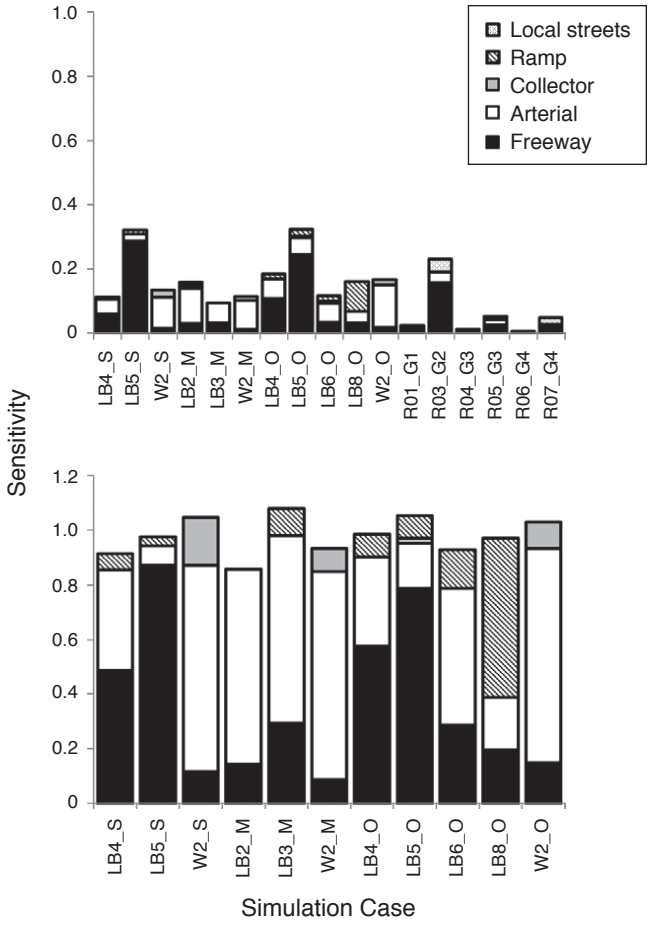

Figure 29. The sensitivity to various types of traffic of (top) modeled particle volume concentration (for particles less than 2.5 μm) and of (bottom) the increment of these particle volumes above background, caused by vehicle emissions within 4 km of the receptor. Caption of Figure 28 provides details on sensitivity measurements and simulations.

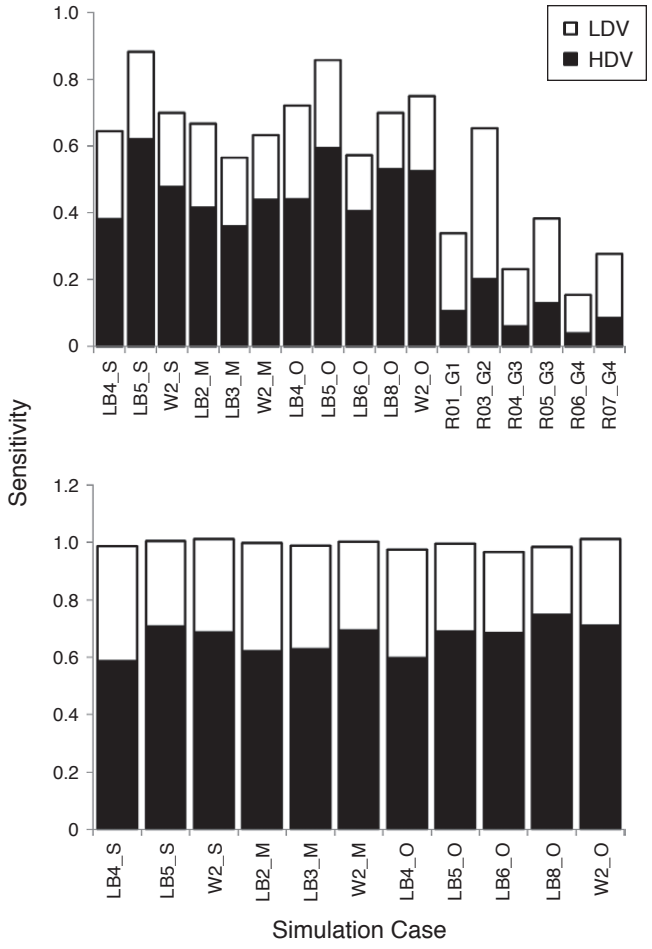

Figure 30. The sensitivity to LDV and HDV emissions of (top) modeled particle number concentrations (for particles greater than 7 nm) and of (bottom) the increment of these concentrations above background, caused by LDV and HDV emissions within 4 km of the receptor. Caption of Figure 28 provides details on sensitivity measurements and simulations.

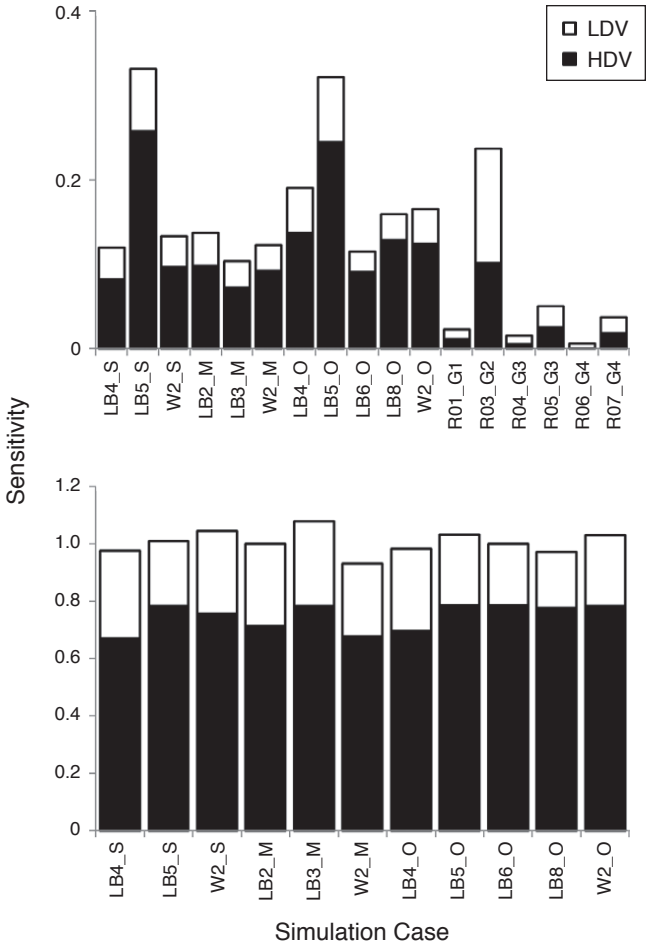

Figure 31. The sensitivity to LDV and HDV emissions of (top) modeled particle volume concentration (for particles less than 2.5 μm) and of (bottom) the increment of these particle volumes above background, caused by LDV and HDV emissions within 4 km of the receptor. Caption of Figure 28 provides details on sensitivity measurements and simulations.

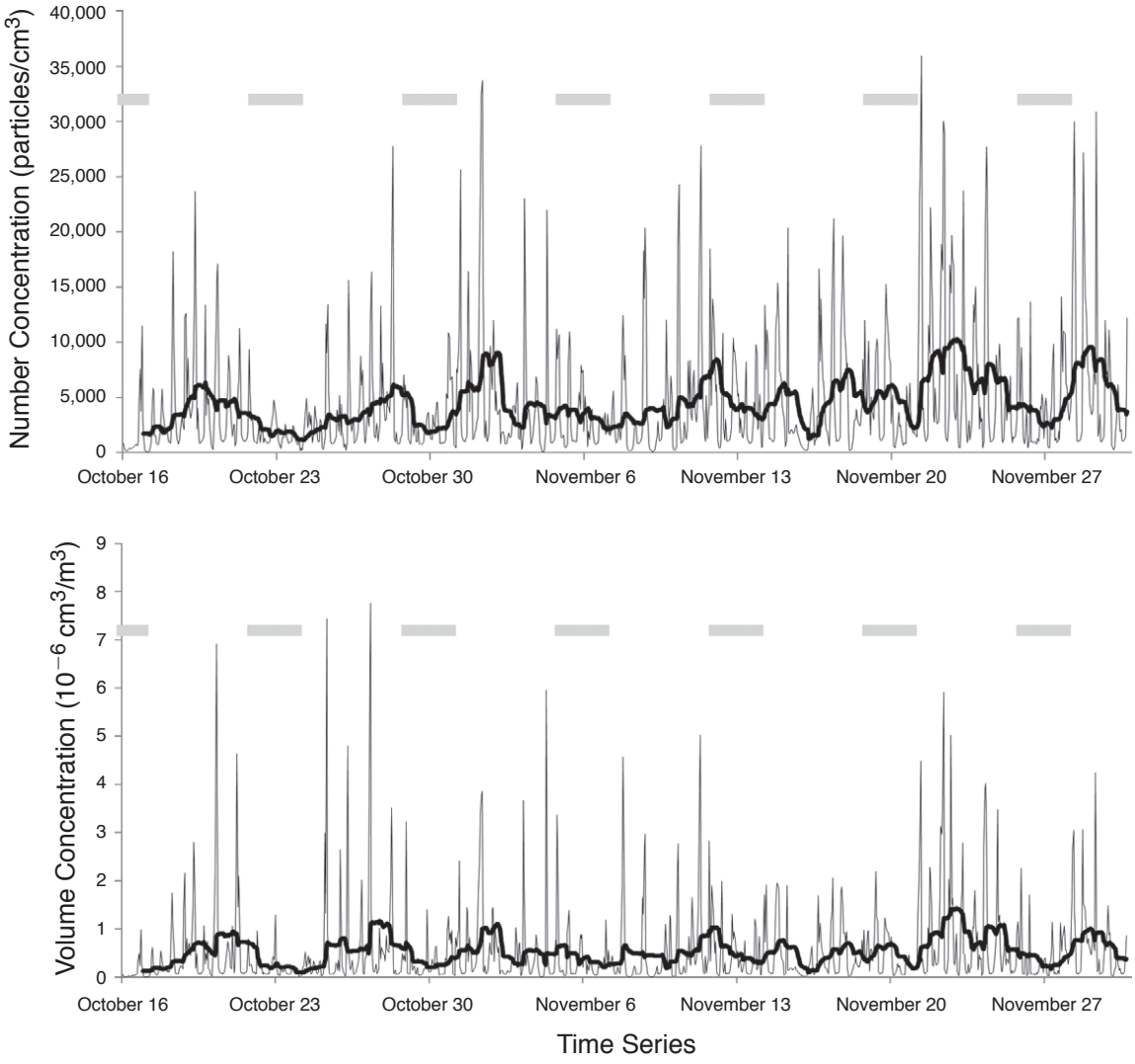

Figure 32. Forty-five-day time series of above-background modeled particle (top) number concentrations and (bottom) volume concentrations, showing the impact of traffic emissions within 4 km of the G1 site. Number concentrations shown in top panel are for particles greater than 7 nm (with background concentration subtracted). Volume concentrations shown in bottom panel are for particles smaller than 2.5 μm. Thick lines indicate 24-hour running averages. Gray bars near the top of each panel indicate weekend hours. Data are from the Run01_G1 simulation for the 45 days from October 16 to November 29, 2005. Multiplying the volume by the particle density gives the $PM_{2.5}$ mass, assuming spherical particles.

receptor, the run time was just over 2 hours. In cases when isolation of the traffic impact on concentration (the increment over background) was needed a second simulation of background size distribution with no emissions was required as well. Without the emissions calculation, the simulation ran more quickly; a 1-hour simulation, for example, required 4.1 seconds. The most computationally demanding subroutines of the simulation were the road–parcel intersection calculation (59% of runtime), the solution of equation 1 (34% of runtime), and the management of the parcels (2% of runtime). All other processes (reading and writing files, outputting to the screen, and housekeeping going into and out of the main computational routines) required 5% of the runtime. Simulation performance for the Long Beach sites was similar (an average runtime of 11.7 seconds per simulation hour per receptor), with two important differences. The spatial resolution was 10 m instead of 50 m, and the domain did not include local roads. These factors offset one another. The integration of aerosol dynamics (equation 1) required 56% of runtime, and the road–parcel intersection calculation was reduced to 39% of runtime. Further optimization of runtime is entirely feasible, by coding the intersection search in FORTRAN instead of Matlab, by reducing the number of road segments and allowing nonrectangular polygons to represent curved roads, and by having a gridded inventory of road emissions for use (instead of precise overlap calculations) when parcels are distant from the receptor.

DISCUSSION AND CONCLUSIONS

As described in the Introduction, a model such as the ASM has several potential applications. The degree to which the ASM might be suitable for these applications can be gauged by considering it in the light of our evaluation against the measured HCMS and CHAPS data. The target applications for the ASM include (1) providing decision support for construction and transportation infrastructure projects, (2) extending the usefulness of UFP-monitoring data through enhanced interpretation of spatial gradients and source–receptor relationships, and (3) producing model-based concentration estimates for health studies for which UFP-monitoring data are sparse, impractical, or unavailable.

SUMMARY OF MODEL SKILL FOR THE ASM

The ASM, a vertically resolved aerosol model, was constructed, tested, and applied. The ASM simulates concentrations at receptors using a slab of parcels that advect from ~4 km upwind to a receptor, filling with emissions as the parcels pass over roads. The model does not take into account topography and does not resolve complex terrain, buildings, roadway barriers, or other similar features. It uses a fixed sectional representation for aerosols. The model simulations use 50 size bins lognormally spaced, from 1 nm to 10 μm. All parcels are assumed to move in the direction and speed of the mean hourly surface wind evaluated at 10 m elevation. By gradient-transfer theory, particles exchange horizontally and vertically between parcels. To reduce the computation time, algorithms were included for variable step sizes of the parcels and for the subdivision of large parcels into smaller ones as needed to meet user-specified resolution goals. Input particle-number emission factors were developed from on-road and tunnel traffic measurements and for LDVs and HDVs in cruise and acceleration modes. For a 7-nm cutoff, the number emission factors developed ranges from 1.41×10^{15} to 16.5×10^{15} particles/kg fuel. Measurements on Minnesota highways in summer 2002 (Kittelson et al. 2006a,b) were influential in the determination of the input size-resolved emission factors. These emission factors had large fractions of particle numbers for particle sizes less than 20 nm; the particle numbers became even larger when corrections for particle losses and CPC-to-SMPS ratios were made. Traffic activity was derived mainly from the SCAG 2008 travel-demand model, supplemented by measured average diurnal patterns for key vehicle and road classes.

Meteorologic data were extracted from 1-km horizontal resolution WRF (version 3.1) simulations with observational nudging. Although measured wind speed and direction can be used in the ASM in place of modeled data, the results below are based on ASM runs using modeled meteorologic data. (One-week simulations were repeated for the LB4 and LB5 sites using measured wind speed and direction. The results were inconclusive; some metrics improved and others did not.)

Evaluation included data on hourly concentrations of aerosols at 11 locations (five of them with size-resolved measurements) in the Long Beach and Los Angeles areas. Measured data were from measurements made from 2005 to 2007, during HCMS and CHAPS. Summing across all the sites, 303 days of paired modeled–measured data were available. The 11 monitoring locations used for evaluations had approximately a 100-fold variation in local HDV traffic activity. At each location, the number of days with paired modeled–measured data ranged from 3 to 72. Mean measured particle concentrations ranged from 6000 to 41,000/cm^3.

The overall model skill for predicting number concentrations and size distributions can be categorized as mixed, with some promising prediction features and some areas where substantial improvements are needed. The r^2 for modeled versus measured long-term average concentrations (averaging hourly measurements over ~15 days) was

0.76 across the 18 simulation cases listed Table 4. Model underprediction was more common than model overprediction, and the average of the absolute normalized bias was 0.30, meaning that, on average, the long-term mean particle concentrations during each simulation case were predicted to within 30%.

Extensive evaluations were made of hourly concentrations, daily averaged concentrations, study average concentrations, diurnal patterns, size distributions, and directional patterns.

Summary of Evaluation for Prediction of 24-Hour Averages

The design goal for the model was to match measured 24-hour number concentrations within a factor of 1.6 on 90% of modeled days. The achieved statistic for this metric was 255 out of 365 days, or 70%. Prediction skill was better at the CHAPS sites than at the Long Beach sites. The ordering of the four CHAPS sites from lowest to highest number concentration was reproduced by the model, 81% of days were within the 1.6:1 envelope, and 94% were within a 2:1 envelope. The corresponding values for the Long Beach sites were 48% and 69%, respectively. This difference was hypothesized to have been caused by the higher LDV fraction (for which the input size distribution might have been more accurate), the absence of port activities, and increased distances from high-traffic roads for the CHAPS sites. However, size-resolved measurements were not available for detailed evaluation.

Summary of Evaluation for Prediction of 1-Hour Averages

Temporal prediction skill at individual monitoring sites was limited. Some time periods modeled with excellent skill, and other time periods of low or high concentrations were missed. Of the 18 hourly simulation cases, for example, only five had r^2 values of 0.25 or higher, and none had values greater than 0.4. The IOA for hourly values for a single site ranged from 0.30 to 0.56. One model performance goal was to simulate hourly concentrations to within a factor of 3.2 for 90% of the simulation hours. Overall, 8111 of 9201 simulated hours (88%) fell within this 3.2:1 envelope. Performance was better at the CHAPS sites (93% within 3.2:1) than at the Long Beach sites (78% within 3.2:1). On an hourly basis, the mean normalized bias for individual sites ranged from −0.51 to 0.78 (median −0.12), and the mean normalized error ranged from 0.39 to 0.99 (median 0.55). So although the model had limited success in predicting hourly variability in concentrations and particle size distributions for individual sites, evaluation based on skill at modeling single-site day-to-day variability and longer averaging time (weekly to monthly) variability across sites lead to a more positive assessment.

Summary of Evaluation for Other Features of Model Skill

The model made significant errors in predicting diurnal features and modes of the aerosol size distribution at the two sites with the most size-resolved SMPS data. (These sites also happened to have high concentrations and to be highly influenced by HDV traffic.) In summary, the morning-to-afternoon transitions in the size distribution associated with the morning-to-afternoon shift in winds were not well reproduced, and the modeled concentrations were too high at sizes less than 15 nm and too low at sizes from about 15 to 500 nm. One cause of these errors is that the emission factor developed from the summertime high-speed on-road chase experiments in Minnesota seems to have had too high of a nucleation mode and too low of an accumulation mode for application in Long Beach.

Diurnal patterns in aerosol particle number could typically be modeled, but some features were missed at specific sites. The reasons for the errors in the diurnal patterns were likely a combination of site-specific factors (e.g., missing sources, such as rail lines and port emissions) and systematic factors (e.g., missing photochemical influences on the aerosol population, errors in horizontal and vertical dispersion, and errors in the number and size of the emission factors).

Comparison with Results from Other Size-Resolved Models

Gidhagen and colleagues (2005) simulated concentrations in Stockholm, Sweden, using an Eulerian model with a 500-m resolution for 10 days and compared the results qualitatively with data from five monitoring stations using a 10-nm cutoff. Agreement was described as very good, but no quantitative measures of model skill were reported, and the modeled and measured size distributions were not compared. It is therefore difficult to compare the model skill of the ASM with that of the model used by Gidhagen and colleagues.

Wang and Zhang (2009) used computational fluid dynamics (CFD) with an unstructured grid of 2.4 million nodes to simulate a small area (~0.04 km^2) near I-405 and I-710. The detailed CFD simulation, which included traffic-produced turbulence, improved the modeled downwind dilution of CO as well as the vertical CO profile. Four representative hours were simulated; particles were not simulated. Comparison with the ASM is, again, not possible, given the differences in approach, number of hours simulated, and other factors. However, Wang and Zhang (2009) did show that it

is important to include traffic-produced turbulence in near-road predictions.

Zhang and Wexler (2004) simulated I-405 and I-710 particle number distributions for representative hours and fitted optimal modal size distributions (up to five modes) and semivolatile fractions for each mode. Zhang and Wexler's model (with semivolatile fractions) achieved much better agreement with measured size distributions than the ASM model. For I-405 southbound, for example, Zhang and Wexler assumed that the mode with the largest number of particles (12.5-nm mode) was 60% semivolatile, and thus could evaporate downwind of the highway, shifting the shape of the size distribution as a function of distance from the road much more than is seen in the ASM model, which assumes nonvolatile particles. A comparison between the model used by Zhang and Wexler (2004) and the ASM shows why the semivolatile treatment needs to be applied to future ASM simulations. Zhang and colleagues (2005) gave further support to the idea that a single nonvolatile emission factor does not predict measurements well. Their results show that different size-resolved emission factors are necessary (if the emissions are not semivolatile), depending on the distance from the receptor, with modes ranging from less than 7 to 12 nm (road-level prediction) up to 70 nm (grid-level prediction). Furthermore, these results show considerable variation in the size-resolved emission factors needed for matching grid-level data. The evaporation evidence reported by Zhang and colleagues is robust to assumptions regarding particle losses.

WEIGHING COST AND COMPLEXITY VERSUS MODEL SKILL AND SUITABILITY FOR APPLICATIONS

One concern about the ASM is that for a screening model it has a relatively large number of complex inputs (e.g., WRF model outputs, detailed street geometry, and link activity), but for a detailed model it has significant structural limitations and parametric uncertainty. It is conceivable that the ASM model could develop along two branches from its current state — a simplified model for screening purposes and a version with increasingly constrained parameters and better-quantified structural limitations. Simplifications that could make screening with the ASM more palatable include default traffic-activity levels for certain street types, gridded (rather than link-specific) traffic emissions as a function of vehicle miles traveled for distant traffic sources, and default meteorologic test cases. The latter were constructed from the Los Angeles WRF simulations from our study, as shown in Appendix D (available on the Web at *www.healtheffects.org*).

However, the potential applications of the ASM and the model skill demonstrated thus far deserve further consideration.

Application 1: Decision Support or Evaluation of Emissions Controls

The ASM could hypothetically be used for applications involving decision support or evaluation of emissions controls requiring multi-day averages (e.g., a week) over a specific portion of a day.

Screening Model As a screening model, the ASM could be used to estimate the impact of emissions reductions, changes in traffic activity, changes in the location of traffic, or the impact of size-dependent particle controls (such as filtration). This could provide useful information on concentrations and sensitivities before more detailed work (e.g., CFD modeling, wind-tunnel testing, computationally intensive treatments of aerosol chemistry, or field sampling). Given the long averaging times involved, the runtime of the ASM (~10 seconds per simulation hour) would be much better than that of a CFD-based detailed model. The use of alternate models for this screening purpose (such as LUR, multivariate regression, literature review and estimation of concentrations and sensitivities, or simpler dispersion models) would be possible but would lack size-resolved aerosol information. Simplification of the ASM by using typical meteorologic cases and reduced information on road networks might lead to a reduction in effort. The computational cost of the ASM and the skill demonstrated indicate that the ASM would serve as a successful screening model for such an application, especially if improvements were made in the HDV emission factor, simplifications to the input data were completed, and comparisons with other dispersion models (e.g., AERMOD, CALINE, or Gaussian plume equations) were established.

Detailed Model Use of the ASM as a detailed (i.e., definitive) model for decision support or evaluation of emissions controls could be warranted depending on the complexity of the topography involved in the project. If complex topography was involved, the ASM would be inappropriate as a detailed model. However, if the topography was reasonably simple, there was a focus on size distribution predictions, and a training data set for a detailed multivariate model was not available, the ASM would be a viable and, compared with other choices, simple model suitable for the task. The model skill levels demonstrated in the current study show that the ASM has promise for serving as a detailed model in such applications.

Application 2: Interpretation and Enhancement of Short-Term Observations

The ASM could hypothetically be used for applications involving the interpretation and enhancement of short-term observations (e.g., source apportionment, extrapolation, interpolation, and gap-filling in space or time) at hourly and day-specific times.

Screening Model This hypothetical application assumes that a measurement data set (such as the one from HCMS) is available and that there is a desire to learn more about specific hours of monitoring or to fill gaps in space and time. However, a screening model is not what is needed in this application; a detailed data-analysis technique is needed.

Detailed Model The current study showed that the ASM failed to model hour- and day-specific variability, probably in large part because of uncertainties in the data on hour- and day-specific traffic activity and weather. The preferred models for application 2 would probably be LUR and multivariate regression. Physical models with improved performance statistics are still appealing because their prediction and sensitivity features (e.g., tracking source–receptor relationships explicitly and simulating source-specific aerosol number separately from photochemical aerosols). For hour- and day-specific applications, all three techniques would require well-constrained data on near-field traffic, fleet information, speed, background concentrations, and weather. The use of the ASM as a detailed model for application 2 is unlikely, unless substantial improvements can be made in the hour-specific prediction skill, perhaps by using measured meteorologic data, measured traffic data, and site-specific size distributions as emission factors.

Application 3: Interpretation and Enhancement of Long-Term Observations

The ASM could hypothetically be used for applications involving the interpretation and enhancement of long-term observations (e.g., source apportionment, extrapolation, interpolation, and gap-filling in space or time) with weekly to yearly time averaging.

Screening Model This hypothetical application assumes that a short-term or spatially incomplete measurement data set (such as the one from HCMS) is available and that there is a desire to learn more about long-term concentrations at a number of spatially distributed receptors. The use of a screening model implies that more measurements are anticipated or that a detailed model is under consideration. The ASM would be a candidate for a screening model in this situation, but because of its data requirements, uncertainties, and runtimes (in its current form, the ASM requires 1 day of calculation to compute 1 year of hourly concentrations at one receptor), it might not be competitive with LUR, multivariate regression, and inferences about the detailed application based on literature searches. It should be noted that the ASM's r^2 for average concentrations for the 18 simulations at 11 sites was 0.76 in this study, the mean normalized bias was −0.30, and the mean normalized error was 0.32. These statistics are competitive with those of a wide range of applications. The ASM might be a good screening model (e.g., in preparation for saturation monitoring) for applications such as the ones considered here (i.e., in application 3), but structural and parametric uncertainties coupled with high input requirements might limit its use.

Detailed Model See Application 2, above. The selection of a modeling or measurement technique for this application might depend on application details such as the availability of monitoring and background data, computer resources, human resources, the complexity of the terrain, and the need for detailed physical and chemical aerosol variables. The same pros and cons of using a physical dispersion model such as the ASM for the interpretation and enhancement of observation described for Application 2 apply to Application 3.

Application 4: Generation of Spatially Resolved Multi-Hour Exposure Estimates

The ASM could hypothetically be used for applications involving the generation of spatially resolved exposure estimates for multi-hour or 24-hour day-specific averaging periods where monitoring is unfeasible.

Screening Model This hypothetical application assumes minimal availability of existing monitoring data. Because the application specifically demands modeled rather than measured data, a detailed model is needed for this application, not a screening model. One exception might be the generation of modeled concentrations to demonstrate exposure variability before the start of epidemiologic work; however, multiple methods would be competitive with the ASM for this application.

Detailed Model The ASM is a good candidate for use as a detailed model in this application, subject to the caveats on day-specific performance (see Application 2, above) and runtimes and complexity (see Application 3, above). When monitoring data are not available, LUR-based models can

be used, but these models are not easily transferable to other locations or times. The accuracy of the ASM's day-specific predictions for specific locations is limited (e.g., day-specific 24-hour mean normalized biases ranged from 0.2 to 0.6 at individual sites but was 0.32 for all 365 location–day pairs simulated). Model skill for diurnal patterns in size distributions, particularly in HDV-affected areas, would need to be improved. More advanced (and computationally intensive) Eulerian models might be useful, especially if large numbers of receptors are involved or background concentrations are not constrained. If epidemiologic analysis depends on temporal variations in concentrations, the ASM's accuracy to date would probably not be acceptable. In summary, the ASM might be applicable for the detailed modeling of size-resolved day-specific multi-hour and 24-hour averaged concentrations, but other techniques would also need to be considered, and improvements in model skill (probably by using day- and location-specific input data) would be needed.

Application 5: Generation of Spatially Resolved 24-Hour Exposure Estimates

The ASM could also hypothetically be used for applications involving the generation of spatially resolved exposure estimates for 24-hour day-specific averaging periods where monitoring is unfeasible.

Screening Model See Screening Model comments in the Application 4 section, above.

Detailed Model See Detailed Model comments in the Application 3 section, above, about the pros and cons of using the ASM for long-term exposure assessment. If LUR is chosen for the application, then model transferability will be a drawback. If the ASM is chosen, then structural and parametric uncertainties will be drawbacks, together with the computation time. ASM accuracy, as in any physical model, will depend on complete and accurate specification of the background and emission terms in the model. The ASM might be competitive with LUR for long-term spatial predictions in areas for which there is no transferable LUR model. However, given the limited track record of both LUR and dispersion models with respect to size-resolved particle number, extreme caution is warranted in the use and interpretation of their findings (because this hypothetical application has minimal evaluation data).

To summarize these hypothetical applications, four of the five have potential use for screening models. Of these four, the ASM would be particularly useful for Application 1, especially if its data inputs could be made more user-friendly for screening-level applications. For the other three applications, the ASM, regression analyses, and other techniques would all be possible for use in screening, and case-by-case features would determine the best tool. All five of the applications might have use for detailed size-resolved predictive models. In these cases, the ASM might be competitive with alternative models, depending on the amount of complex terrain, available training data for regression, and temporal averaging times. Spatial (rather than temporal) prediction and lack of training data for regression lend themselves to use of the ASM; dense training data sets and a need for accuracy at high time resolutions are currently best handled with regression analyses.

SENSITIVITY CALCULATIONS

As an example of the ability of the ASM to quantify the sensitivity of concentrations to emissions, the sensitivity of each receptor to LDV traffic, HDV traffic, and road class was calculated. The sensitivity of overall particle number to all types of traffic ranged from 0.87 at the most traffic-affected site to 0.28 at the least traffic-affected site. At the Long Beach sites, HDV and freeway–arterial traffic had greater influence on particle number and traffic-related particle mass than LDV and other road types. At the more residential CHAPS sites, conversely, LDV and local traffic had greater influence on particle number.

OTHER SENSITIVITIES

The ASM and similar models are sensitive to a number of structural and parametric uncertainties.

The major structural uncertainties of the ASM include the neglecting of topography, gradient-transfer theory parameterization of dispersion, and neglecting of aerosol evaporation and photochemical aerosol sources, as well as the inherent limitations of the Lagrangian modeling framework.

The major parametric uncertainties include sensitivity to background aerosol concentrations, emission factors, traffic activity (e.g., total, HDV, and LDV fractions; distribution across road classes; and acceleration fraction), weather, and the parameterization and estimation involved in specifying K_{zz} and K_{yy}. Of these, the sensitivity of concentrations to emission factors and traffic activity were quantified earlier, in the demonstration of the model's ability to perform sensitivity calculations. Especially for particle number and (at the Long Beach sites) particle volume, the sensitivity to traffic activity and emission factors is high. In addition, both traffic activity (from a traffic-demand model) and emission factors (from a limited number of studies, processed and harmonized to make them model-ready) are uncertain. Some

of the limitations of travel-demand models were reviewed by the HEI Panel on the Health Effects of Traffic-Related Air Pollution (2010), and the frequently found sensitivity of physically based models to emission factors was well documented by Kumar and colleagues (2011). Of the six limitations of travel-demand models discussed in the HEI review, four affect the current study: these models were not rigorously evaluated against observational data for the baseline period, they did not provide accurate distributions of speed by link, they did not distinguish accurately between traffic patterns for LDV and HDV vehicles, and they did not provide traffic outputs for specific small- and moderate-size collector roads.

Although it is clear that our model is sensitive to emission factors and traffic activity, quantitative uncertainty of these inputs has not yet been established. Comparison with automated traffic-count data and automated weight-in-motion records would (at least for the larger road classes) allow quantification.

Background concentrations are very important to overall modeling results. Sensitivity results (Figures 28 and 29) quantify the influence of such background concentrations. For example, at three of the eleven sites, modeled number concentration was more sensitive to the specified background than it was to vehicle emissions within 4 km. In the panels showing LB4 results for 3 AM in Figures 23 and 25, the modeled particle number and volume distributions are largely attributable to the background, because the influence of traffic is minimal at that time. Depending on the application, detailed information about background concentrations can be critical. For parameters other than aerosol number (which is most sensitive to nearby sources) and aerosol volume (i.e., mass), parameters for which there is a relatively dense sampling network in most urban areas, other compounds, such as air toxics, are even more difficult to specify accurately at model boundaries.

Sensitivity to meteorologic data has not been assessed except by using the measured wind speed and direction in the modeling (instead of the WRF-modeled values). Although it is clear that individual hours are very sensitive to the wind speed and direction used, the overall model performance statistics were not sensitive to the use of measured winds compared with WRF-modeled winds. In part, this insensitivity likely reflects the fact that certain meteorologic data errors can compensate for bias in emissions data. It also partly reflects uncertainty from other important sources, parametric and structural, in addition to wind speed and direction. In addition, it might also reflect difficulties in measuring wind and comparing wind observations. We note, however, that mean errors in wind direction (~65° in any given hour) were important contributors to limited model skill. Although the use of the WRF model at high resolutions is growing in popularity for dispersion calculations (Wyszogrodzki et al. 2012; Yerramilli et al. 2012; Sandeepan et al. 2013), optimization of its settings and configuration for improved performance would likely improve hourly modeling results.

Detailed sensitivity to aspects of the K_{yy} and K_{zz} parameterization (i.e., selection of $K_{yy,\min}$ and $K_{zz,\min}$, as well as the equations for K_{yy} for stable and unstable time periods) requires further testing and optimization as well.

Future Model-Improvement Priorities

Higher-priority modifications to the ASM include the following:

1. Emission factors can be improved by considering a wider universe of chase and near-road studies; they can also be fitted to match the measured data using this model framework, and more dependence of emissions on speed and load (e.g., grade) are likely needed.
2. Although including evaporation of the nuclei mode particles from exhaust and the photochemical growth of particles is a challenge and will introduce additional complexity to the modeling, analysis, and input data needs, it is likely required for detailed matching of the aerosol size distribution.
3. Modeling of CO_2 as an on- and near-road dilution tracer and the use of ratios of particles to conservative tracers such as CO and CO_2 (including the development of analytic expressions giving size-resolved particle number as a ratio to commonly simulated and measured species) are needed. CO is a simulated species in the model, but evaluation of CO has been difficult because of the high variability of background CO in the Los Angeles area and the high ratio of background to on-road CO. Because particle emissions are already based on fuel use, CO_2 emissions can be easily modeled. Having information on ratios of the more commonly measured combustion tracers will make incorporation of UFPs into existing LUR and multivariate statistical models more accurate.
4. The use of best practices for urban meteorologic modeling appropriate to the computational and accuracy goals of the ASM needs to be further refined through partnerships with the CFD and urban-scale meteorologic modeling communities. The WRF model seems to render conditions both too stable (at night) and too unstable (in the afternoon).

5. Improvements in the treatment of K_{yy} and H_{mix} are needed, including the use of K_{yy} from the WRF model, vertical variations in K_{yy}, the use of observed wind direction standard deviation, comparison with additional observations of near-road vertical and horizontal concentration profiles, and consideration of thermal plumes rising from roadway sources.
6. Integration with the MOVES emissions model is needed.
7. Comparisons with other models are needed to further identify strengths and weaknesses.
8. A simplified screening-only version of the ASM, with simplified input needs and default traffic and meteorologic fields, should be developed.

Lower-priority improvements include the following:

1. Simulations in other locations should be carried out. The domains that have been used to test the ASM have been limited to a coastal area, with a very heavy influence from I-405 and I-710. The modeling approach of the current study, for example, is not well suited to locations with stagnant conditions. However, stagnant conditions are somewhat rare at coastal sites, such as Long Beach, compared with what might develop in nighttime conditions at inland sites. Stagnant conditions are difficult to model at high resolution and will likely require detailed consideration of traffic-produced turbulence and flow.
2. Enabling two- or one-way nesting with a 3D air-quality model continues to be an important goal. Although not presented in the current study, limited size resolution for aerosols and in the ultrafine range, limited spatial resolution in readily available 3D-model input files (e.g., emissions), and limited skill for subdaily variations in $PM_{2.5}$ and combustion tracers remain difficult problems in terms of nesting with 3D air-quality models for background concentrations.
3. Inclusion of the locations of stop lights and separation of on and off ramps would help in ensuring that the model is truly accurate at high spatial resolutions.
4. Further improvements are needed in the adaptive step size, and adaptive parcel algorithms are needed to reduce computation time.
5. Representation of the mechanical wake of roadways is likely important, especially at low wind speeds. Wakes are not naturally represented in the framework of the ASM, although increasing the effective width of roadways based on wakes might be a fruitful approach.
6. Enabling simulation of photochemical nucleation.

IMPLICATIONS OF FINDINGS

The implications of this study are that high-resolution modeling (down to 10 m) of vehicle sources is possible in a relatively simple modeling framework, although improvements to the meteorologic inputs and assumed emission factors are needed. In one of the largest (in terms of number of hours and sites) evaluations of a UFP model to date, site-to-site variations in long-term (~15 days) mean number concentrations in the Los Angeles area could be predicted with an r^2 of 0.76, and 45% and 79% of modeled days at Long Beach and the CHAPS sites, respectively, could be modeled to within a 1.6:1 envelope.

Particle losses for particles less than 50 nm, and especially less than 20 nm, can be large, and differences between particle losses for CPC and SMPS measurements and other differences between the two kinds of equipment need to be carefully considered. Detailed reporting of assumed or measured inlet and instrument losses, for example, is critical.

Atmospheric processing of semivolatile primary traffic particles was not addressed in the current work but will likely be required for detailed matching of size distributions. The current modeling effort relied on on-road measured size distributions. An alternate approach would be to fit the emission factors for model–measurement agreement. Both approaches are needed. It is likely that speed and load (e.g., road grade) affect emissions in ways that are important to include in the model and that would improve the ASM's prediction capability.

Sensitivity calculations for the ASM indicated that particle number concentration from LDV traffic likely exceeded that from HDV traffic in some locations. The ASM highlighted the fact that emission impacts from roadways depend on traffic volume and distance: in other words, both low traffic volume at close proximity and high traffic volume at distances up to several kilometers need to be considered in health and planning studies.

A range of potential applications of the ASM were reviewed in the current study. Although the Lagrangian methods of the ASM are not likely to suit every application, the ASM as both a screening model and a detailed model is probably competitive for estimating exposure in several scenarios.

ACKNOWLEDGMENTS

We wish to acknowledge the contributions of Costas Sioutas (University of Southern California) and Ralph Delfino (University of California–Irvine) and their scientific staffs

for discussions, encouragement, and data as well as the assistance of Nicole Riemer (University of Illinois) and Rahul Zaveri (Pacific Northwest National Laboratory) with PartMC–MOSAIC. We also acknowledge the following students and staff at the University of Iowa: Jay Raife, who contributed to the development of the emission factors; Jeremie Moen, who helped provide computing resources; and Jaemeen Baek, with whom we consulted regarding CMAQ. In addition, we appreciate our conversations with Jun Wu (University of California–Irvine) and Yifang Zhu (University of California–Los Angeles) on urban-scale modeling and UFPs as well as the assistance of those at the California Air Resources Board who provided traffic-demand model data, including Alberto Ayala, Todd Sax, and Pranay Avlani.

REFERENCES

Adams PJ, Seinfeld JH. 2002. Predicting global aerosol size distributions in general circulation models. J Geophys Res-Atmos 107(D19):AAC 12-1–AAC 12-14.

Aggarwal S, Jain R, Marshall JD. 2012. Real-time prediction of size-resolved ultrafine particulate matter on freeways. Environ Sci Technol 46(4):2234–2241.

Asmi A, Wiedensohler A, Laj P, Fjaeraa AM, Sellegri K, Birmili W, Weingartner E, Baltensperger U, Zdimal V, Zikova N, Putaud JP, Marinoni A, Tunved P, Hansson HC, Fiebig M, Kivekas N, Lihavainen H, Asmi E, Ulevicius V, Aalto PP, Swietlicki E, Kristensson A, Mihalopoulos N, Kalivitis N, Kalapov I, Kiss G, de Leeuw G, Henzing B, Harrison RM, Beddows D, O'Dowd C, Jennings SG, Flentje H, Weinhold K, Meinhardt F, Ries L, Kulmala M. 2011. Number size distributions and seasonality of submicron particles in Europe 2008–2009. Atmos Chem Phys 11(11): 5505–5538.

Ayala A, Olson B, Cantrell B, Drayton M, Barsic N. 2003. Estimation of diffusion losses when sampling diesel aerosol: A quality assurance measure. Society of Automotive Engineers Technical Paper Series, paper number 2003-01-1896.

Baker D, Ku M, Hao W, Sistia G, Kiss M, Johnson M, Brown D. 2010. Sensitivity testing of WRF physics parameterizations for meteorological modeling and protocol in support of regional SIP air quality modeling in the OTR. Report of the Ozone Transport Commission Modeling Committee. *http://otcair.org/upload/Documents/Meeting%20Materials/OTC%20WRF%20Protocol%203_11_10.pdf*

Baron PA, Willeke K. 2001. Aerosol Measurement: Principles, Techniques, and Applications. John Wiley & Sons, New York, NY.

Baumer D, Vogel B, Fiedler F. 2005. A new parameterisation of motorway-induced turbulence and its application in a numerical model. Atmos Environ 39(31):5750–5759.

Benson PE. 1992. Review of the development and application of the CALINE3 and CALINE4 models. Atmos Environ Part B. Urban Atmospheres 26(3):379–390.

Berkowicz R, Ketzel M, Jensen SS, Hvidberg M, Raaschou-Nielsen O. 2008. Evaluation and application of OSPM for traffic pollution assessment for a large number of street locations. Environ Modell Softw 23(3):296–303.

Capaldo K, Pandis S. 2001. Lifetimes of Ultrafine Diesel Aerosol. In: Report for the University of Minnesota and the Coordinating Research Council under the E-43 project diesel aerosol sampling methodology. Carnegie Mellon University, Pittsburgh, PA.

Capaldo KP, Kasibhatla P, Pandis SN. 1999. Is aerosol production within the remote marine boundary layer sufficient to maintain observed concentrations? J Geophys Res-Atmos 104(D3):3483–3500.

Carpentieri M, Kumar P, Robins A. 2011. An overview of experimental results and dispersion modelling of nanoparticles in the wake of moving vehicles. Environ Pollut 159(3):685–693.

Clifford S, Choy SL, Hussein T, Mengersen K, Morawska L. 2011. Using the Generalised Additive Model to model the particle number count of ultrafine particles. Atmos Environ 45(32):5934–5945.

Cook R, Isakov V, Touma JS, Benjey W, Thurman J, Kinnee E, Ensley D. 2008. Resolving local-scale emissions for modeling air quality near roadways. J Air Waste Manage Assoc 58(3):451–461.

Delfino RJ, Sioutas C, Malik S. 2005. Potential role of ultrafine particles in associations between airborne particle mass and cardiovascular health. Environ Health Perspect 113(8):934–946.

Delfino RJ, Staimer N, Tjoa T, Gillen DL, Polidori A, Arhami M, Kleinman MT, Vaziri ND, Longhurst J, Sioutas C. 2009. Air pollution exposures and circulating biomarkers of effect in a susceptible population: Clues to potential causal component mixtures and mechanisms. Environ Health Perspect 117(8):1232–1238.

Delfino RJ, Staimer N, Tjoa T, Polidori A, Arhami M, Gillen DL, Kleinman MT, Vaziri ND, Longhurst J, Zaldivar F, Sioutas C. 2008. Circulating biomarkers of inflammation, antioxidant activity, and platelet activation are associated with primary combustion aerosols in subjects with coronary artery disease. Environ Health Perspect 116(7):898–906.

Di Sabatino S, Kastner-Klein P, Berkowicz R, Britter RE, Fedorovich E. 2003. The modelling of turbulence from traffic in urban dispersion models. Part I: Theoretical considerations. Environ Fluid Mech 3(2):129–143.

Emery C, Tai E, Yarwood G. 2001. Enhanced Meteorological Modeling and Performance Evaluation for Two Texas Ozone Episodes. Final report submitted to Texas Natural Resources Conservation Commission, Austin, Texas.

Feng J. 2008. A size-resolved model and a four-mode parameterization of dry deposition of atmospheric aerosols. J Geophys Res-Atmos 113(D12).

Fissan H, Hummes D, Stratmann F, Buscher P, Neumann S, Pui DYH, Chen D. 1996. Experimental comparison of four differential mobility analyzers for nanometer aerosol measurements. Aerosol Sci Tech 24(1):1–13.

Fossum HE, Reif BAP, Tutkun M, Gjesdal T. 2012. On the use of computational fluid dynamics to investigate aerosol dispersion in an industrial environment: A case study. Bound-Layer Meteor 144(1):21–40.

Fruin S, Westerdahl D, Sax T, Sioutas C, Fine PM. 2008. Measurements and predictors of on-road ultrafine particle concentrations and associated pollutants in Los Angeles. Atmos Environ 42:207–219.

Fuchs NA. 1964. Mechanics of Aerosols. Pergamon, New York.

Fuller CH, Brugge D, Williams PL, Mittleman MA, Durant JL, Spengler JD. 2012. Estimation of ultrafine particle concentrations at near-highway residences using data from local and central monitors. Atmos Environ 57:257–265.

Funk TH, Coe DL, Chinkin LR. 2001. Weekday versus weekend on-road mobile source emissions activity patterns in California's South Coast Air Basin. In: Proceedings of the 10th International Emissions Inventory Conference, May 1–3, 2001. U.S. Environmental Protection Agency, Denver, CO.

Gaydos TM, Stanier CO, Pandis SN. 2005. Modeling of in situ ultrafine atmospheric particle formation in the eastern United States. J Geophys Res-Atmos 110(D07S12).

Geller VD, Sardar SB, Phuleria H, Fine PM, Sioutas C. 2005. Measurements of particle number and mass concentrations and size distributions in a tunnel environment. Environ Sci Technol 39(22):8653–8663.

Gidhagen L, Johansson C, Langner J, Foltescu VL. 2005. Urban scale modeling of particle number concentration in Stockholm. Atmos Environ 39(9):1711–1725.

Gidhagen L, Johansson C, Langner J, Olivares G. 2004a. Simulation of NO_x and ultrafine particles in a street canyon in Stockholm, Sweden. Atmos Environ 38(14):2029–2044.

Gidhagen L, Johansson C, Omstedt G, Langner J, Olivares G. 2004b. Model simulations of NO_x and ultrafine particles close to a Swedish highway. Environ Sci Technol 38(24): 6730–6740.

Gidhagen L, Johansson C, Strom J, Kristensson A, Swietlicki E, Pirjola L, Hansson HC. 2003. Model simulation of ultrafine particles inside a road tunnel. Atmos Environ 37(15): 2023–2036.

HEI Panel on the Health Effects of Traffic-Related Air Pollution. 2010. Traffic-Related Air Pollution: A Critical Review of the Literature on Emissions, Exposure, and Health Effects. Special Report 17. Health Effects Institute, Boston, MA.

Hinds WC. 1999. Aerosol Technology: Properties, behavior, and measurement of airborne particles. John Wiley & Sons, New York.

Hoek G, Beelen R, Kos G, Dijkema M, van der Zee SC, Fischer PH, Brunekreef B. 2011. Land use regression model for ultrafine particles in Amsterdam. Environ Sci Technol 45(2):622–628.

Hölz S. 2006. Polygon Clipper. Matlab Central File Exchange. *www.mathworks.com/matlabcentral/fileexchange/8818-polygon-clipper*

Hu SS, Fruin S, Kozawa K, Mara S, Paulson SE, Winer AM. 2009. A wide area of air pollutant impact downwind of a freeway during pre-sunrise hours. Atmos Environ 43(16): 2541–2549.

Hudda N, Eckel SR, Knibbs LD, Sioutas C, Delfino RJ, Fruin SA. 2012. Linking in-vehicle ultrafine particle exposures to on-road concentrations. Atmos Environ 59:578–586.

Isakov V, Touma JS, Burke J, Lobdell DT, Palma T, Rosenbaum A, Ozkaynak H. 2009. Combining regional- and local-scale air quality models with exposure models for

use in environmental health studies. J Air Waste Manage Assoc 59(4):461–472.

Jacobson MZ, Seinfeld JH. 2004. Evolution of nanoparticle size and mixing state near the point of emission. Atmos Environ 38(13):1839–1850.

Johnson JP, Kittelson DB, Watts WF. 2005. Source apportionment of diesel and spark ignition exhaust aerosol using on-road data from the Minneapolis metropolitan area. Atmos Environ 39(11):2111–2121.

Johnson M, Isakov V, Touma JS, Mukerjee S, Ozkaynak H. 2010. Evaluation of land-use regression models used to predict air quality concentrations in an urban area. Atmos Environ 44(30):3660–3668.

Jones AM, Harrison RM. 2006. Estimation of the emission factors of particle number and mass fractions from traffic at a site where mean vehicle speeds vary over short distances. Atmos Environ 40(37):7125–7137.

Karner AA, Eisinger DS, Niemeier DA. 2010. Near-roadway air quality: Synthesizing the findings from real-world data. Environ Sci Technol 44(14):5334–5344.

Ketzel M, Berkowicz R. 2005. Multi-plume aerosol dynamics and transport model for urban scale particle pollution. Atmos Environ 39(19):3407–3420.

Khlystov A, Stanier CO, Pandis SN. 2004. An algorithm for combining electrical mobility and aerodynamic size distributions data when measuring ambient aerosol. Aerosol Sci Tech 38(S1):229–238.

Kim E, Hopke PK. 2004. Comparison between conditional probability function and nonparametric regression for fine particle source directions. Atmos Environ 38(28):4667–4673.

Kim S, Shen S, Sioutas C, Zhu YF, Hinds WC. 2002. Size distribution and diurnal and seasonal trends of ultrafine particles in source and receptor sites of the Los Angeles basin. J Air Waste Manage Assoc 52(3):297–307.

Kittelson DB, Watts WF, Johnson JP. 2004. Nanoparticle emissions on Minnesota highways. Atmos Environ 38(1):9–19.

Kittelson DB, Watts WF, Johnson JP. 2006a. On-road and laboratory evaluation of combustion aerosols: Part 1. Summary of diesel engine results. J Aerosol Sci 37(8):913–930.

Kittelson DB, Watts WF, Johnson JP, Schauer JJ, Lawson DR. 2006b. On-road and laboratory evaluation of combustion aerosols: Part 2. Summary of spark ignition engine results. J Aerosol Sci 37(8):931–949.

Knibbs LD, Cole-Hunter T, Morawska L. 2011. A review of commuter exposure to ultrafine particles and its health effects. Atmos Environ 45(16):2611–2622.

Krudysz M, Moore K, Geller M, Sioutas C, Froines J. 2009. Intra-community spatial variability of particulate matter size distributions in Southern California/Los Angeles. Atmos Chem Phys 9(3):1061–1075.

Kumar P, Ketzel M, Vardoulakis S, Pirjola L, Britter R. 2011. Dynamics and dispersion modelling of nanoparticles from road traffic in the urban atmospheric environment: A review. J Aerosol Sci 42(9):580–603.

Liu MK, Seinfeld JH. 1975. Validity of grid and trajectory models of urban air pollution. Atmos Environ 9(6–7):555–574.

Maricq MM, Podsiadlik DH, Chase RE. 1999. Examination of the size-resolved and transient nature of motor vehicle particle emissions. Environ Sci Technol 33(10):1618–1626.

McAuley TR, Ferro A, Spengler JD, Hopke PK, Jaques PA. 2010. Spatial measurements of ultrafine particles using an engine exhaust particle sizer within a local community downwind of a major international trade bridge in Buffalo, New York. Aerosol Sci Tech 44(12):1096–1104.

McMurry PH, Woo KS. 2002. Size distributions of 3–100-nm urban Atlanta aerosols: Measurement and observations. J Aerosol Med: Deposition, Clearance, and Effects in the Lung 15(2):169–178.

McRae GJ, Goodin WR, Seinfeld JH. 1982. Development of a second-generation mathematical model for urban air pollution. I. Model formulation. Atmos Environ 16(4):679–696.

Michael S. 2008. KD Tree Nearest Neighbor and Range Search. Matlab Central File Exchange. *www.mathworks.com/matlabcentral/fileexchange/7030-kd-tree-nearest-neighbor-and-range-search*

Molgaard B, Hussein T, Corander J, Hameri K. 2012. Forecasting size-fractionated particle number concentrations in the urban atmosphere. Atmos Environ 46:155–163.

Moore K, Krudysz M, Pakbin P, Hudda N, Sioutas C. 2009. Intra-community variability in total particle number concentrations in the San Pedro Harbor area (Los Angeles, California). Aerosol Sci Tech 43(6):587–603.

Oberdörster G. 2001. Pulmonary effects of inhaled ultrafine particles. Int Arch Occup Environ Health 74:1–8.

Padro-Martinez LT, Patton AP, Trull JB, Zamore W, Brugge D, Durant JL. 2012. Mobile monitoring of particle number concentration and other traffic-related air pollutants in a near-highway neighborhood over the course of a year. Atmos Environ 61:253–264.

Pohjola M, Pirjola L, Kukkonen J, Kulmala M. 2003. Modelling of the influence of aerosol processes for the dispersion of vehicular exhaust plumes in street environment. Atmos Environ 37(3):339–351.

Pohjola MA, Pirjola L, Karppinen A, Harkonen J, Korhonen H, Hussein T, Ketzel M, Kukkonen J. 2007. Evaluation and modelling of the size fractionated aerosol particle number concentration measurements nearby a major road in Helsinki: Part I. Modelling results within the LIPIKA project. Atmos Chem Phys 7(15):4065–4080.

Polidori A, Arhami M, Sioutas C, Delfino RJ, Allen R. 2007. Indoor/outdoor relationships, trends, and carbonaceous content of fine particulate matter in retirement homes of the Los Angeles basin. J Air Waste Manage Assoc 57(3):366–379.

Robert MA, Kleeman MJ, Jakober CA. 2007a. Size and composition distributions of particulate matter emissions: Part 2. Heavy-duty diesel vehicles. J Air Waste Manage Assoc 57(12):1429–1438.

Robert MA, VanBergen S, Kleeman MJ, Jakober CA. 2007b. Size and composition distributions of particulate matter emissions: Part 1. Light-duty gasoline vehicles. J Air Waste Manage Assoc 57(12):1414–1428.

Rogak SN, Flagan RC. 1992. Coagulation of aerosol agglomerates in the transition regime. J Colloid Interface Sci 151(1):203–224.

Roldin P, Swietlicki E, Massling A, Kristensson A, Londahl JL, Eriksson A, Pagels J, Gustafsson S. 2011. Aerosol ageing in an urban plume: Implication for climate. Atmos Chem Phys 11(12):5897–5915.

Russell A, Dennis R. 2000. NARSTO critical review of photochemical models and modeling. Atmos Environ 34(12–14):2283–2324.

Sandeepan BS, Rakesh PT, Venkatesan R. 2013. Observation and simulation of boundary layer coherent roll structures and their effect on pollution dispersion. Atmos Res 120:181–191.

Seinfeld JH, Pandis SN. 2006. Atmospheric Chemistry and Physics. John Wiley & Sons, Hoboken, NJ.

Shi JP, Evans DE, Khan AA, Harrison RM. 2001. Sources and concentration of nanoparticles (< 10 nm diameter) in the urban atmosphere. Atmos Environ 35(7):1193–1202.

Sousan S. 2012. Optimal Interpolation Schemes to Constrain $PM_{2.5}$ in Regional Modeling over the United States [dissertation]. Department of Chemical and Biochemical Engineering, University of Iowa, Iowa City, IA.

Steffens JT, Wang YJ, Zhang KM. 2012. Exploration of effects of a vegetation barrier on particle size distributions in a near-road environment. Atmos Environ 50:120–128.

Stein AF, Isakov V, Godowitch J, Draxler RR. 2007. A hybrid modeling approach to resolve pollutant concentrations in an urban area. Atmos Environ 41(40):9410–9426.

Tiwary A, Robins A, Namdeo A, Bell M. 2011. Air flow and concentration fields at urban road intersections for improved understanding of personal exposure. Environ Int 37(5):1005–1018.

U.S. Environmental Protection Agency. 1976. The General Motors/Environmental Protection Agency Sulfate Dispersion Experiment. Research Triangle Park, NC. EPA-600/3-76-035.

Wang YG, Hopke PK, Chalupa DC, Utell MJ. 2011. Long-term study of urban ultrafine particles and other pollutants. Atmos Environ 45(40):7672–7680.

Wang YJ, Zhang KM. 2009. Modeling near-road air quality using a computational fluid dynamics model, CFD-VIT-RIT. Environ Sci Technol 43(20):7778–7783.

Wyszogrodzki AA, Miao SG, Chen F. 2012. Evaluation of the coupling between mesoscale-WRF and LES-EULAG models for simulating fine-scale urban dispersion. Atmos Res 118:324–345.

Yerramilli A, Dodla VBR, Challa VS, Myles L, Pendergrass WR, Vogel CA, Dasari HP, Tuluri F, Baham JM, Hughes RL, Patrick C, Young JH, Swanier SJ, Hardy MG. 2012. An integrated WRF/HYSPLIT modeling approach for the assessment of $PM_{2.5}$ source regions over the Mississippi Gulf Coast region. Air Qual Atmos Health 5(4):401–412.

Zhang KM, Wexler AS. 2004. Evolution of particle number distribution near roadways: Part I. Analysis of aerosol dynamics and its implications for engine emission measurement. Atmos Environ 38(38):6643–6653.

Zhang KM, Wexler AS, Niemeier DA, Zhu YF, Hinds WC, Sioutas C. 2005. Evolution of particle number distribution near roadways: Part III. Traffic analysis and on-road

size resolved particulate emission factors. Atmos Environ 39(22): 4155–4166.

Zhang KM, Wexler AS, Zhu YF, Hinds WC, Sioutas C. 2004. Evolution of particle number distribution near roadways: Part II. The "Road-to-Ambient" process. Atmos Environ 38(38):6655–6665.

Zhou Y, Levy JI. 2007. Factors influencing the spatial extent of mobile source air pollution impacts: A meta-analysis. BMC Public Health 7:89.

Zhu YF, Hinds WC, Kim S, Sioutas C. 2002. Concentration and size distribution of ultrafine particles near a major highway. J Air Waste Manage Assoc 52(9):1032–1042.

Zhu YF, Kuhn T, Mayo P, Hinds WC. 2006. Comparison of daytime and nighttime concentration profiles and size distributions of ultrafine particles near a major highway. Environ Sci Technol 40(8):2531–2536.

APPENDIX A. Assumed Instrument Sampling Efficiencies

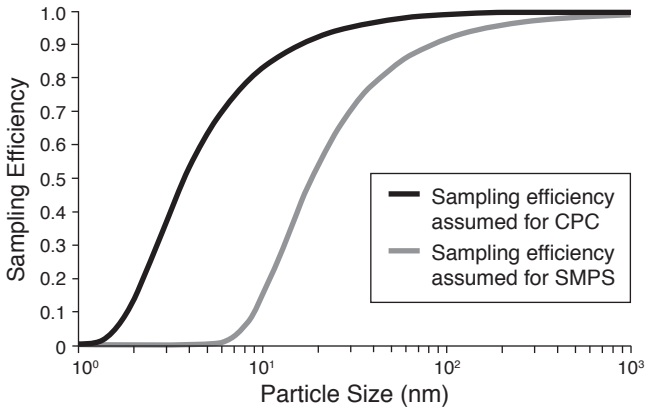

Figure A.1. Sampling efficiency assumed for converting the ambient size distribution to instrumental particle number concentration or instrument-reported size distribution. Efficiency curves are also used to convert emission factors to lower emission factors that would be derived from instrumentation with these assumed losses occurring, but without correction or adjustment for those losses (see, for example, Table 7). The SMPS curve is developed based on work by Kittelson and colleagues (2006a) and is described in the report. The CPC curve is based on diffusional losses in a 2-m inlet with flow rates and diameter as described in the Evaluation Data section.

APPENDIX B. Model–Observation Statistical Tables

Table B.1. Statistics for Hourly Model–Measurement Pairs of Particle Number Concentrations

Internal University of Iowa Identification Code	Simulation Case	n	Modeled Mean (particles/cm^3)	Measured Mean (particles/cm^3)	Modeled SD (particles/cm^3)	Measured SD (particles/cm^3)	Mean Bias (particles/cm^3)	Mean Error (particles/cm^3)	Mean Normal Bias (particles/cm^3)	Mean Normal Error	Fractional Bias	Fractional Error	r	IOA	RMSE (particles/cm^3)	RMSEs (particles/cm^3)	RMSEu (particles/cm^3)	Hours Within 3.2:1 (n)	Hours Within 4:1 (n)
20130217T134752	Run01LB4_Sept	355	8,687	13,103	2,938	7,169	−4,417	6,346	−0.05	0.54	−0.27	0.54	0.18	0.46	8,485	7,978	2,888	321	341
20130217T134752	Run02LB5_Sept	355	14,255	30,596	10,614	18,011	−16,341	19,528	−0.38	0.57	−0.67	0.80	0.00	0.42	26,536	24,327	10,599	228	253
20130217T134752	Run03W2_Sept	305	8,679	14,112	3,541	8,813	−5,433	8,656	0.10	0.78	−0.28	0.71	−0.03	0.41	11,016	10,434	3,534	242	272
20130217T134752	Run04LB2_May	77	7,336	13,280	3,095	5,720	−5,944	7,017	−0.33	0.48	−0.53	0.64	−0.15	0.38	9,072	8,548	3,040	62	68
20130218T091223	Run05LB3_May	159	6,131	16,135	2,368	9,069	−10,003	10,422	−0.51	0.57	−0.78	0.83	0.12	0.43	13,500	13,295	2,343	107	129
20130218T112010	Run06W2_May	180	6,910	13,797	2,949	8,071	−6,888	8,202	−0.28	0.56	−0.53	0.70	−0.10	0.38	11,211	10,823	2,926	135	158
20130218T112010	Run07LB4_Oct	305	17,545	24,426	10,491	11,564	−6,881	12,199	−0.12	0.54	−0.33	0.58	0.25	0.54	15,151	11,259	10,138	273	292
20130218T112010	Run08LB5_Oct	305	31,798	41,423	26,205	23,019	−9,625	26,802	0.05	0.78	−0.36	0.75	0.07	0.43	34,929	23,216	26,096	217	245
20130218T112010	Run09LB6_Oct	294	11,435	26,582	7,404	14,741	−15,147	16,706	−0.46	0.56	−0.74	0.81	0.04	0.43	22,177	20,911	7,385	199	236
20130218T112010	Run10LB8_Oct	286	16,489	24,316	8,054	11,626	−7,827	11,415	−0.17	0.47	−0.34	0.54	0.22	0.51	14,814	12,569	7,842	264	275
20130218T112010	Run11W2_Oct	305	17,750	25,299	13,586	13,991	−7,549	16,253	−0.01	0.74	−0.37	0.73	0.02	0.40	20,725	15,672	13,562	232	262
20130219T091425	Run01G1	1,053	9,802	13,476	5,219	5,365	−3,673	5,519	−0.20	0.40	−0.33	0.47	0.33	0.56	7,125	5,157	4,917	996	1034
20130219T091425	Run02G2	821	12,358	13,757	6,808	6,091	−1,399	6,654	0.11	0.56	−0.11	0.48	0.07	0.41	8,934	5,807	6,789	773	801
20130219T091425	Run03G2	1,008	19,929	22,989	17,279	9,050	−3,060	12,196	−0.09	0.51	−0.28	0.55	0.35	0.53	16,743	4,294	16,183	910	963
20130219T091425	Run04G3	650	7,148	6,225	2,328	3,414	924	3,173	0.78	0.99	0.24	0.50	0.00	0.30	4,228	3,531	2,326	576	596
20130219T091425	Run05G3	904	9,246	12,663	4,303	6,327	−3,416	5,255	−0.12	0.42	−0.26	0.46	0.29	0.54	7,373	6,118	4,115	845	881
20130219T091425	Run06G4	972	7,173	6,689	1,555	2,096	484	1,828	0.23	0.39	0.10	0.28	0.09	0.39	2,540	2,014	1,547	937	956
20130219T091425	Run07G4	867	6,646	9,256	2,358	4,518	−2,610	3,834	−0.12	0.41	−0.27	0.47	0.25	0.49	5,246	4,722	2,284	794	826

Table B.2. Statistics for 24-Hour Average (Midnight to Midnight) Model–Measurement Pairs of Particle Number Concentrations

Internal University of Iowa Identification Code	Simulation Case	*n*	Modeled Mean (particles/cm^3)	Measured Mean (particles/cm^3)	Modeled SD (particles/cm^3)	Measured SD (particles/cm^3)	Mean Bias (particles/cm^3)	Mean Error (particles/cm^3)	Mean Normal Bias (particles/cm^3)	Mean Normal Error	Fractional Bias	Fractional Error	*r*	IOA	RMSE (particles/cm^3)	RMSEs (particles/cm^3)	RMSEu (particles/cm^3)	Hours Within 3.2:1 (*n*)	Hours Within 4:1 (*n*)
20130217T134752	Run01LB4_Sept	15	8,669	13,118	1,841	4,370	−4,450	5,216	−0.22	0.43	−0.35	0.48	0.54	0.53	5,719	5,519	1,499	6	13
20130217T134752	Run02LB5_Sept	15	14,203	30,595	5,505	7,882	−16,392	16,649	−0.51	0.53	−0.74	0.76	0.17	0.41	18,470	17,711	5,240	4	6
20130217T134752	Run03W2_Sept	12	8,674	14,422	2,142	2,656	−5,748	5,748	−0.39	0.39	−0.50	0.50	0.24	0.42	6,417	6,101	1,988	6	9
20130217T134752	Run04LB2_May	3	7,495	12,665	911	3,274	−5,170	5,170	−0.38	0.38	−0.49	0.49	−0.11	0.42	5,904	5,857	739	2	2
20130218T091223	Run05LB3_May	7	6,163	16,677	670	5,681	−10,515	10,515	−0.60	0.60	−0.88	0.88	0.18	0.37	11,724	11,708	610	0	2
20130218T112010	Run06W2_May	7	6,970	12,970	1,087	2,994	−6,000	6,000	−0.44	0.44	−0.58	0.58	0.04	0.35	6,670	6,594	1,006	3	3
20130218T112010	Run07LB4_Oct	13	17,362	24,185	5,107	7,176	−6,824	7,395	−0.25	0.29	−0.32	0.36	0.60	0.61	8,812	7,888	3,930	9	11
20130218T112010	Run08LB5_Oct	13	31,490	41,249	9,584	10,543	−9,760	12,649	−0.20	0.30	−0.27	0.37	0.38	0.54	14,574	11,817	8,530	9	12
20130218T112010	Run09LB6_Oct	12	10,900	25,584	3,492	7,569	−14,683	14,683	−0.55	0.55	−0.79	0.79	0.21	0.41	16,407	16,078	3,270	3	5
20130218T112010	Run10LB8_Oct	12	16,481	24,302	3,475	6,235	−7,821	8,093	−0.29	0.32	−0.36	0.39	0.66	0.57	9,029	8,679	2,490	9	11
20130218T112010	Run11W2_Oct	13	17,518	25,251	6,512	4,004	−7,733	8,129	−0.31	0.33	−0.41	0.43	0.48	0.40	9,521	7,779	5,489	8	10
20130219T091425	Run01G1	43	9,846	13,486	2,159	3,411	−3,639	3,844	−0.24	0.26	−0.30	0.32	0.47	0.53	4,738	4,346	1,887	34	40
20130219T091425	Run02G2	31	12,254	13,745	2,561	3,902	−1,491	3,780	−0.05	0.27	−0.10	0.28	0.18	0.47	4,461	3,707	2,480	25	31
20130219T091425	Run03G2	41	19,606	22,759	5,442	4,238	−3,153	4,442	−0.13	0.19	−0.17	0.22	0.57	0.68	5,547	3,349	4,422	35	41
20130219T091425	Run04G3	21	7,078	6,513	581	2,516	565	2,075	0.40	0.57	0.16	0.34	−0.11	0.26	2,642	2,582	563	17	18
20130219T091425	Run05G3	35	9,328	12,617	1,219	3,234	−3,288	4,082	−0.19	0.33	−0.27	0.36	0.13	0.43	4,630	4,474	1,191	25	33
20130219T091425	Run06G4	36	7,248	6,828	724	1,239	420	1,041	0.12	0.19	0.07	0.16	0.03	0.36	1,459	1,273	714	33	35
20130219T091425	Run07G4	36	6,648	9,258	1,645	1,912	−2,610	2,702	−0.27	0.28	−0.34	0.35	0.42	0.53	3,228	2,873	1,471	27	30
Using all 24-hour averages		365	11,878	16,297	6,723	9,360	−4,419	5,352	−0.18	0.32	−0.27	0.37	0.76	0.79	7,554	6,145	4,394	255	312

Table B.3. Statistics for Overall Mean Particle Number Concentrations for the 18 Model Cases

n	18
Model mean (particles/cm^3)	12,184
Measured mean (particles/cm^3)	18,229
Modeled SD (particles/cm^3)	6,579
Measured SD (particles/cm^3)	9,178
Mean bias (particles/cm^3)	−6,045
Mean error (particles/cm^3)	6,201
Mean normalized bias	−0.30
Mean normalized error	0.32
Fractional bias	−0.38
Fractional error	0.40
r	0.87
IOA	0.80
RMSE (particles/cm^3)	7,568
RMSEs (particles/cm^3)	6,902
RMSEu (particles/cm^3)	3,105

MATERIALS AVAILABLE ON THE WEB

Appendices C through H and Additional Materials 1 through 4 contain supplemental material not included in the printed report. They are available on the HEI Web site *http://pubs.healtheffects.org*.

Appendix C. WRF Namelist

Appendix D. Description of Modeled Meteorologic Data and Development of Test Cases

Appendix E. Speed- and Temperature-Dependent CO Emission Factors from EMFAC

Appendix F. Descriptive Statistics for Roads in G1 Domain

Appendix G. Traffic near Receptors as a Function of Road Class, Distance, Direction, and Vehicle Type

Appendix H. Wind Data from LB4 Site

Additional Materials 1 through 4: Colorplots of Number Size Distributions

ABOUT THE AUTHORS

Charles Stanier is an associate professor of chemical and biochemical engineering at the University of Iowa, Iowa City, Iowa. He is also active in the university's IIHR–Hydroscience & Engineering Institute and the Center for Global and Regional Environmental Research.

Sang-Rin Lee works on engineering and environmental issues for Doosan Heavy Industries & Construction, Changwon, Korea. From 2007 to 2011, he was a postdoctoral research associate in IIHR–Hydroscience & Engineering at the University of Iowa. He holds a Ph.D. in environmental engineering from the University of Florida, Gainesville, Florida.

ABBREVIATIONS AND OTHER TERMS

3D	three-dimensional
ASM	Aerosol Screening Model
CFD	computational fluid dynamics
CHAPS	Coronary Health and Air Pollution Study
CMAQ	Community Multiscale Air Quality model
CO	carbon monoxide
CO_2	carbon dioxide
CPC	condensation particle counter
EPA	(U.S.) Environmental Protection Agency
GIS	geographic information systems
HCMS	Harbor Community Monitoring Study
HDV	heavy-duty vehicle
I-405	Interstate 405
I-710	Interstate 710
IMPROVE	Interagency Monitoring of Protected Visual Environments
IOA	index of agreement
LDV	light-duty vehicle
LUR	land-use regression
NWS	National Weather Service
PM	particulate matter
$PM_{2.5}$	particulate matter ≤ 2.5 μm in aerodynamic diameter
RMSE	root mean squared error
SCAG	Southern California Association of Governments
SMPS	scanning mobility particle sizer
USC	University of Southern California
UFPs	ultrafine particles less than 0.1 μm in aerodynamic diameter
UTM	Universal Transverse Mercator
WRF	Weather Research and Forecasting

Research Report 179, *Development and Application of an Aerosol Screening Model for Size-Resolved Urban Aerosols*, C. O. Stanier and S.-R. Lee

INTRODUCTION

Ambient particulate matter (PM*) is a complex mixture of solid and liquid airborne particles, ranging from approximately 5 nm to 100 μm in aerodynamic diameter. On the basis of epidemiologic findings, the U.S. Environmental Protection Agency has promulgated National Ambient Air Quality Standards for PM with an aerodynamic diameter ≤ 2.5 μm ($PM_{2.5}$, also referred to as fine particles) to protect the general population and the groups considered most vulnerable to adverse effects of PM exposure.

In the urban atmosphere, the subset of $PM_{2.5}$ with an aerodynamic diameter less than 100 nm, conventionally referred to as ultrafine particles (UFPs), originates primarily from motor vehicle emissions. These particles contribute very little to the total $PM_{2.5}$ mass in ambient air but are the dominant contributors to particle number. Because of the small size and physical properties of UFPs, concerns have been raised about whether UFPs might have specific or enhanced toxicity compared with other particle size fractions. However, the epidemiologic evidence for short-term effects of UFPs is limited, and there are no studies of long-term exposure, in part because of the challenges in assessing exposure of the study populations (caused by the fact that measurements taken at central sites do not capture the spatial contrast in concentrations across an urban area).

In January 2006, Dr. Charles O. Stanier of the University of Iowa, Iowa City, submitted an application under Request for Applications 06-3, the "Walter A. Rosenblith New Investigator Award," entitled "Development and Application of a Personal Exposure Screening Model for Size-Resolved Urban Aerosols." He proposed to construct and test an advanced exposure model (based on several existing models) to predict concentrations of UFPs in near-road environments with high spatial resolution (~10 m). The HEI Health Research Committee thought that the development of an improved model would be valuable for future studies of the health effects of UFPs and recommended the study for funding.

BACKGROUND

A large proportion of the world's population lives in close proximity to roads and highways with heavy vehicular traffic. Studies have shown that the number concentration of UFPs is highest on roads and decreases with distance from the roads as a result of dilution, dispersion, and transformation processes such as coagulation, condensation, and evaporation (Karner et al. 2010; Kumar et al. 2011). The dispersion of UFPs is also influenced by weather and geography. Given the steep gradients in UFP concentrations near traffic sources, the concentrations of UFPs vary greatly within an urban area and are not adequately captured by measurements taken at one or a few central monitoring sites.

Efforts to estimate exposure to UFP number concentrations have relied in part on models developed specifically to capture the small area variations in these concentrations. Various models that address the dispersion of pollutants are available. These are referred to as dispersion models and use as model inputs motor-vehicle-emission factors, traffic data, data on background concentrations of the pollutant of interest, and meteorologic data. The models vary in complexity and in how they describe the dispersion of pollutants and their chemical–physical transformations. The most commonly used dispersion models are Gaussian — that is, they assume that the dispersion of a pollutant plume can be described with a Gaussian equation. After the data requirements have been met, the model computes the pollutant concentrations at specific sites (referred to as receptors).

Recently, dispersion models have been integrated with geographic information system data, such as data on road types and traffic, and travel-demand models to provide

Dr. Stanier's 3-year study, "Development and Application of a Personal Exposure Screening Model for Size-Resolved Urban Aerosols," began in October 2007. Total expenditures were $276,263. The draft Investigators' Report from Drs. Stanier and Lee was received for review in August 2012. A revised report, received in February 2013, was accepted for publication in March 2013. During the review process, the HEI Health Review Committee and the investigators had the opportunity to exchange comments and to clarify issues in both the Investigators' Report and the Review Committee's Critique.

* A list of abbreviations and other terms appears at the end of the Investigators' Report.

more detailed spatial resolution of traffic patterns, as well as with more advanced model frameworks to improve the simulation of physical–chemical atmospheric processes and dispersion of pollutants over complex terrain. These integrated air pollution dispersion models include fluid dynamics models, so-called Lagrangian models, and grid models, among others (Sharma et al. 2004.)

The application of dispersion models to UFPs is challenging because particle number emission factors are seldom available and, when available, have large uncertainties associated with them. In addition, UFPs undergo complex physical–chemical changes in time and space that are difficult to model. A review of the dispersion models applied to UFPs can be found in Kumar and colleagues (2011).

A different type of model that has recently been applied to UFPs is the land-use regression (LUR) model, which combines monitoring of air pollution at specific locations with predictor variables such as land use and traffic characteristics (Hoek et al. 2011; Abernethy et al. 2013.) LUR models typically focus on long-term concentrations; dispersion models also incorporate short-term variability.

One important component of model development is model evaluation. This can include comparing modeled pollutant concentrations at the receptors with measured concentrations, as well as comparing model predictions with those of other models for the same locations.

The study described in this report aimed at developing a physically based Lagrangian dispersion model to estimate UFPs and fine PM concentrations at high spatial resolution. This Critique is intended to aid the sponsors of HEI and the public by highlighting both the strengths and limitations of the study and by placing it into scientific perspective.

SPECIFIC AIMS

The main goal of the study, conducted by Stanier and his colleague Sang-Rin Lee, was to develop, test, and evaluate an aerosol screening model (ASM) of hourly size-resolved particle concentrations in the size range of 3 nm to 2.5 μm. The investigators hoped that the ASM would prove to be useful as a screening model in near-road environments and that it would be widely applied to decide whether a more complex model or additional pollutant measurements were needed.

The specific aims of the study were the following:

1. To develop a computationally efficient ASM combining analytic dispersion equations and two-dimensional and three-dimensional aerosol dynamics. The ASM would model UFPs and fine PM concentrations at 11 sites in Los Angeles and Riverside counties in California where field measurements were available from previous studies;
2. To evaluate the model by comparing the modeled concentrations with the measured concentrations; and
3. To evaluate the sensitivity of the model output to aerosol dynamic processes and meteorologic data selection and the computational cost of these design choices.

STUDY DESIGN

Model design and construction were guided by the desire for the model, first, to have the ability to model concentrations over short (1-hour) and longer (24-hour) periods at sites with various traffic volumes and patterns and at various distances from roads and, second, to use a large database of road segments and emission factors derived from different data sources. It was also important that the model estimates could be compared with field measurements made with a condensation particle counter (CPC), which counted particles > 14 nm in size, and a scanning mobility particle sizer (SMPS), which measured number-based and volume-based size distributions of particles > 7 nm (as well as total particle number). The volume metric from the SMPS was assumed to be an indicator of mass. Although the CPC measures a large range of particle sizes, the size distributions measured in the Harbor Community Monitoring Study (HCMS) showed that a large proportion of particle number was in the UFP range (Krudysz et al. 2009.) The investigators thus assumed that particle number is primarily a measure of UFP number.

After the model was developed, the next phase of the study consisted of obtaining and processing appropriate inputs for the model. The model was then run to predict hourly and 24-hour concentrations and size distributions of particle number and volume (an indicator of mass) at 11 sites where real-time measurements were made in previous studies. These included seven sites around the port of Long Beach (one of the busiest commercial ports in the United States) that were part of the HCMS (Krudysz et al. 2009; Moore et al. 2009) and four sites near retirement communities in Los Angeles and Riverside counties that were part of the Cardiovascular Health and Air Pollution Study (CHAPS) (Polidori et al. 2007; Delfino et al. 2008). The measurements at the HCMS sites were made from February to

December 2007, using a CPC and an SMPS. The measurements at the CHAPS sites were made during two 6-week periods between July 2005 and February 2006, using a CPC.

The measurement sites varied in their distance from roads with heavy traffic. Overall, compared with the HCMS sites (which had on average 107,700 vehicles/km per day), three of the CHAPS sites (G1, G3, and G4) had lower total traffic volume (20,300 vehicles/km per day) within 500 m. The CHAPS G2 site had 180,000 vehicles/km per day. The HCMS LB4 and LB5 sites were the most affected by traffic.

The performance of the model in predicting particle number concentrations was assessed through comparison with the measurements made in the HCMS and CHAPS. The performance of the model in predicting particle-weighted size distributions was assessed through comparison with the size distributions measured at the seven HCMS sites.

MODEL DESCRIPTION AND INPUTS

The ASM is an integrated model based on the Lagrangian modeling framework. It follows multiple interacting, vertically resolved columns of air traveling at the local wind velocity. The columns can be viewed as a moving wall or slab made up of computational parcels. The model follows emissions and their nonlinear transformations and deposition. The assumptions used by the ASM include rapid mixing of tailpipe emissions, emissions evenly mixed horizontally across the road width and carried beyond the edge of the road by diffusion and advection with the wind (i.e., downwind transportation), and rapid mixing into a predefined vertical distribution. As designed, the parcel wall moves in larger steps when far from receptors and in smaller steps when close to receptors.

The ASM inputs were meteorologic variables, parameters describing the movement of the air parcels from the source to the receptor, emission factors, road locations and types, traffic data, and background UFP concentrations and size distributions. These are briefly described below.

- Meteorologic variables were derived using the Weather Research and Forecasting (WRF) model, which was run at 1-km spatial resolution using observations from 11 nearby stations of the National Weather Service. Meteorologic output was evaluated relative to the Long Beach National Weather Service station and the meteorologic variables measured in the HCMS.
- Parameters of deposition, coagulation, and vertical and horizontal dispersion were used to describe the size-specific movement of PM between parcels. The starting location of the slab of parcels was set at 4000 m upwind from the receptor or, during hours of low wind speed, at an upwind distance equal to the distance wind traveled during a 1-hour period. Several assumptions were made in determining the vertical dispersion profiles.
- Road network and daily traffic volume data for heavy- and light-duty vehicles were obtained from the Southern California Association of Governments travel-demand model, which includes nine road classes. Traffic data are available for 4-hour periods and are differentiated by day of the week but do not correspond to any particular day. The investigators derived hourly diurnal patterns and weekday/weekend ratios using Long Beach–specific analyses of hourly total traffic counts and heavy- and light-duty vehicle counts. The CHAPS sites were modeled to have a lower fraction of heavy-duty vehicles within 500 m than the HCMS sites (0.05 versus 0.1).
- Size-resolved emission factors for cruise and acceleration modes and for light- and heavy-duty vehicles were obtained from a vehicle chase experiment using the CPC and SMPS that was conducted by Kittelson and colleagues (2006a; 2006b) in Minnesota in summer 2002. These data were supplemented with measurements in the accumulation and coarse size ranges from a California tunnel study in the summer of 2004 (Geller et al. 2005) and measurements from a chassis dynamometer study of some in-use light-duty gasoline and heavy-duty diesel vehicles in 2002 and 2003, respectively (Robert et al. 2007a and 2007b). The emission factors were corrected for the vehicles' acceleration fraction, diffusional losses for particles < 20 nm during sampling, and differences in transmission efficiencies (i.e., lower size cut-offs) between the CPC and SMPS.
- Parcel dimensions and sizes were set by the investigators.
- Background mass-weighted and number-weighted size distributions were derived for each parcel, by interpolating the $PM_{2.5}$ mass concentrations from the U.S. Environmental Protection Agency or Interagency Monitoring of Protected Visual Environments (IMPROVE) hourly and daily monitoring values with kriging, using an assumed distribution based on the size distribution at one of the receptor locations in the wind direction with the lowest $PM_{2.5}$ mass.

SUMMARY OF KEY RESULTS

MODEL OUTPUT

The model simulated particle number concentrations at 1-hour resolution (based on a lower size cut-off of either 7 or 14 nm) and concentrations averaged over a day (24 hours). The hourly concentrations are reported in plots showing the diurnal patterns for all 11 sites on specific days; the 24-hour concentrations are shown in scatterplots comparing them with the measured concentrations. The Investigators' Report also includes plots that show number or volume size distributions for specific days.

OVERALL MODEL PERFORMANCE

Correlations Between Modeled and Measured 24-Hour and 1-Hour Average Number Concentrations

For 24-hour modeled concentrations, the investigators' performance goal for the ASM was that 90% of the concentrations were to be no more than a factor of 1.6 higher or lower than the measured concentrations. In actual performance, 70% (255 out of 365) of the modeled concentrations fell within this range. The model's performance was better for the CHAPS sites than for the Long Beach sites. The investigators found that when the modeled values failed to fall within the targeted range, the model typically underestimated particle concentrations.

For hourly concentrations, the investigators' performance goal for the ASM was that 90% of the concentrations were to be no more than a factor of 3.2 higher or lower than the measured concentrations. In actual performance, 88% (that is, 8111 of 9201 total hours of simulation across all sites) of the concentrations fell within this range. Again, the model's performance was better at the CHAPS sites (93% within the range) than at Long Beach sites (78% within the range). Only four of the 18 simulation periods at the 11 sites had a correlation coefficient between 0.25 and 0.4 compared with the measured concentrations; the others all had a lower correlation coefficient. For modeled 24-hour concentrations, eight of the 18 simulation periods had correlation coefficients in excess of 0.25 (as shown in Appendix B.)

Diurnal Patterns

To evaluate the model's ability to predict the diurnal patterns of number concentrations, the model's estimates for Long Beach sites were compared with diurnal patterns based on measurements made using the SMPS. The results indicated that the model underpredicted particle number during certain times (for example, during the morning rush hours) at particular sites and did not reproduce the variability in concentrations sufficiently well. The investigators noted that the issue of model underprediction was not as evident when they compared the model's estimates for Long Beach sites with the diurnal patterns based on measurements using the CPC (which included particles > 7 nm). A similar comparison (i.e., using the CPC-based measurements) for the CHAPS sites showed that the diurnal patterns and concentrations were predicted with more accuracy than for the Long Beach sites.

Size Distribution Patterns

The investigators compared modeled and measured size distributions at two Long Beach sites, LB4 and LB5. The modeled distributions differed from the measured distributions for many of the simulations. The simulations typically had a bimodal size distribution reflecting the assumed emission size distribution, while measured size distributions generally had a single mode.

The investigators concluded that the model underpredicts number concentrations for all particles sizes $\geq$ 15 nm and overpredicts concentrations for particle sizes < 15 nm, possibly because of uncertainties in emission factors.

SENSITIVITY CALCULATIONS

To evaluate the sensitivity of the modeled concentrations to model inputs that could affect resulting emission factors, Stanier and Lee performed sensitivity tests for each receptor by varying seven inputs: light-duty vehicle traffic, heavy-duty vehicle traffic, and total traffic on each of five types of roads (e.g., highway and arterial). Sensitivity to emission variables was quantified as the fractional reduction in concentration divided by the fractional reduction for the emission variable being tested. The investigators found that model predictions of particle number were sensitive to traffic type and road class. More specifically, at the Long Beach sites, heavy-duty vehicles and freeway and arterial traffic affected particle number more than light-duty vehicles and the other road classes did. At the CHAPS sites, which were more residential, light-duty vehicles and traffic on local roads were found to have a greater effect on particle number than at the Long Beach sites. The investigators noted that analyses of background concentrations showed that they can be very important because they represent a major component of the modeled particle number when the influence of traffic is low.

Sensitivity to weather was tested by replacing parameters from the WRF model with those available from the HCMS; this replacement did not result in any changes in model performance. It should be noted that, based on

comparisons at the LB4 and LB5 sites, (1) there was poor agreement between the measured wind direction and speed and the corresponding WRF-modeled values and (2) measured particle numbers showed only a limited dependence on wind direction.

REVIEW COMMITTEE EVALUATION

In its independent review of the study, the HEI Health Review Committee noted that overall this ambitious study was carefully planned and performed and the work was of high quality. Improved modeling of number and size distributions of UFPs is needed for epidemiologic studies; only a limited number of approaches have so far been tested. Thus the Committee thought that the study addressed an important research need.

On the whole, the Committee felt that the investigators had chosen a high level of complexity for a screening model, that the model would require additional simplifications for actual screening applications, and that additional information (including improved meteorologic data and consideration of aerosol dynamics, wind speed and direction [shear], atmospheric chemistry, secondary aerosol formation, and topography) would be needed for more detailed applications.

Stanier and Lee conducted a comprehensive study to develop and evaluate various inputs into an aerosol screening model of size-resolved urban aerosols and were successful in producing estimates of particle number concentrations and size distributions at the target sites. The strengths of the model are its flexibility for adding inputs, the automated procedure for processing road network and traffic data, and the ability to perform the complex task of synthesizing emission data for particle number by size from various research groups. The investigators made reasonable interpretations and corrections to account for differing lower limits on the size of particles detected by different instruments and for particle losses during sampling.

Model limitations are implicit in the Lagrangian approach, which assumes that all the air parcels in slabs move downwind at the same rate and communicate by diffusion but does not allow movement through their boundaries in association with changes in wind speed and direction. In addition, the model did not include local sources other than road traffic, such as rail or marine traffic, which would have been especially important in the Long Beach area.

The evaluation of the model indicated that its prediction skills for 24-hour average particle number concentrations were close to the preset performance targets; the prediction skills for 1-hour average number concentrations were poor and did not capture the diurnal variations observed at several sites. The model performed better in predicting 1-hour averages at the CHAPS sites, which were less affected by heavy-duty vehicles and further from freeways than the Long Beach sites. This result might also reflect the importance of off-road sources at the Long Beach sites. Particle size distributions were not well captured by the model. The Committee agreed that the poor performance of the model in simulating size distributions could be attributed, at least in part, to uncertainties in the emission factors, which were derived from a different fleet of vehicles driving at high speeds.

Sensitivity analysis showed that the model was sensitive to traffic volume and type as well as road class. Sensitivity to the various dispersion parameters and assumptions and to the emission factors was not evaluated, and sensitivity to background concentrations was assessed in a limited fashion. The Committee thought that the detailed evaluation, such as long simulation periods and comparison of modeled with measured data, was a strength of the study. Comparison of the ASM performance with other modeling approaches would be useful.

Even with the limitations discussed above, the Committee agreed with the investigators' conclusion that light-duty vehicles can have greater impact on particle number than heavy-duty vehicles, especially for locations farther away from freeways. The finding that UFP concentrations were affected by both traffic type and road class was also considered valid.

The Committee agreed with the investigators' overall assessment that the performance of the model in predicting particle number and size distribution was mixed. The Committee thought that improvements in the model would be required for future applications, as discussed by the investigators. The results suggest that the model might be more suitable for studies that require longer-term (i.e., 24-hour or longer) averages, rather than 1-hour averages.

In summary, the study reflected the challenges involved in modeling dynamic concentrations of UFPs in urban areas, including the complex behavior of UFPs in the atmosphere as well as our limited knowledge not only of size-resolved emission factors as a function of vehicle types and operating modes, but also of emissions from non-mobile sources. Given the complexity of the ASM and the limitations of the Lagrangian framework in modeling the behavior of UFPs, it remains unclear what the most useful application of this model will be. However, the model offers promise for further improvements and has the flexibility of incorporating additional inputs such as fleet information and emissions from off-road sources.

ACKNOWLEDGMENTS

The Health Review Committee thanks the ad hoc reviewers for their help in evaluating the scientific merit of the Investigators' Report. The Committee is also grateful to Annemoon van Erp for her oversight of the study, to Maria Costantini for her assistance in preparing its Critique, to Mary Katherine Brennan for science editing of this Report and its Critique, to DG Communications for its composition, and to Barbara Gale, Hope Green, Fred Howe, and Bernard Jacobson for their roles in preparing this Research Report for publication.

REFERENCES

Abernethy RC, Allen RW, McKendry IG, Brauer M. 2013. A land use regression model for ultrafine particles in Vancouver, Canada. Environ Sci Technol 47(10):5217–5225.

Delfino RJ, Staimer N, Tjoa T, Polidori A, Arhami M, Gillen DL, Kleinman MT, Vaziri ND, Longhurst J, Zaldivar F, Sioutas C. 2008. Circulating biomarkers of inflammation, antioxidant activity, and platelet activation are associated with primary combustion aerosols in subjects with coronary artery disease. Environ Health Perspect 116(7):898–906.

Geller VD, Sardar SB, Phuleria H, Fine PM, Sioutas C. 2005. Measurements of particle number and mass concentrations and size distributions in a tunnel environment. Environ Sci Technol 39(22):8653–8663.

Hoek G, Beelen R, Kos G, Dijkema M, van der Zee SC, Fischer PH, Brunekreef B. 2011. Land use regression model for ultrafine particles in Amsterdam. Environ Sci Technol 45(2):622–628.

Karner AA, Eisinger DS, Niemeier DA. 2010. Near-roadway air quality: Synthesizing the findings from real-world data. Environ Sci Technol 44(14):5334–5344.

Kittelson DB, Watts WF, Johnson JP. 2006a. On-road and laboratory evaluation of combustion aerosols — part 1: Summary of diesel engine results. J Aerosol Sci 37:913–930.

Kittelson DB, Watts WF, Johnson JP, Schauer JJ, Lawson DR. 2006b. On-road and laboratory evaluation of combustion aerosols — part 2: Summary of spark ignition engine results. J Aerosol Sci 37:931–949.

Krudysz M, Moore K, Geller M, Sioutas C, Froines J. 2009. Intra-community spatial variability of particulate matter size distributions in Southern California/Los Angeles. Atmos Chem Phys 9:1061–1075.

Kumar P, Ketzel M, Vardoulakis S, Pirjola L, Britter R. 2011. Dynamics and dispersion modelling of nanoparticles from road traffic in the urban atmospheric environment: A review. J Aerosol Sci 42(9):580–603.

Moore K, Krudysz M, Pakbin P, Hudda N, Sioutas C. 2009. Intra-community variability in total particle number concentrations in the San Pedro Harbor Area (Los Angeles, California). Aerosol Sci Technol 43(6):587–603.

Polidori A, Arhami M, Sioutas C, Delfino RJ, Allen R. 2007. Indoor/outdoor relationships, trends, and carbonaceous content of fine particulate matter in retirement homes of the Los Angeles Basin. J Air Waste Manage Assoc 57(3):366–379.

Robert MA, Kleeman MJ, Jakober CA. 2007a. Size and composition distributions of particulate matter emissions: Part 2. Heavy-duty diesel vehicles. J Air Waste Manage Assoc 57(12):1429–1438.

Robert MA, VanBergen S, Kleeman MJ, Jakober CA. 2007b. Size and composition distributions of particulate matter emissions: Part 1. Light-duty gasoline vehicles. J Air Waste Manage Assoc 57(12):1414–1428.

Sharma N, Chaudhry KK, Rao CVC. 2004. Vehicular pollution prediction modelling: A review of highway dispersion models. Transport Rev 24(4):409–435.

RELATED HEI PUBLICATIONS: ULTRAFINE PARTICLES

Number	Title	Principal Investigator	Date
Research Reports			
180	Characterizing Ultrafine Particles and Other Air Pollutants In and Around School Buses	Y. Zhu	2014
173	Selective Detection and Characterization of Nanoparticles from Motor Vehicles	M.V. Johnston	2013
166	Advanced Collaborative Emissions Study (ACES) Subchronic Exposure Results: Biologic Responses in Rats and Mice and Assessment of Genotoxicity		2012
	Part 1. Biologic responses in rats and mice to subchronic inhalation of diesel exhaust from U.S. 2007-compliant engines: report on 1-, 3-, and 12-month exposures in the ACES bioassay	J.D. McDonald	
	Part 2. Assessment of genotoxicity after exposure to diesel exhaust from U.S. 2007-compliant diesel engines: report on 1- and 3-month exposures in the ACES bioassay	J.C. Bemis	
	Part 3. Assessment of genotoxicity and oxidative stress after exposure to diesel exhaust from U.S. 2007-compliant diesel engines: report on 1- and 3-month exposures in the ACES bioassay	L.M. Hallberg	
	Part 4. Effects of subchronic diesel engine emissions exposure on plasma markers in rodents: report on 1- and 3-month exposures in the ACES bioassay	D.J. Conklin	
164	Pulmonary Particulate Matter and Systemic Microvascular Dysfunction	T. Nurkiewicz	2011
159	Role of Neprilysin in Airway Inflammation Induced by Diesel Exhaust Emissions	S.S. Wong	2011
158	Air Toxics Exposure from Vehicle Emissions at a U.S. Border Crossing: Buffalo Peace Bridge Study	J.D. Spengler	2011
156	Concentrations of Air Toxics in Motor Vehicle–Dominated Environments	E.M. Fujita	2011
153	Improved Source Apportionment and Speciation of Low-Volume Particulate Matter Samples	J.J. Schauer	2010
151	Pulmonary Effects of Inhaled Diesel Exhaust in Young and Old Mice: A Pilot Project	D.L. Laskin	2010
147	Atmospheric Transformation of Diesel Emissions	B. Zielinska	2010
145	Effects of Concentrated Ambient Particles and Diesel Engine Exhaust on Allergic Airway Disease in Brown Norway Rats	J.R. Harkema	2009
138	Health Effects of Real-World Exposure to Diesel Exhaust in Persons with Asthma	J. Zhang	2009
136	Uptake and Inflammatory Effects of Nanoparticles in a Human Vascular Endothelial Cell Line	I.M. Kennedy	2009
129	Particle Size and Composition Related to Adverse Health Effects in Aged, Sensitive Rats	F.F. Hahn	2005

Continued

Printed copies of these reports can be obtained from HEI; pdf's are available for free downloading at http://pubs.healtheffects.org.

RELATED HEI PUBLICATIONS: ULTRAFINE PARTICLES

Number	Title	Principal Investigator	Date
126	Effects of Exposure to Ultrafine Carbon Particles in Healthy Subjects and Subjects with Asthma	M.W. Frampton	2004
124	Particulate Air Pollution and Nonfatal Cardiac Events		2005
	Part I. Air Pollution, Personal Activities, and Onset of Myocardial Infarction in a Case–Crossover Study	A. Peters	
	Part II. Association of Air Pollution with Confirmed Arrhythmias Recorded by Implanted Defibrillators	D. Dockery	
98	Daily Mortality and Fine and Ultrafine Particles in Erfurt, Germany *Part I.* Role of Particle Number and Particle Mass	H-E. Wichmann	2000
96	Acute Pulmonary Effects of Ultrafine Particles in Rats and Mice	G. Oberdörster	2000
HEI Special Reports			
17	Traffic-Related Air Pollution: A Critical Review of the Literature on Emissions, Exposure, and Health Effects		2010
HEI Communications			
17	Advanced Collaborative Emissions Study (ACES). Phase 3A: Characterization of U.S. 2007-Compliant Diesel Engine and Exposure System Operation	J.L. Mauderly	2012
16	The Future of Vehicle Fuels and Technologies: Anticipating Health Benefits and Challenges		2011
HEI Perspectives			
3	Understanding the Health Effects of Ambient Ultrafine Particles		2013
2	Understanding the Health Effects of Components of the Particulate Matter Mix: Progress and Next Steps		2002

Printed copies of these reports can be obtained from HEI; pdf's are available for free downloading at http://pubs.healtheffects.org.

HEI BOARD, COMMITTEES, and STAFF

Board of Directors

Richard F. Celeste, Chair *President Emeritus, Colorado College*

Sherwood Boehlert *Of Counsel, Accord Group; Former Chair, U.S. House of Representatives Science Committee*

Enriqueta Bond *President Emerita, Burroughs Wellcome Fund*

Purnell W. Choppin *President Emeritus, Howard Hughes Medical Institute*

Michael T. Clegg *Professor of Biological Sciences, University of California–Irvine*

Jared L. Cohon *President Emeritus and Professor, Civil and Environmental Engineering and Engineering and Public Policy, Carnegie Mellon University*

Stephen Corman *President, Corman Enterprises*

Linda Rosenstock *Dean Emerita and Professor of Health Policy and Management, Environmental Health Sciences and Medicine, University of California–Los Angeles*

Henry Schacht *Managing Director, Warburg Pincus; Former Chairman and Chief Executive Officer, Lucent Technologies*

Warren M. Washington *Senior Scientist, National Center for Atmospheric Research; Former Chair, National Science Board*

Archibald Cox, Founding Chair *1980–2001*

Donald Kennedy, Vice Chair Emeritus *Editor-in-Chief Emeritus, Science; President Emeritus and Bing Professor of Biological Sciences, Stanford University*

Health Research Committee

David L. Eaton, Chair *Dean and Vice Provost of the Graduate School, University of Washington–Seattle*

David Christiani *Elkan Blout Professor of Environmental Genetics, Harvard School of Public Health*

Francesca Dominici *Professor of Biostatistics and Senior Associate Dean for Research, Harvard School of Public Health*

David E. Foster *Phil and Jean Myers Professor Emeritus, Department of Mechanical Engineering, Engine Research Center, University of Wisconsin–Madison*

Uwe Heinrich *Professor, Hannover Medical School; Executive Director, Fraunhofer Institute for Toxicology and Experimental Medicine, Hanover, Germany*

Barbara Hoffmann *Professor of Environmental Epidemiology and Head of Environmental Epidemiology of Aging, IUF-Leibniz Research Institute for Environmental Medicine, and Professor, Medical Faculty, Heinrich Heine University of Düsseldorf, Germany*

Allen L. Robinson *Raymond J. Lane Distinguished Professor and Head, Department of Mechanical Engineering, and Professor, Department of Engineering and Public Policy, Carnegie Mellon University*

Richard L. Smith *Director, Statistical and Applied Mathematical Sciences Institute, University of North Carolina–Chapel Hill*

James A. Swenberg *Kenan Distinguished Professor of Environmental Sciences, Department of Environmental Sciences and Engineering, University of North Carolina–Chapel Hill*

HEI BOARD, COMMITTEES, and STAFF

Health Review Committee

Homer A. Boushey, Chair *Professor of Medicine, Department of Medicine, University of California–San Francisco*

Michael Brauer *Professor, School of Environmental Health, University of British Columbia, Canada*

Bert Brunekreef *Professor of Environmental Epidemiology, Institute of Risk Assessment Sciences, University of Utrecht, the Netherlands*

Mark W. Frampton *Professor of Medicine and Environmental Medicine, University of Rochester Medical Center*

Stephanie London *Senior Investigator, Epidemiology Branch, National Institute of Environmental Health Sciences*

Roger D. Peng *Associate Professor, Department of Biostatistics, Johns Hopkins Bloomberg School of Public Health*

Armistead Russell *Howard T. Tellepsen Chair of Civil and Environmental Engineering, School of Civil and Environmental Engineering, Georgia Institute of Technology*

Lianne Sheppard *Professor of Biostatistics, School of Public Health, University of Washington–Seattle*

Officers and Staff

Daniel S. Greenbaum *President*
Robert M. O'Keefe *Vice President*
Rashid Shaikh *Director of Science*
Barbara Gale *Director of Publications*
Jacqueline C. Rutledge *Director of Finance and Administration*
April Rieger *Corporate Secretary*

Kate Adams *Senior Scientist*
Hanna Boogaard *Staff Scientist*
Aaron J. Cohen *Principal Scientist*
Maria G. Costantini *Principal Scientist*
Philip J. DeMarco *Compliance Manager*
Hope Green *Editorial Assistant*
L. Virgi Hepner *Senior Science Editor*
Anny Luu *Administrative Assistant*
Francine Marmenout *Senior Executive Assistant*
Nicholas Moustakas *Policy Associate*
Hilary Selby Polk *Senior Science Editor*
Jacqueline Presedo *Research Assistant*
Evan Rosenberg *Staff Accountant*
Margarita Shablya *Science Administrative Assistant*
Robert A. Shavers *Operations Manager*
Geoffrey H. Sunshine *Senior Scientist*
Annemoon M.M. van Erp *Managing Scientist*
Donna J. Vorhees *Senior Scientist*
Katherine Walker *Senior Scientist*

HEALTH
EFFECTS
INSTITUTE

101 Federal Street, Suite 500
Boston, MA 02110, USA
+1-617-488-2300
www.healtheffects.org

RESEARCH
REPORT

Number 179
June 2014